



Universidad EAFIT  
*Escuela de Ingeniería*  
Grupo de Investigación de Mecánica Aplicada  
MSc.Thesis

---

# Wave propagation in a phase transforming cellular material

Author  
**Sara Elena Rodríguez Gómez**  
srodri13@eafit.edu.co

Advisor:  
**Prof. Juan David Gómez Cataño**

Co-Advisor:  
**Prof. Pablo Zavattieri**

Medellín, Colombia  
October 2016

*To Marinis and Jorge, thank you for all the love...*

## **Abstract**

The aim of this project is to explore the wave propagation properties in a phase transforming cellular material suitable for energy dissipation applications. We pretend to understand how to control the dispersion behavior and switch the propagation properties when the phase transition is triggered. In the long-term, the main objective is to achieve a device with tunable band gaps and wave guide properties.

The first part of this document presents the theoretical background of wave propagation in periodic materials. The second part is dedicated to the Bloch analysis of the phase transforming cellular material.

# Contents

<b>Introduction</b>	<b>5</b>
<b>State of the art</b>	<b>7</b>
<b>I Wave propagation in periodic materials</b>	<b>9</b>
<b>1 Bloch analysis</b>	<b>10</b>
1.1 Bloch-periodicity as boundary condition . . . . .	11
1.2 Fourier expansion of $w(\mathbf{r})$ . . . . .	13
1.3 The reciprocal space . . . . .	14
1.4 The diffraction condition . . . . .	15
1.5 First Brillouin zone . . . . .	17
1.6 The band structure . . . . .	21
1.7 Dispersion relations for one dimensional lattice models . . . . .	25
<b>2 Bloch-periodicity in the Finite Element Method</b>	<b>29</b>
2.1 Implementation . . . . .	32
2.1.1 Code for Abaqus input files . . . . .	32
2.2 Construction of the band structure . . . . .	36
<b>3 Classical problems in periodic materials</b>	<b>37</b>
3.1 Elastic, homogeneous and isotropic infinite space . . . . .	37
3.2 Square inclusion . . . . .	42
<b>II Wave propagation in a bistable material</b>	<b>47</b>
<b>1 A cellular material that exhibits bistability</b>	<b>48</b>
<b>2 Building an open cell</b>	<b>51</b>
<b>3 Dispersion diagrams of the stable configurations</b>	<b>68</b>
<b>4 Considering pre-stresses</b>	<b>74</b>

5 Modifying the topology	78
Conclusions	87

# Introduction

Cellular materials offer a unique combination of properties making them highly appealing and with a strong potential in different fields. They can exhibit high strength-to-weight and stiffness-to-weight ratios; high compressive failure strains at nearly constant stress; low thermal conductivity combined with high mechanical strength at elevated temperatures; high surface area per unit volume together with high mechanical strength and low density, among others [1–3]. With a controlled topology, relative density and geometry, novel materials are now possible thus widening its range of applications covering areas like medicine, package protection, chemical processing, waste management, aerospace and construction engineering.

Using the extended notion of solid state phase transformations to cellular solids, Restrepo et al. [4] designed a material that can switch its effective properties under a phase transformation. A phase transformation represents a change in the geometry of the unit cell in such conditions that the topology remains unmodified, while experiencing changes in its effective properties. Thus, it is possible to generate programmable devices with the advantages of cellular materials changing “on the fly”. On the other hand, the resulting phase transforming cellular material also offers good energy dissipation characteristics. This is achieved through an elastic bistable mechanism which produces a long stress-strain plateau, usually found in association to plastic behavior of materials.

A cellular material can also be regarded as a periodic material which inherently implies the existence of interesting phenomena associated to its wave propagation characteristics. First, periodic materials may exhibit stop bands introduced by Bragg scattering which produce frequency regions where waves are forbidden to propagate. Secondly, periodic materials may possess specific directions of preferred wave propagation or so-called directionality effects. The study of the effects known to exist in periodic materials in combination with the idea of bi-stable elemental cells with energy dissipation capabilities is a problem of interest on its own. In the particular case of *Grupo de Investigación en Mecánica Aplicada* of *Universidad EAFIT*, there is interest in exploring new alternatives to mitigate and attenuate elastic waves. In this project we conduct a preliminary study of phase transforming cellular materials aiming at identifying its potential in the frequency ranges of seismic waves.

*Grupo de Investigación en Mecánica Aplicada* has at its core interest, the identification of low-cost alternatives for earthquake resistant structures and as a conse-

quence, it has directed its attention to the study of elastic wave propagation [5–8]. In the case of a phase transforming cellular material, we are interested in exploring the mechanisms that lead to wave control and energy dissipation (the last one already covered in [4]). In general, with this work we seek to understand how a phase transformation changes the wave propagation properties of the cellular material and how to design appropriate unit cell geometries to achieve band gap tunability.

In the first part of the document we summarize the theoretical aspects of elastic wave propagation in periodic materials. In the first section of part I we present fundamental concepts on Bloch analysis, while in the second we describe the basis of Bloch-periodicity conditions in the finite element method. The last section of part I is dedicated to two cases of elastic periodic materials studied with Bloch analysis (the homogeneous and isotropic material and the square inclusion).

In part II we present the analysis on wave propagation of a phase transforming cellular material. The first section of part II contains the mechanical description of the cellular material, and the second section is dedicated to study the evolution of the wave propagation properties while building an open cell in five stages. The next section describes dispersion diagrams for each stable phase of the material while the fourth section study the change of these propagation properties when considering pre-stresses. The last section explores the influence of topological modification on the band diagrams in a closed cell.

# State of the art

The study of periodic materials and structures can be traced back to Newton’s work on sound propagation in air and to Lord Rayleigh’s work in continuous periodic structures. Rayleigh showed that such materials can exhibit band gaps in the frequency spectrum, i.e., forbidden bands where waves can not propagate [10]. These and other early developments in the field are described in Brillouin’s book on periodic structures [11].

The fundamental analysis tool for the study of infinite periodic media can be identified in a theorem proved by G. Floquet [12] in 1880 and extended by F. Bloch in 1929 [13]. Bloch stated that in a crystal, the energy eigenstates for an electron can be written as a plane wave times a periodic function; this fact underlies the concept of electronic band structures and crystals properties<sup>1</sup> which are well known in solid-state physics. It turns out that a description in terms of Bloch waves applies to any wave-like phenomenon present in a periodic medium.

Periodic structures are differentiated as photonic crystals in electromagnetism and phononic crystals in acoustics and elasticity. The applications of phononic crystals are found, as expected, in wave control and filtering [14–19]. Also, there is important literature on the subjects of non-destructive testing [20], waveguiding and localization [21–25], signal sensing [26], wave demultiplexers passive devices [27–29], logic gates [30], liquid sensors [31], microfluidic manipulation [32], ultrahigh sensitivity mass sensing above 100 GHz [33], sound collimation [34], refraction and focusing of sound waves [35, 36], wave rectification and acoustic diodes [37, 38], and “phoX-onic” crystals<sup>2</sup> [39].

Another extension of phononic crystals applications, of particular interest to us, is active control or tunability. This branch focuses on the development of devices with the capability to change the location and size of band gaps “on the fly”, as well as the shapes of its band diagrams. For example, crystals where the orientation of the inclusions with respect to the incoming waves may be tuned during operation [40]; piezoelectricity to alter the cells [41–44]; light-induced substrate potential and electrorheological materials in which tuning is done via an external electric field [45, 46];

---

<sup>1</sup>The classification of all crystals to metals, semiconductors and insulators is based on these phenomena.

<sup>2</sup>Crystals that exhibit simultaneous phononic and photonic bandgaps coinciding at the same range of wavevectors.

magnetism to alter material elastic properties [47] and temperature control [48]. Also, there are some works related to the control of elastic waves like those using finite elastic pre-straining [49], mechanical instabilities to trigger large deformations [50] and nonlinear materials to tune band gaps [51–54].

To optimize the band gap characteristics, researches have identified two features in the design of phononic crystals: the unit cell topology [20, 55–65] and the lattice symmetry [66]. The choice of the constitutive material phases and interweaving more than one lattice also provide possibilities for improving band gap characteristics [67].

Particularly in mechanics, before the introduction of phononic crystals theory as reported by Hussein [10], periodic structures had applications in composite materials (modeled as periodic) [68, 69], aircraft structures [70, 71], multiblade turbines [72, 73], impact resistant foam/cellular materials [74, 75], periodic foundations for buildings [76, 77], and multistory buildings and multispans bridges [78]. The field has been enriched notably with migration of concepts from phononic crystal treatment and recently, with the boom in metamaterials, broadly considered as examples of phononic materials except they have the added feature of exhibiting local resonance [9].

Starting in the 90s, we found contributions in elastic wave propagation for 2D spaces [79–83] and 3D phononic crystals [84–86]; sonic crystals, consisting of multiple phases of liquids and/or gases [14, 80, 87–89]; Rayleigh-type Bloch waves propagating along free surfaces in 2D semi-infinite domains [90–93]; phononic crystals in the form of plates of finite thickness [26, 94–103]; phononic crystals as MEMS [104, 105]; other configurations as radial phononic crystals [106], quasicrystals [107] and fractals [108, 109], and techniques to compute modes of evanescent Bloch waves [110, 111].

The reader is encouraged to review the work of Hussein et al. [10] where the historical origins, recent progress and future outlook in phononic materials are exposed in detail.

## Part I

# Wave propagation in periodic materials

A periodic material (PM) is defined as the repetition of a given motif in one, two or three space directions. The motif can be in the constituent material phases, the internal geometry, or the boundary conditions [10, 112, 113].



Figure 1: To every lattice point, the motif is added till is formed the material structure.

The description of a PM involves just the association of the motif to a **lattice**, which is a set of mathematical points (Figure 1). The material is then formed by the addition of the motif to each point with the final result allowing the condition that: “in every point of the lattice the arrangement of the whole structure must look the same”. The lattice is thus said to be **primitive** and such condition implies that a PM is invariant under any translation of the form (for three dimensions <sup>3</sup>):

$$\mathbf{T} = n_1 \mathbf{a}_1 + n_2 \mathbf{a}_2 + n_3 \mathbf{a}_3, \quad (1)$$

where  $n_i \in \mathbb{Z}$  and  $\mathbf{a}_i$  are basis vectors called **primitive translation vectors** (with  $i = 1, 2, 3$ ). They are formed by connecting the nearest neighboring points in the lattice and explicitly define the axes of periodicity. Figure 2 shows the primitive lattice in the description of a PM.

---

<sup>3</sup>For a peridodicity in 2D, the translation is expressed with  $\mathbf{a}_1$  and  $\mathbf{a}_2$ . Similarly, in 1D the primitive vector would be  $\mathbf{a}_1$ .

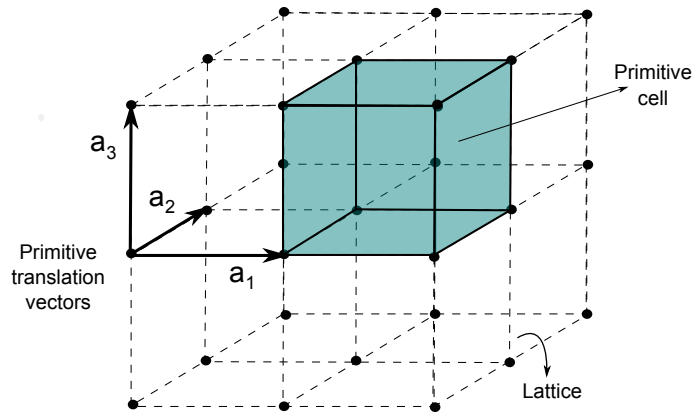


Figure 2: Description of a periodic material in 3D.

The parallelepiped formed by the primitive axes  $\mathbf{a}_1$ ,  $\mathbf{a}_2$  and  $\mathbf{a}_3$  contains the motif and is called a **primitive cell**. This cell serves as building block of the material structure and will fill all the space by the repetition of suitable translation operations. Any local physical property of the PM is invariant under  $\mathbf{T}$ , thus, the behavior of the whole material can be obtained just by studying the primitive cell.

## 1 Bloch analysis

The study of wave propagation in a PM can be conducted through Bloch-Floquet's theorem which states that the wave function for a periodically repeated medium can be defined as:

$$u(\mathbf{r}) = w(\mathbf{r})e^{i\mathbf{k}\cdot\mathbf{r}} \quad (2)$$

where,  $\mathbf{r}$  is the vector of spatial coordinates,  $\mathbf{k}$  the wavevector and  $w(\mathbf{r})$  is a function with the same periodicity of the associated lattice, i.e.,  $w(\mathbf{r} + \mathbf{T}) = w(\mathbf{r})$ .

The theorem was originally proved in the context of the Schrödinger equation with a periodic potential<sup>4</sup>. According to [114]:

---

<sup>4</sup>The Schrödinger equation describes how the quantum state of a quantum system changes with time, it predicts that wave functions can form standing waves, called stationary states:  $\hat{H}\Psi(\mathbf{r}) = E\Psi(\mathbf{r})$ , where  $E$  the energy of the wave function  $\Psi(\mathbf{r})$  and  $\hat{H}$  the Hamiltonian operator.

*The eigenfunctions of the wave equation for a periodic potential are the product of a plane wave  $e^{i\mathbf{k}\cdot\mathbf{r}}$  times a function  $w(\mathbf{r})$  with the periodicity of the crystal lattice.*

In general, equation (2) is a suitable solution for any wave equation where a physical property is represented as periodic, i. e.,

$$Lu(\mathbf{r}) = \omega^2 u(\mathbf{r}) + \mathbf{f}(\omega),$$

where  $L$  is a differential operator and  $\mathbf{f}(\omega)$  a harmonic body force with angular frequency  $\omega$  that is applied with the same periodicity of the lattice.

If we express equation (2) for a point in the space  $\mathbf{r} + \mathbf{T}$ , we will obtain

$$u(\mathbf{r} + \mathbf{T}) = w(\mathbf{r} + \mathbf{T})e^{i\mathbf{k}\cdot(\mathbf{r}+\mathbf{T})},$$

with  $\mathbf{T} = n_i \mathbf{a}_i$  being the translation vector. The function  $w(\mathbf{r})$  has the periodicity of the lattice, thus

$$u(\mathbf{r} + \mathbf{T}) = w(\mathbf{r})e^{i\mathbf{k}\cdot(\mathbf{r}+\mathbf{T})}.$$

Replacing  $w(\mathbf{r})$  in equation (2) we have

$$u(\mathbf{r}) = u(\mathbf{r} + \mathbf{T})e^{-i\mathbf{k}\cdot(\mathbf{r}+\mathbf{T})}e^{i\mathbf{k}\cdot\mathbf{r}},$$

which gives;

$$u(\mathbf{r} + \mathbf{T}) = u(\mathbf{r})e^{i\mathbf{k}\cdot\mathbf{T}}. \quad (3)$$

Equation (3) is known as the Bloch-periodicity condition and is used as the boundary condition for a Boundary Value Problem (BVP) when studying PMs.

## 1.1 Bloch-periodicity as boundary condition

The elastodynamic wave equation in the frequency domain (reduced wave equation) reads [115]:

$$(\lambda + \mu)\nabla(\nabla \cdot \mathbf{u}) + \mu\nabla^2 \mathbf{u} + \rho \mathbf{f} = -\omega^2 \rho \mathbf{u}, \quad (4)$$

where  $\lambda$  and  $\mu$  are the Lamé parameters, and  $\rho$  is the volumetric mass density. Writing the displacement field  $\mathbf{u}$  in terms of scalar and vector potentials  $\phi$  and  $\boldsymbol{\psi}$ , respectively yields:

$$\mathbf{u} = \nabla\phi + \nabla \times \boldsymbol{\psi},$$

where  $\nabla \cdot \boldsymbol{\psi} = 0$  [115].

If we neglect body forces  $\mathbf{f}$ , equation (4) is satisfied when:

$$\begin{aligned}\nabla^2\phi &= -\frac{\omega^2}{\alpha^2}\phi, \\ \nabla^2\boldsymbol{\psi} &= -\frac{\omega^2}{\beta^2}\boldsymbol{\psi}.\end{aligned}$$

The fact that these expressions are also wave equations, implies that the displacement field is formed by two decoupled types of waves: a dilatational (gradient) term  $\nabla\phi$  corresponding to longitudinal waves or P-waves propagating with velocity  $\alpha = \left(\frac{\lambda+2\mu}{\rho}\right)^{1/2}$ , and a distortional (rotational) term  $\nabla \times \boldsymbol{\psi}$  corresponding to shear waves or S-waves propagating with velocity  $\beta = \left(\frac{\mu}{\rho}\right)^{1/2}$ . Applying Bloch-Floquet's theorem to the above (see equation (3)) gives:

$$\begin{aligned}\phi(\mathbf{r} + \mathbf{T}) &= \phi(\mathbf{r})e^{i\mathbf{k}\cdot\mathbf{T}}, \\ \boldsymbol{\psi}(\mathbf{r} + \mathbf{T}) &= \boldsymbol{\psi}(\mathbf{r})e^{i\mathbf{k}\cdot\mathbf{T}},\end{aligned}$$

then,

$$\begin{aligned}\mathbf{u}(\mathbf{r} + \mathbf{T}) &= \nabla\phi(\mathbf{r} + \mathbf{T}) + \nabla \times \boldsymbol{\psi}(\mathbf{r} + \mathbf{T}), \\ &= e^{i\mathbf{k}\cdot\mathbf{T}}\nabla\phi(\mathbf{r}) + e^{i\mathbf{k}\cdot\mathbf{T}}\nabla \times \boldsymbol{\psi}(\mathbf{r}), \\ &= e^{i\mathbf{k}\cdot\mathbf{T}} [\nabla\phi(\mathbf{r}) + \nabla \times \boldsymbol{\psi}(\mathbf{r})], \\ &= \mathbf{u}(\mathbf{r})e^{i\mathbf{k}\cdot\mathbf{T}},\end{aligned}$$

which shows that Bloch-Floquet's theorem is also satisfied for the displacement field  $\mathbf{u}$ .

The complete BVP for equation (4) over a domain  $\Omega$  bounded by a boundary surface  $\Gamma$ , using Bloch-periodicity condition reads:

$$(\lambda + \mu)\nabla(\nabla \cdot \mathbf{u}) + \mu\nabla^2\mathbf{u} = -\omega^2\rho\mathbf{u} \quad \text{in } \Omega, \quad (5)$$

$$\mathbf{u}(\mathbf{r} + \mathbf{T}) = \mathbf{u}(\mathbf{r})e^{i\mathbf{k}\cdot\mathbf{T}} \quad \text{in } \Gamma, \quad (6)$$

$$\mathbf{t}(\mathbf{r} + \mathbf{T}) = -\mathbf{t}(\mathbf{r})e^{i\mathbf{k}\cdot\mathbf{T}} \quad \text{in } \Gamma. \quad (7)$$

In the above  $\mathbf{t}(\mathbf{r})$  is the surface traction vector.

## 1.2 Fourier expansion of $w(\mathbf{r})$

It has been stated that  $w(\mathbf{r})$  is a periodic function of  $\mathbf{r}$ , with period  $\mathbf{a}_1$ ,  $\mathbf{a}_2$  and  $\mathbf{a}_3$  in the directions of the three material axes, respectively. It follows that the condition  $w(\mathbf{r}) = w(\mathbf{r} + \mathbf{T})$  is better understood when expanded in Fourier series. Following [114] for a one-dimensional periodic function  $w(x)$  with period  $a$  in the direction of  $x$ , it is found that its sine and cosine Fourier expansion can be written like:

$$w(x) = w_0 + \sum_{p>0} [C_p \cos(2\pi px/a) + S_p \sin(2\pi px/a)], \quad (8)$$

where  $p$  are positive integers, and  $C_p$ ,  $S_p$  are real constants.

It must be noticed that the factor  $2\pi/a$  renders periodic the function  $w(\mathbf{x})$  with period  $a$ . Similarly, it shall be noticed that  $2\pi p/a$  is a point in the **reciprocal lattice** or Fourier space of the material<sup>5</sup>. A term or point is allowed if it is consistent with the periodicity of the material.

Equation (8) can be simplified into:

$$w(x) = \sum_p w_p e^{i2\pi px/a},$$

where the sum extends over all integers ( $p \in \mathbb{Z}$ ) and  $w_p$  is a complex coefficient. The extension to three dimensions of this last expression follows:

$$w(\mathbf{r}) = \sum_{\mathbf{G}} w_{\mathbf{G}} e^{i\mathbf{G}\cdot\mathbf{r}}, \quad (9)$$

---

<sup>5</sup>In one dimension, these points lie on a line.

where the set of vectors  $\mathbf{G}$  leaves the equation invariant under  $\mathbf{T}$ . These vectors are called the **reciprocal lattice vectors**.

### 1.3 The reciprocal space

The points in the reciprocal lattice can be defined by the set of vectors

$$\mathbf{G} = m_1\mathbf{b}_1 + m_2\mathbf{b}_2 + m_3\mathbf{b}_3,$$

where  $m_i \in \mathbb{Z}$  and the basis vectors  $\mathbf{b}_i$  are **primitive vectors of the reciprocal lattice**, with  $i = 1, 2, 3$ . A vector  $\mathbf{G}$  of this form is a reciprocal lattice vector and must keep the invariance of equation (9) under translations  $\mathbf{T} = n_1\mathbf{a}_1 + n_2\mathbf{a}_2 + n_3\mathbf{a}_3$ :

$$w(\mathbf{r} + \mathbf{T}) = \sum_{\mathbf{G}} w_{\mathbf{G}} e^{i\mathbf{G}\cdot\mathbf{r}} e^{i\mathbf{G}\cdot\mathbf{T}} = w(\mathbf{r}) \implies e^{i\mathbf{G}\cdot\mathbf{T}} = 1.$$

To ensure the invariance, we construct the axis vectors  $\mathbf{b}_i$  of the reciprocal lattice using the expressions:

$$\mathbf{b}_1 = 2\pi \frac{\mathbf{a}_2 \times \mathbf{a}_3}{\mathbf{a}_1 \cdot \mathbf{a}_2 \times \mathbf{a}_3}, \quad \mathbf{b}_2 = 2\pi \frac{\mathbf{a}_3 \times \mathbf{a}_1}{\mathbf{a}_1 \cdot \mathbf{a}_2 \times \mathbf{a}_3}, \quad \mathbf{b}_3 = 2\pi \frac{\mathbf{a}_1 \times \mathbf{a}_2}{\mathbf{a}_1 \cdot \mathbf{a}_2 \times \mathbf{a}_3}. \quad (10)$$

It shall be observed that  $\mathbf{a}_1$ ,  $\mathbf{a}_2$  and  $\mathbf{a}_3$  are primitive vectors of the material lattice (physical space) while  $\mathbf{b}_1$ ,  $\mathbf{b}_2$  and  $\mathbf{b}_3$  are primitive vectors of the reciprocal lattice (reciprocal space). They have the property

$$\mathbf{b}_i \cdot \mathbf{a}_j = 2\pi\delta_{ij} \quad \text{with} \quad \begin{aligned} \delta_{ij} &= 1 \text{ for } i = j, \\ \delta_{ij} &= 0 \text{ for } i \neq j. \end{aligned}$$

From the above it is now evident that every material implicitly has two lattices: a material (direct) and a reciprocal lattice. Vectors in the direct lattice have dimensions of [length] while vectors in the reciprocal lattice have dimensions of [1/length], i.e., they have the units of wavelength and wavevector, respectively.

It has been shown that the reciprocal lattice is a lattice in the Fourier space representation of the material. It is also observed that wavevectors  $\mathbf{k}$  are always represented in a general Fourier space and where every point in that space describes a wave [114]. There is a special phenomenon associated to waves defined by the set of vectors  $\mathbf{G}$ , which is known as the diffraction condition as will be discussed next.

## 1.4 The diffraction condition

Consider the diffraction of an elastic wave of wavevector  $\mathbf{k}$  by a volume element  $dV$  of a PM. The diffracted wave will have an outgoing wavevector  $\mathbf{k}'$  with a phase difference and amplitude  $A_d$  (see Figure 3).

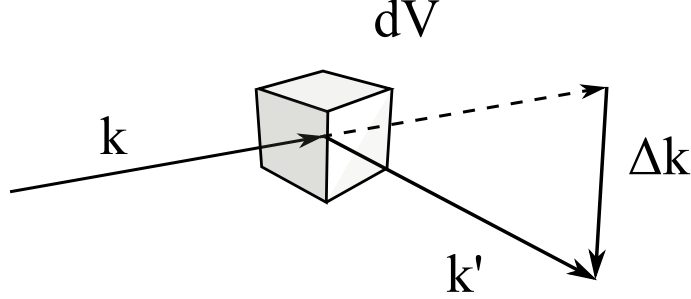


Figure 3: Diffraction of a plane wave by a volume element  $dV$  in which  $\mathbf{k} + \Delta\mathbf{k} = \mathbf{k}'$ .

It can be assumed that the amplitude  $A_d$  is proportional to the local properties [114] (density  $\rho$ , Young's Modulus  $E$  and Poisson's ratio  $\nu$ ). Since these properties also have the periodicity of the lattice, the proportionality results in a periodic function having the form (see (9)):

$$w(\mathbf{r}) = \sum_{\mathbf{G}} w_{\mathbf{G}} e^{i\mathbf{G}\cdot\mathbf{r}}.$$

The total amplitude  $A_d$  of the diffracted wave in the direction of  $\mathbf{k}'$  is proportional to the integral over the PM of  $w(\mathbf{r})dV$  times the phase factor  $e^{i(\mathbf{k}-\mathbf{k}')\cdot\mathbf{r}}$ . Then,

$$A_d = \int e^{i(\mathbf{k}-\mathbf{k}')\cdot\mathbf{r}} w(\mathbf{r}) dV \equiv \int e^{-i\Delta\mathbf{k}\cdot\mathbf{r}} w(\mathbf{r}) dV,$$

where  $\mathbf{k} - \mathbf{k}' = -\Delta\mathbf{k}$  and  $\Delta\mathbf{k}$  measures the change in the wavevector when the wave is diffracted, i.e., a phase factor. Replacing for the Fourier components of  $w(\mathbf{r})$  (Eq.(9)), the diffraction amplitude becomes:

$$A_d = \int e^{-i\Delta\mathbf{k}\cdot\mathbf{r}} \sum_{\mathbf{G}} w_{\mathbf{G}} e^{i\mathbf{G}\cdot\mathbf{r}} dV \equiv \sum_{\mathbf{G}} \int w_{\mathbf{G}} e^{i(\mathbf{G}-\Delta\mathbf{k})\cdot\mathbf{r}} dV,$$

If the phase difference  $\Delta\mathbf{k}$  is equal to a particular reciprocal vector  $\mathbf{G}$ , i. e.,

$$\Delta\mathbf{k} = \mathbf{G}, \quad (11)$$

the argument of the exponential vanishes and the integral is equal to  $Vw_{\mathbf{G}}$ . Also, if  $\Delta\mathbf{k}$  differs significantly from  $\mathbf{G}$ ,  $A_d$  is negligibly small which means that diffraction is highly influenced by the periodicity of the material and it is interesting to identify which vectors satisfy this requirement. To this aim, it is convenient to write the expression given in (11) like:

$$\begin{aligned} \mathbf{k} + \mathbf{G} &= \mathbf{k}', \\ (\mathbf{k} + \mathbf{G})^2 &= k'^2. \end{aligned}$$

On the other hand, since we are considering elastic scattering, the energy of the incident wave is the same as that in the outgoing wave, in other terms: the angular frequencies must be the same  $\omega = \omega'$ . From relation  $\omega = c|\mathbf{k}|$ , where  $c$  is a wave velocity, it follows that  $|\mathbf{k}| = |\mathbf{k}'|$ . Substituting the above in the last expression gives the well known **diffraction condition**:

$$2\mathbf{k} \cdot \mathbf{G} + G^2 = 0. \quad (12)$$

Since both  $\mathbf{G}$  and  $-\mathbf{G}$  are reciprocal lattice vectors, the result can also be written like:

$$2\mathbf{k} \cdot \mathbf{G} = G^2,$$

where one of the vectors satisfying the condition is recognized to be:

$$\mathbf{k} = \pm \frac{1}{2}\mathbf{G}.$$

This phenomenon is maximized when  $\Delta\mathbf{k} = \mathbf{G}$ , where the diffracted beams are the result of a constructive interference<sup>6</sup>. From the superposition of two plane sine waves with the same wavelength, it is clear that:

$$\begin{aligned} u(\mathbf{r}) &= A_1 \sin(\mathbf{k} \cdot \mathbf{r}) + A_2 \sin(\mathbf{k} \cdot \mathbf{r} + \varphi), \\ &= [A_1 + A_2] \cos(\varphi/2) \sin(\mathbf{k} \cdot \mathbf{r} + \varphi/2), \end{aligned}$$

---

<sup>6</sup>Diffraction phenomenon is described as the interference of waves according to the Huygens-Fresnel principle [116].

which gives a wave whose amplitude depends on the phase  $\varphi$ . When the two waves are in phase ( $\varphi = 0$ ), they interfere constructively; when the waves have opposite phase ( $\varphi = \pi$ ), they interfere destructively. For an incident wave vector of the form  $\mathbf{k} = \pm 1/2\mathbf{G}$ , the periodicity always causes a constructive interference, i.e., waves add in phase and yield the maximum amplitude for  $A_d$ .

## 1.5 First Brillouin zone

A Brillouin zone is said to be a vivid geometrical interpretation of the diffraction condition  $2\mathbf{k} \cdot \mathbf{G} = G^2$  [114] and it can be constructed as follows. Divide both sides by 4 gives <sup>7</sup>

$$\mathbf{k} \cdot \frac{1}{2}\mathbf{G} = \left(\frac{1}{2}G\right)^2. \quad (13)$$

and select a vector  $\mathbf{G}$  from the origin to a reciprocal lattice point. Then construct a plane normal to the vector  $\mathbf{G}$  at its midpoint. The resulting plane forms a part of a boundary zone as shown in Figure 4. The wave vectors  $\mathbf{k}$  having the magnitude and direction required by (13) will be diffracted. It may be observed that this Brillouin construction encloses all such vectors, i.e., they go from the origin to any point along the constructed plane.

---

<sup>7</sup>Notice that geometrically, we are working in the reciprocal space.

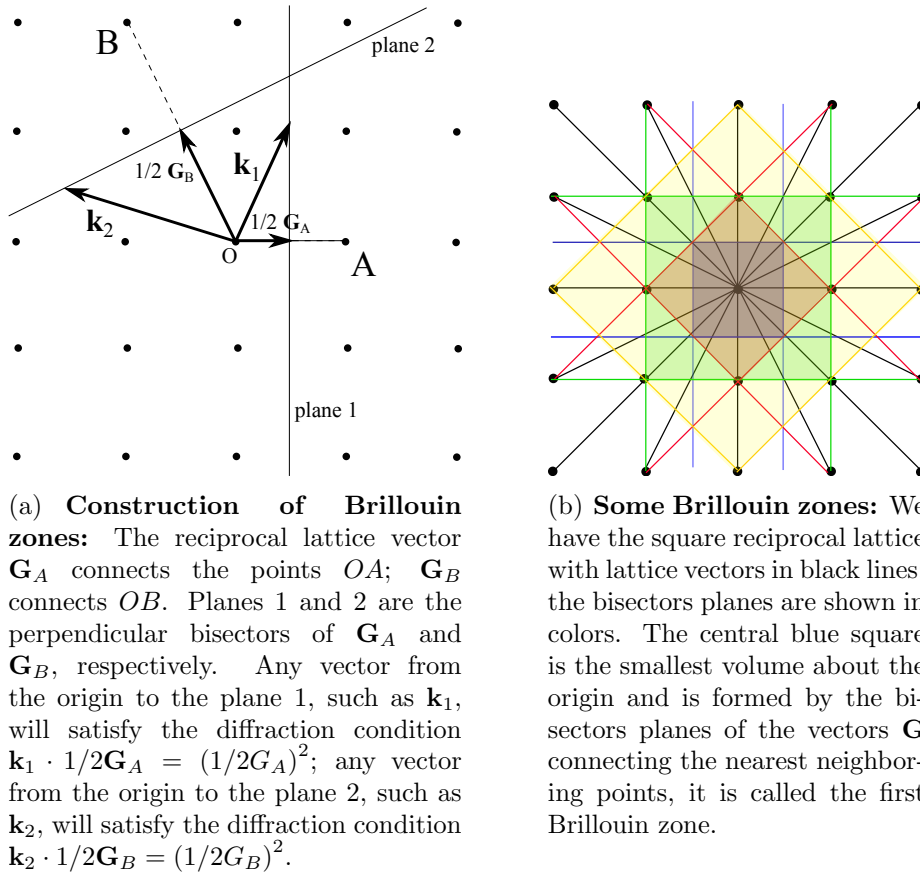


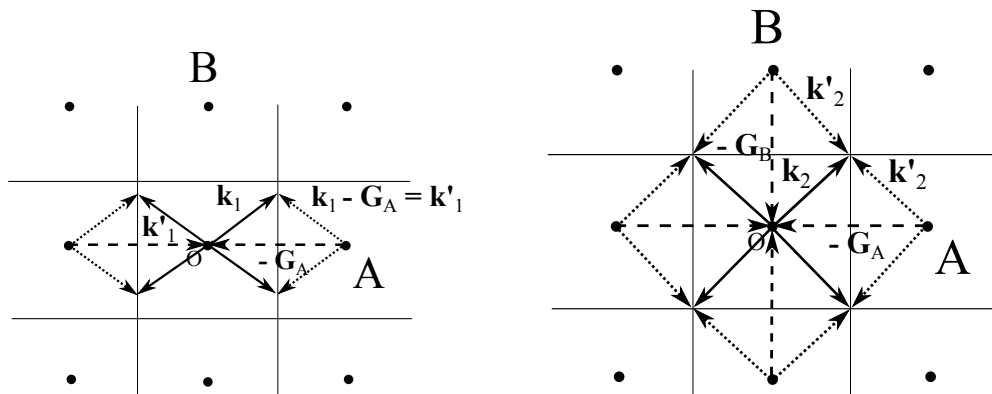
Figure 4: Definition and construction of the first Brillouin zone.

From (11)<sup>8</sup> it is known that  $\mathbf{k} + \Delta\mathbf{k} = \mathbf{k}'$  and  $\Delta\mathbf{k} = -\mathbf{G}$  which means that diffracted beams will be in the direction of  $\mathbf{k} - \mathbf{G}$ . In Figure 5 it is shown that a special geometric condition for all the diffracted beams corresponds to an incident wave generating a diffracted wave with direction  $\mathbf{k} - \mathbf{G}$ . Similarly, this last wave generates another diffracted wave and so on (all of them with the same magnitude).

A wave vector  $\mathbf{k}$  drawn from the origin  $O$  to any corner will satisfy the diffraction condition for both  $\mathbf{G}_A$  and  $\mathbf{G}_B$ , thus, this wave generates two diffracted waves with opposite directions that will act as new incident waves. As a result, the wave that points to a corner generates diffracted waves that point to the opposite corners. Such a feature will lead to a key concept in periodic materials as is the existence of **band**

<sup>8</sup>Both  $\mathbf{G}$  and  $-\mathbf{G}$  satisfy the diffraction condition.

gaps due to the formation of standing waves.



(a) Diffraction of a wave vector  $\mathbf{k}_1$ . The diffracted wave will be in the direction of  $\mathbf{k}_1 - \mathbf{G}_A$  like a mirror image, this last wave act as a new incident wave and generate another one in the direction of  $\mathbf{k}_1$ . This process continues infinite times.

(b) Diffraction of a wave vector  $\mathbf{k}_2$  that points to a corner of the first Brillouin zone. This wave generate diffracted waves that point in the direction of the rest of the corners, i.e., waves travelling in opposite directions.

Figure 5: Direction of diffracted waves for the first Brillouin zone.

The set of planes that are perpendicular bisectors of the reciprocal lattice vectors divide the Fourier space into fragments, as shown in Figure 4. The central square is a primitive cell of the reciprocal lattice, called the **first Brillouin zone** and it is the smallest volume entirely enclosed by the bisectors planes.

It must be recalled that the reciprocal lattice space contains the information of the material periodicity: the set of vectors  $\mathbf{G}$  render invariant any periodic function under translations  $\mathbf{T}$ . Considering again Bloch-Floquet's theorem from equation (2), and increasing the wave vector  $\mathbf{k}$  by a factor  $p$  times  $\mathbf{G}$ , i.e.,  $\mathbf{k} + p\mathbf{G}$  with  $p$  an integer, gives:

$$\begin{aligned} u(\mathbf{r}) &= w(\mathbf{r})e^{i(\mathbf{k}+p\mathbf{G})\cdot\mathbf{r}}, \\ &= w(\mathbf{r} + \mathbf{T})e^{i(\mathbf{k}+p\mathbf{G})\cdot\mathbf{r}}, \end{aligned}$$

after using  $w(\mathbf{r} + \mathbf{T})$ . From equation (9) it follows that:

$$\begin{aligned}
u(\mathbf{r}) &= \sum_{\mathbf{G}} w_{\mathbf{G}} e^{i\mathbf{G}\cdot(\mathbf{r}+\mathbf{T})} e^{i(\mathbf{k}+p\mathbf{G})\cdot\mathbf{r}}, \\
&= \sum_{\mathbf{G}} w_{\mathbf{G}} e^{i\mathbf{G}\cdot\mathbf{r}} e^{i\mathbf{G}\cdot\mathbf{T}} e^{i\mathbf{k}\cdot\mathbf{r}} e^{ip\mathbf{G}\cdot\mathbf{r}}, \\
&= \sum_{\mathbf{G}} w_{\mathbf{G}} e^{ip\mathbf{G}\cdot\mathbf{r}} e^{i\mathbf{G}\cdot\mathbf{T}} e^{i\mathbf{k}\cdot\mathbf{r}}, \\
&= \sum_{\mathbf{G}} w_{\mathbf{G}} e^{ip\mathbf{G}\cdot(\mathbf{r}+\mathbf{T})} e^{i\mathbf{k}\cdot\mathbf{r}},
\end{aligned}$$

where the property  $\mathbf{b}_i \cdot \mathbf{a}_j = 2\pi\delta_{ij}$  (with  $i, j = 1, 2, 3$ ) in the term  $e^{ip\mathbf{G}\cdot\mathbf{T}}$ , yields:

$$\begin{aligned}
e^{ip\mathbf{G}\cdot\mathbf{T}} &= e^{[ip(m_1\mathbf{b}_1+m_2\mathbf{b}_2+m_3\mathbf{b}_3)\cdot(n_1\mathbf{a}_1+n_2\mathbf{a}_2+n_3\mathbf{a}_3)]}, \\
&= e^{[i2\pi p(m_1n_1+m_2n_2+m_3n_3)]}, \\
&= 1.
\end{aligned}$$

The argument of the exponential contains the term  $2\pi$  times an integer  $p$  because  $m_1n_1 + m_2n_2 + m_3n_3$  is also an integer. Thus, increasing the wave vector by a factor of  $p\mathbf{G}$  means a translation of  $2\pi p$  in the reciprocal lattice space and then, the initial expression  $u(\mathbf{r})$  remains invariant. It can be said that the information in  $\mathbf{k} + p\mathbf{G}$  is redundant, therefore, it is only necessary to consider the values of  $\mathbf{k}$  in the interval of  $[0, 2\pi]$  in all directions. The region enclosed by the interval will be defined around one node of the reciprocal lattice space where the origin is defined, this means that the **first Brillouin zone** fills the whole region of analysis: all the wave vectors  $\mathbf{k}$  are considered in this zone. The primitive cell contains the information of the whole lattice and the other Brillouin zones have redundant information.

A related concept is that of the **Irreducible Brillouin Zone** (IBZ), which is the first Brillouin zone reduced by all of the symmetries in the point group of the lattice. Figure 6 shows the irreducible Brillouin zone for a square lattice.

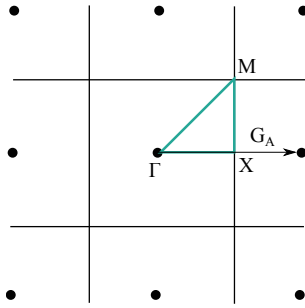


Figure 6: The irreducible Brillouin zone for a square lattice. The triangle  $\Gamma - X - M$  can describe completely the first Brillouin zone using symmetry operations.

## 1.6 The band structure

In a dispersive material (i.e., when the wave propagation velocity depends upon frequency) the **dispersion relation**  $\omega = c|\mathbf{k}|$  is no longer linear. This requires the distinction between two quantities: **phase velocity** and **group velocity**. The **phase velocity**  $c_p$  is the velocity at which the phase of the wave (of any frequency component) propagates in the space. It is defined as

$$\mathbf{c}_p = \frac{\omega}{|\mathbf{k}|} \hat{\mathbf{k}}. \quad (14)$$

The **group velocity**, on the other hand, is the velocity of propagation of the envelope of a wave package. It is defined by the relation:

$$\mathbf{c}_g = \nabla_{\mathbf{k}} \omega, \quad (15)$$

where  $\nabla_{\mathbf{k}}$  is the gradient of the angular frequency  $\omega$  when written as a function of the wave vector  $\mathbf{k}$ , and  $\hat{\mathbf{k}}$  is the unit vector in direction of  $\mathbf{k}$ . The group velocity is often thought of as the velocity at which wave energy or information is transported. In most cases this is accurate, however, if the wave is travelling through a dissipative medium, the group velocity ceases to have a clear physical meaning, [117]. Figure 7 taken from [113], illustrates the distinction between a dispersive and a non-dispersive medium.

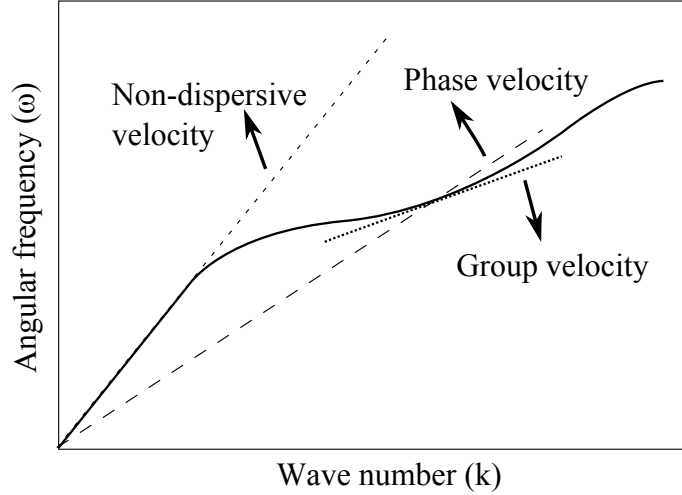


Figure 7: Dispersion relation for a dispersive medium. The black solid line represent the dispersion curve, the phase velocity is the slope of the secant cutting the curve and the group velocity is the slope of the tangent in that cutting point.

The dispersion relation is also known as the **band structure** of a material as it describes the behavior of waves in terms of frequency bands. Among the methods to determine the band structure of complex systems one can identify wave expansions, finite difference time domain methods, finite element methods, multiple scattering theory, Rayleigh multipole and Green’s function methods (see [118]). Most of them cast the problem in the form of a generalized eigenvalue problem of the form:

$$[\mathbf{K}(\mathbf{k}) - \omega^2 \mathbf{M}] \mathbf{u} = 0, \quad (16)$$

and where  $\mathbf{K}$  and  $\mathbf{M}$  are matrices containing information about the geometry and material parameters and  $\mathbf{u}$  is the vector of degrees of freedom in the system. The band structure is found after finding the eigenfrequencies associated to the wave vectors  $\mathbf{k}$  along the borders of an irreducible Brillouin zone. .

As discussed earlier, the diffraction condition<sup>9</sup> affects the dispersion relation of a PM causing the formation of standing waves and the appearance of band gaps. Moreover, at Bragg’s diffraction wavelike solutions do not exist [114].

---

<sup>9</sup>Usually called Bragg’s diffraction and considered to be a special feature of wave propagation in periodic materials.

The diffraction condition,  $(\mathbf{k} + \mathbf{G})^2 = k^2$ , for a wave vector  $\mathbf{k}$  in one-dimensional space becomes:

$$k = \pm \frac{1}{2}G = \pm q \frac{\pi}{a},$$

where  $G = 2\pi q/a$  is a reciprocal lattice vector and  $q$  is an integer. The first diffraction (and the first energy gap) occurs at  $k = \pm\pi/a$ , which in the wave vector space belongs to the region between  $[-\pi/a, \pi/a]$  and thus, to the **first Brillouin zone** of the 1D lattice. Other energy gaps occur for other values of the integer  $q$ .

As discussed previously, an incident wave vector  $\mathbf{k}$  satisfying the diffraction condition will trigger the diffraction of waves traveling in opposite directions. In the current case of a 1D-space, the wave functions at  $k = \pm q\pi/a$  are not traveling waves of the form  $e^{ikx}$  or  $e^{-ikx}$ , but at these special values of  $k$  the waves are composed of equal parts traveling to the right and left thus forming a standing wave.

The Bragg diffraction condition is satisfied by the wave vector  $k = \pm q\pi/a$ , therefore, in the 1D case a wave traveling to the right is Bragg-diffracted to travel to the left, and vice versa. Each subsequent Bragg diffraction will reverse the direction of the wave. A wave that travels neither to the right nor to the left is a standing non-propagating wave as explained next. From the two traveling waves:

$$e^{\pm i\pi x/a} = \cos\left(\frac{\pi x}{a}\right) \pm i \sin\left(\frac{\pi x}{a}\right),$$

two different standing waves are formed and given by:

$$\begin{aligned} u(+) &= e^{i\pi x/a} + e^{-i\pi x/a} = 2 \cos\left(\frac{\pi x}{a}\right), \\ u(-) &= e^{i\pi x/a} - e^{-i\pi x/a} = 2i \sin\left(\frac{\pi x}{a}\right). \end{aligned}$$

Both standing waves are composed of equal parts of right and left directed traveling waves.

The energy of a system defined by equation (16), depends upon  $\omega$  since the contributions to the potential and kinetic energy depend upon  $\omega$ :

$$\begin{aligned} E &= E_P + E_K, \\ &= \frac{1}{2}K(\omega)u^2(x) + \frac{1}{2}\omega^2 Mu^2(x), \end{aligned}$$

where  $\omega(k)$  indicates that the frequency is a function of  $k$ .

A band gap in the band structure corresponds to an energy gap and there is an energy gap when a wave vector  $\mathbf{k}$  satisfies the diffraction condition therefore, leading to the appearance of standing waves. The energy of the system when  $k = \pm\pi/a$  is given by:

$$E = E_P = \frac{1}{2}K(\omega)u^2.$$

and it is evident that it only depends upon the potential energy due to the non-propagating nature of the standing waves.

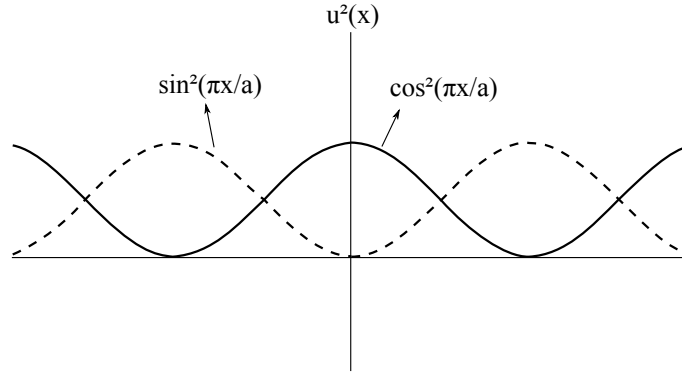


Figure 8: Distribution of  $u^2(x)$  in space.  $u(+)\propto\cos^2(\pi x/a)$  and  $u(-)\propto\sin^2(\pi x/a)$ .

Figure 8 shows the space distribution of  $u^2(x)$ . The energy of the system would be proportional to the envelope of this graph if  $K(\omega)$  were a constant. However, there is an energy difference between the standing waves since  $K(\omega)$  is also distributed in the space. That is, it contains the information of the material properties and then, the information of the material periodicity. The energy difference between the standing waves creates an energy gap  $E_g$  [114] given by:

$$E_g = \frac{1}{2}K(\omega)[u(+)-u(-)].$$

The wave functions at the boundary of the Brillouin zone  $k = \pi/a$ , normalized over unit length of line, are  $\sqrt{2}\cos(\pi x/a)$  and  $\sqrt{2}\sin(\pi x/a)$ . Assuming that  $K(\omega)$  is a periodic function of the form

$$K(\omega) = K\cos(2\pi x/a),$$

leads to an energy difference between the two standing wave given by:

$$\begin{aligned} E_g &= \int_0^1 \frac{1}{2} K \cos(2\pi x/a) [u^2(+)-u^2(-)] dx, \\ &= 2 \int_0^1 \frac{1}{2} K \cos(2\pi x/a) [\cos^2(\pi x/a) - \sin^2(\pi x/a)] dx, \end{aligned}$$

which after some manipulation<sup>10</sup> becomes:

$$E_g = 2 \int_0^1 \frac{1}{2} K \cos(2\pi x/a) [\cos^2(\pi x/a) - \sin^2(\pi x/a)] dx = \frac{1}{2} K.$$

It can be observed that the energy gap is equal to the Fourier component of the material properties.

## 1.7 Dispersion relations for one dimensional lattice models

In elastodynamics, many complex structures can be represented by simple lattice models described in terms of systems of masses and springs. This section discusses the response of two of such systems, one corresponding to a simple mass and spring (Figure 9) and the other with two different masses (Figure 11).

The period of the structure shown in Figure 9 is  $a$ , while the lumped masses and spring stiffness are  $m$  and  $K$  respectively. The displacement at the arbitrary location  $x_j$  is  $u_j$  and the unit cell is repeated infinitely.

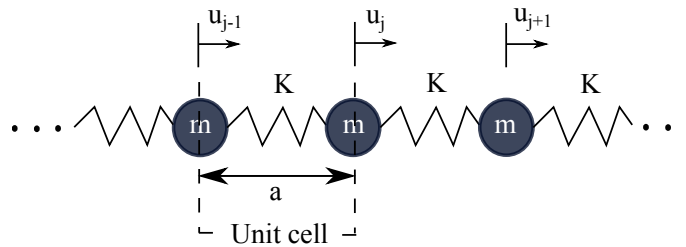


Figure 9: Simple mass-spring lattice.

Now, consider the motion for the  $j$ -th mass governed by:

---

<sup>10</sup>We have used the identity  $\cos^2(\theta) - \sin^2(\theta) = \cos(2\theta)$

$$K(u_{j+1} - u_j) - K(u_j - u_{j-1}) = m\ddot{u}_j.$$

If this motion is time harmonic with frequency  $\omega$ , it follows that:

$$K(u_{j+1} - u_j) - K(u_j - u_{j-1}) + m\omega^2 u_j = 0.$$

The Bloch-periodicity condition between consecutive masses reads:

$$u_{j-1} = u_j e^{-ika} \quad \text{and} \quad u_{j+1} = u_j e^{ika},$$

therefore

$$K u_j (2 - e^{ika} - e^{-ika}) - m\omega^2 u_j = 0.$$

On the other hand  $e^{ika} + e^{-ika} = 2 \cos(ka)$  and  $1 - \cos(ka) = 2 \sin^2(ka/2)$  which leads to:

$$\left[ \frac{4K}{m} \sin^2(ka/2) - \omega^2 \right] u_j = 0.$$

Since  $\omega > 0$ , it follows that for real values of  $k$  this equation has a nontrivial solution only if

$$\omega(k) = 2 \sqrt{\frac{K}{m}} |\sin(ka/2)| =: 2\omega_0 |\sin(ka/2)|, \quad (17)$$

with  $\omega_0 = \sqrt{\frac{K}{m}}$ . This is the dispersion relation for the structure (see Figure 10). It should be noticed that in the quasistatic limit  $k \rightarrow 0$ ,  $\sin(ka/2) = ka/2$  and  $\omega(k) = ka\sqrt{K/m}$ . The group velocity in this limit is  $d\omega/dk = a\sqrt{K/m}$ .

In the band diagram of Figure 10, frequency is a periodic function of  $k$  with period of  $2\pi/a$ . It is observed that the frequency is zero every time  $k$  becomes an integer multiple of  $2\pi/a$ . Thus, it is only necessary to consider just a small range of values of  $k$  in order to capture the response of the system for all  $k$ . The shaded region corresponds to the first Brillouin zone and contains the complete information of the system. At the boundaries of the first Brillouin zone it holds that  $\omega = 2\omega_0$  and the group velocity  $d\omega/dk$  becomes zero; standing waves are present for values of  $k$  which are odd integer multiples of  $\pi/a$ .

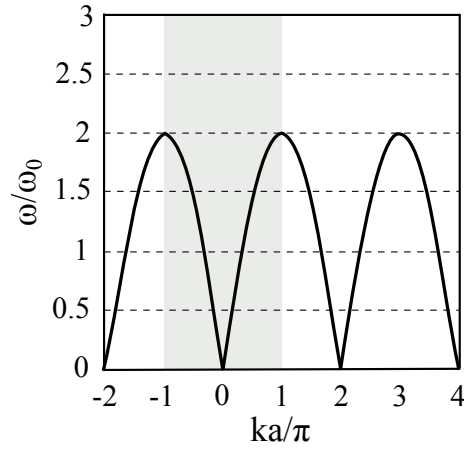


Figure 10: Dispersion curve for a simple mass-spring lattice. The shaded region corresponds to the first Brillouin zone. This eigenmode is called an acoustic mode because both  $\omega$  and  $k$  go to zero simultaneously for some values.

In this simple one-degree-of-freedom system, there is only one eigenmode (called the acoustic mode) and therefore only one branch in the band diagram because there is only one direction of wave propagation. More eigenmodes and branches can be observed after increasing the complexity in the model.

For instance, consider now a two-mass-system (Figure 11) with equations of motion given by:

$$\begin{aligned} K(2U_j - u_j - u_{j+1}) - \omega^2 M U_j &= 0, \\ K(2u_j - U_{j-1} - U_j) - \omega^2 m u_j &= 0. \end{aligned}$$

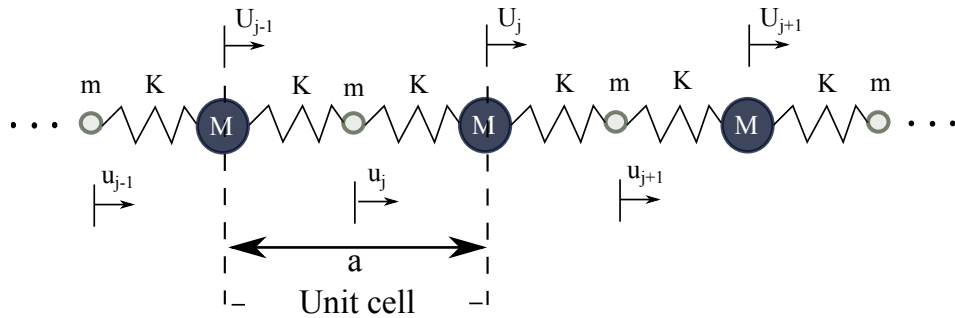


Figure 11: Mass-spring lattice with two species of masses.

Using the Bloch-periodicity condition

$$u_{j+1} = u_j e^{ika} \quad \text{and} \quad U_{j-1} = U_j e^{-ika},$$

yields,

$$\begin{aligned} K [2U_j - u_j(1 + e^{ika})] - \omega^2 M U_j &= 0, \\ K [2u_j - U_j(1 + e^{-ika})] - \omega^2 m u_j &= 0; \end{aligned}$$

or using the matrix form  $(\bar{\mathbf{K}} - \omega^2 \bar{\mathbf{M}})\bar{\mathbf{u}} = \bar{\mathbf{0}}$  as

$$\begin{bmatrix} 2K - \omega^2 M & -K(1 + e^{ika}) \\ -K(1 + e^{-ika}) & 2K - \omega^2 m \end{bmatrix} \begin{bmatrix} U_j \\ u_j \end{bmatrix} = \begin{bmatrix} 0 \\ 0 \end{bmatrix}.$$

The resultant eigenvalue problem has a nontrivial solution if  $\det(\bar{\mathbf{K}} - \omega^2 \bar{\mathbf{M}}) = 0$  or equivalently if:

$$mM\omega^4 - 2K(m + M)\omega^2 + 4K^2 \sin^2(ka/2) = 0.$$

It can be shown that positive eigenvalues correspond to:

$$\omega(k) = \left[ K \frac{m + M}{mM} \pm \frac{K}{mM} \sqrt{m^2 + M^2 + 2mM \cos(ka)} \right]^{1/2},$$

and the dispersion relation is shown in Figure 12. Notice that there is now one extra mode called the optical mode. At  $k = 0$ , the group velocity of the optical mode is zero and standing waves exist. This time we obtain a frequency band gap that depends upon the difference between  $m$  and  $M$ ; high contrast composites are more likely to exhibit band gaps.

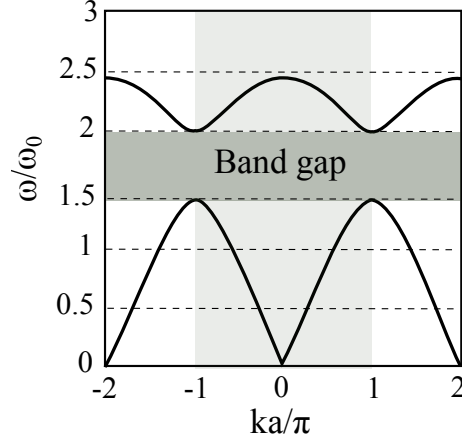


Figure 12: Dispersion relation for a mass-spring lattice with two species of masses.

## 2 Bloch-periodicity in the Finite Element Method

The total potential energy functional of the system corresponding to equations (5)-(7) is given by (see [113]):

$$\Pi(\omega) = \int_{\Omega} \epsilon_{rs}^*(\mathbf{r}) C_{rskl}(\mathbf{r}) \epsilon_{kl}(\mathbf{r}) d\Omega - \omega^2 \int_{\Omega} \rho(\mathbf{r}) u_r^*(\mathbf{r}) u_r(\mathbf{r}) d\Omega - \int_{\Gamma} u_r^*(\mathbf{r}) t_r(\mathbf{r}) d\Gamma,$$

where the Einstein summation convention is implicit in the index notation and the complex conjugate is denoted by \*. In the above expression the last term on the right corresponds to the work of the external traction and it implicitly contains the corresponding Bloch-periodicity conditions. After using standard finite element discretization ideas over the variational equation associated to  $\Pi$ , yields the following direct formulation:

$$[\mathbf{K} - \omega^2 \mathbf{M}] \mathbf{u} = \mathbf{f}.$$

In the above, the Bloch-periodicity conditions can be expressed through relations between the degrees of freedom (DOF) of opposite boundaries for the primitive cell of the PM.

Figure 13 shows the primitive cell with the nodal DOF corresponding to boundary and domain nodes.

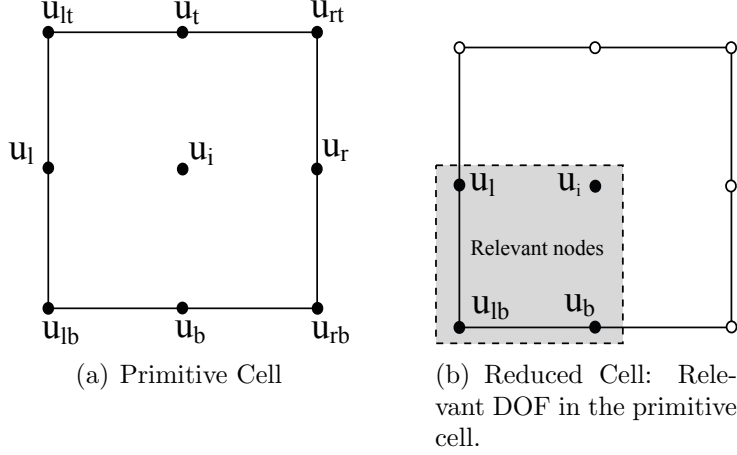


Figure 13: Primitive cell of finite elements. In the perimeter nodes, the subindex  $\mathbf{b}$  denotes bottom,  $\mathbf{t}$ =top,  $\mathbf{r}$ =right and  $\mathbf{l}$ =left. The domain nodes not in the perimeter are denoted as  $\mathbf{i}$ =internal.

In the discretized domain, all of the elements will lie completely within the primitive cell and all boundary nodes will lie on the perimeter of the primitive cell. On the other hand, there is no energy associated with  $\mathbf{M}$  or  $\mathbf{K}$  belonging to a neighboring primitive cell. However, there are extra degrees of freedom in  $\mathbf{u}$  since the nodal DOF at the top and right boundaries of the primitive cell belong to neighboring primitive cells. For plane waves, the Bloch-periodicity conditions translate into a reduction of these nodal DOF. In the particular case of the primitive cell shown in Figure 13, the system of equations correspond to the vectors:

$$\mathbf{u} = [u_l \quad u_r \quad u_b \quad u_t \quad u_{lb} \quad u_{rb} \quad u_{lt} \quad u_{rt} \quad u_i]^T,$$

$$\mathbf{f} = [f_l \quad f_r \quad f_b \quad f_t \quad f_{lb} \quad f_{rb} \quad f_{lt} \quad f_{rt} \quad f_i]^T.$$

From Bloch-Floquet's theorem it follows that:

$$\begin{aligned} u_r &= u_l e^{ik_x T_x}, & u_t &= u_b e^{ik_y T_y}, \\ u_{rb} &= u_{lb} e^{ik_x T_x}, & u_{lt} &= u_{lb} e^{ik_y T_y}, \\ u_{rt} &= u_{lb} e^{i(k_x T_x + k_y T_y)}, \end{aligned}$$

where  $(k_x, k_y)$  are the wave vector components and  $T_x$  and  $T_y$  are the translation vector components. Notice that the terms  $\mathbf{k} \cdot \mathbf{T}$  correspond to a phase shift in every

direction  $x$  and  $y$ .

The above relations can be expressed in matrix form as

$$\underbrace{\begin{bmatrix} u_l \\ u_r \\ u_b \\ u_t \\ u_{lb} \\ u_{rb} \\ u_{lt} \\ u_{rt} \\ u_i \end{bmatrix}}_{\mathbf{u}} = \underbrace{\begin{bmatrix} I_l & 0 & 0 & 0 \\ I_l e^{ik_x T_x} & 0 & 0 & 0 \\ 0 & I_b & 0 & 0 \\ 0 & I_b e^{ik_y T_y} & 0 & 0 \\ 0 & 0 & I_{lb} & 0 \\ 0 & 0 & I_{lb} e^{ik_x T_x} & 0 \\ 0 & 0 & I_{lb} e^{ik_y T_y} & 0 \\ 0 & 0 & I_{lb} e^{i(k_x T_x + k_y T_y)} & 0 \\ 0 & 0 & 0 & I_i \end{bmatrix}}_{\mathbf{A}} \underbrace{\begin{bmatrix} u_l \\ u_b \\ u_{lb} \\ u_i \end{bmatrix}}_{\mathbf{u}_R},$$

where  $I$  are identity matrices with subindex  $l$  and  $b$  denoting the boundary. Similarly, considering the equilibrium conditions

$$\begin{aligned} f_r + f_l e^{ik_x T_x} &= 0, & f_t + f_b e^{ik_y T_y} &= 0, \\ f_{rt} + f_{rb} e^{ik_x T_x} + f_{lt} e^{ik_y T_y} + f_{lb} e^{i(k_x T_x + k_y T_y)} &= 0, \end{aligned}$$

or using its matrix form:

$$\underbrace{\begin{bmatrix} 0 \\ 0 \\ 0 \\ f_i \end{bmatrix}}_{\mathbf{f}_R} = \underbrace{\begin{bmatrix} I_l & I_l e^{-ik_x T_x} & 0 & 0 & 0 & 0 & 0 & 0 & 0 \\ 0 & 0 & I_b & I_b e^{-ik_y T_y} & 0 & 0 & 0 & 0 & 0 \\ 0 & 0 & 0 & 0 & I_{lb} & I_{lb} e^{-ik_x T_x} & I_{lb} e^{-ik_y T_y} & I_{lb} e^{-i(k_x T_x + k_y T_y)} & 0 \\ 0 & 0 & 0 & 0 & 0 & 0 & 0 & 0 & I_i \end{bmatrix}}_{\mathbf{A}^H} \underbrace{\begin{bmatrix} f_l \\ f_r \\ f_b \\ f_t \\ f_{lb} \\ f_{rb} \\ f_{lt} \\ f_{rt} \\ f_i \end{bmatrix}}_{\mathbf{f}},$$

where  $\mathbf{A}^H$  is the Hermitian transpose of  $\mathbf{A}$ .

The direct formulation of the problem can be written in compact form as:

$$\left[ \underbrace{\mathbf{A}^H \mathbf{K} \mathbf{A}}_{\mathbf{K}_R} - \omega^2 \underbrace{\mathbf{A}^H \mathbf{M} \mathbf{A}}_{\mathbf{M}_R} \right] \mathbf{u}_R = \mathbf{f}_R,$$

and after neglecting the body forces  $\mathbf{f}_R$  as the reduced system

$$\mathbf{K}_R \mathbf{u}_R = \omega^2 \mathbf{M}_R \mathbf{u}_R.$$

## 2.1 Implementation

A finite element implementation of the Bloch-analysis formulation can be developed following [113] through:

- A modification of the connectivity and also of the shape functions of the finite element method.
- An assembly of the mass and stiffness matrices without the boundary conditions and then, using elementary row/column operations to impose the boundary conditions.

In this work we have used the multi-point constraints tool (MPCs) from the commercial finite element code Abaqus in order to impose Bloch-periodicity conditions

### 2.1.1 Code for Abaqus input files

The used computer code writes the input files for the implementation of Bloch-periodicity conditions in Abaqus . The conditions are imposed through the multi-point constraint equation that describes a linear constraint between individual DOF. The equation used by Abaqus is

$$A_1 u_1^P + A_2 u_2^Q + \dots + A_k u_k^S = 0,$$

where the subindex  $k$  =integer, represents the component of the solution vector  $\mathbf{u}$ ;  $A$  is the amplitude and  $P$  the selected point or node, i.e,  $A_1 u_1^P$  represents the amplitude times the solution for the component 1 of the  $P$ -node. The Abaqus command line reads

*\*EQUATION*  
*Number of terms in the equation*

*Node, Component, Amplitude, Node, Component, Amplitude, ...*

A particular case could be given by

*\*EQUATION*

3

3, 1, 1, 45, 1,  $-\cos(k_x)$ , 128, 1,  $-\sin(k_x)$

that belongs to the equation

$$u_1^3 - \cos(k_x)u_1^{45} - \sin(k_y)u_1^{128} = 0.$$

The implemented code works for 2D rectangular cells and uses a rectangular window for the sampling of the wave vector space. This is a grid of  $S_x \times S_y$  data points in direction of the Cartesian coordinates  $x$  and  $y$ . The pseudo codes are described in [1](#) and [2<sup>11</sup>](#).

---

<sup>11</sup>It is important to state that the method requires to duplicate the mesh to consider the imaginary part, in this sense, the phase shift in the Bloch conditions is assigned to the solution using Euler's equation:

$$e^{\pm i\theta} = \cos(\theta) \pm i \sin(\theta).$$

---

**Algorithm 1:** Creates Abaqus input files with Bloch-periodicity conditions through MPCs.

---

**Input :**

Mesh: Nodes, Elements, Material Sets  
# Eigenvalues  
Element Type  
Material Properties  
Wave vector space sampling  $S_x, S_y$ .

**Output:**

$S_x \times S_y$  input files with Bloch-BC through MPCs.

```
/* Rectangular window of the wave vector space */
1  $k_x \leftarrow \text{linspace}(-\pi, \pi, S_x)$ ;
2  $k_y \leftarrow \text{linspace}(-\pi, \pi, S_y)$ ;
3  $[k_x, k_y] \leftarrow \text{Meshgrid}(k_x, k_y)$ ;

/* Phase assignment for every  $k$  */
4  $Ckx \leftarrow \cos(k_x)$ ;  $Skx \leftarrow \sin(k_x)$ ;
5  $Cky \leftarrow \cos(k_y)$ ;  $Sky \leftarrow \sin(k_y)$ ;
6  $Ckxky \leftarrow \cos(k_x + k_y)$ ;  $Skxky \leftarrow \sin(k_x + k_y)$ ;

/* Identical mesh for the imaginary part */
7  $RNodes \leftarrow Nodes$ ;
8  $RElmts \leftarrow Elmts$ ;
9  $[INodes, IElmts] = \text{CopyMesh}(RNodes, RElmts)$ ;
10  $Nodes \leftarrow [RNodes; INodes]$ ;
11  $Elmts \leftarrow [RElmts; IElmts]$ ;

/* Bloch-periodicity conditions */
12 Bloch-BC( $Nodes, Phases$ );
```

---

---

**Algorithm 2:** Function to impose Bloch-periodicity conditions through MPCs.

---

```

1 Bloch-BC(Nodes, Phases);

   /* Perimeter nodes in the real and imaginary meshes */
2 Rre; RIm; /* Right */
3 Lre; LIm; /* Left */
4 Tre; TIm; /* Top */
5 Bre; BIm; /* Bottom */
6 LTre; LTIm; /* LeftTop */
7 RTre; RTIm; /* RightTop */
8 LBre; LBIm; /* LeftBottom */
9 RBre; RBIm; /* RightBottom */
10 for  $i = 1 : S_x \times S_y$  do
11   print('EQUATION');
   /* The following procedure will also apply for bottom and top
      nodes with the respective phases */
12   for  $j = 1 : \#LeftNodes$  do
   /* Real part */
13   print('3');
14   print('Rre(j),1,1,Lre(j),1,-Ckx(i),Lim(j),1,-Skx(i)');
15   print('Rre(j),2,1,Lre(j),2,-Ckx(i),Lim(j),2,-Skx(i)');
   /* Imaginary part */
16   print('3');
17   print('Rim(j),1,1,Lim(j),1,-Ckx(i),Lre(j),1,-Skx(i)');
18   print('Rim(j),2,1,Lim(j),2,-Ckx(i),Lre(j),2,-Skx(i)');
19   end
   /* Corner points: same procedure for LT and RB with the
      respective phases */
   /* Real part */
20   print('3');
21   print('RTre(j),1,1,LBre(j),1,-Ckxky(i),LBim(j),1,-Skxky(i)');
22   print('RTre(j),2,1,LBre(j),2,-Ckxky(i),LBim(j),2,-Skxky(i)');
   /* Imaginary part */
23   print('3');
24   print('RTim(j),1,1,LBim(j),1,-Ckxky(i),LBre(j),1,-Skxky(i)');
25   print('RTim(j),2,1,LBim(j),2,-Ckxky(i),LBre(j),2,-Skxky(i)');
26 end

```

---

## 2.2 Construction of the band structure

The determination of the band structure of a PM, requires the solution of an eigenvalue problem for every  $\mathbf{k}$ -point in the wave vector space. The required number of eigenvalues is approximately fixed by the desired number of curves in the dispersion relation.

The band structure is constructed for the wave vector values along the borders of the IBZ. The complete dispersion relation depends upon the cell dimension, i.e., for a 2D cell the wave vector will have two components,  $k_x$  and  $k_y$  in Cartesian coordinates, then, the complete dispersion relation  $\omega(k_x, k_y)$  will be formed by surfaces.

Figure 14 shows the construction of a band structure in a 1D problem, where there are twenty  $k$ -points between  $[0, \pi]$  and around seven eigenvalues for each value of  $k$ .

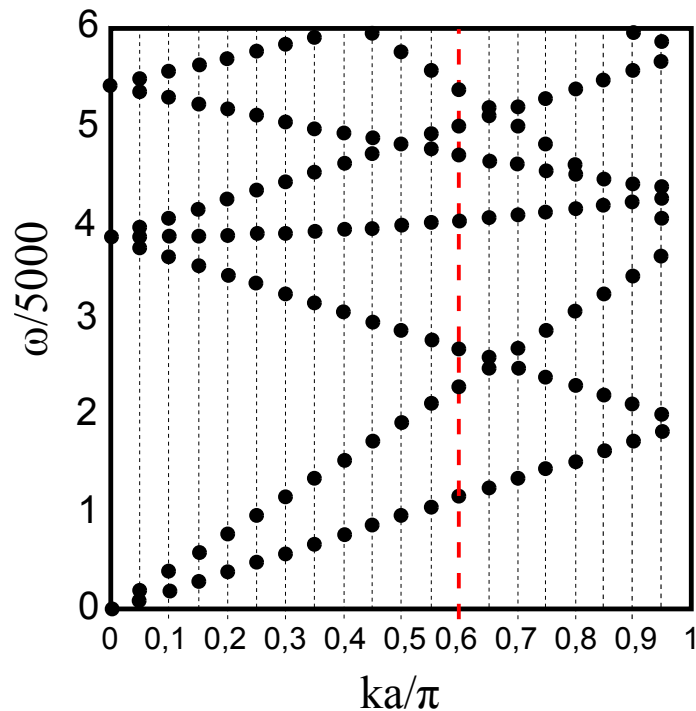


Figure 14: Band structure of a 1D PM: a homogeneous and isotropic material. To construct the graph we solved twenty eigenvalue problems that correspond to the values of  $k$ -points between  $[0, \pi]$ . Every value of the wave vector has around seven eigenvalues as it is shown in the red dashed line with  $ka/\pi = 0.6$ .

### 3 Classical problems in periodic materials

This section, used for further reference, describes the results of previous analysis reported in the literature, see [112, 113]. The section describes the following cases:

1. A homogeneous and isotropic material.
2. A square inclusion.

#### 3.1 Elastic, homogeneous and isotropic infinite space

The material is infinite and uniform in the three space directions and is formulated in the  $xy$  plane after using a plane strain idealization. The primitive cell can be chosen arbitrarily since the material is homogeneous and isotropic (Figure 15). The elastic properties of the material (Aluminum) are  $E = 7.31 \times 10^{10} Pa$  for the Young's modulus,  $\nu = 0.325$  for the Poisson's ratio,  $\rho = 2770 kg/m^3$  for the mass density and the longitudinal  $\alpha$  and transversal  $\beta$  velocities are  $\alpha = 6198 m/s$  and  $\beta = 3157 m/s$ .

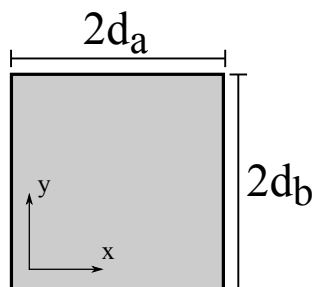


Figure 15: Primitive cell: infinite isotropic and homogeneous elastic material.

For traveling plane waves, the wave vector norm or wave number is:

$$k = \sqrt{k_x^2 + k_y^2}.$$

Since there is no dispersion in a homogeneous and isotropic medium, the phase and group velocities coincide and the angular frequency is a linear function of the wave number

$$\omega = ck = c\sqrt{k_x^2 + k_y^2}, \quad (18)$$

and where the constant  $c$  can be either  $\alpha$  or  $\beta$ .

The dispersion relation in equation (18) represents the positive part of a cone in Cartesian coordinates, this cone must be obtained for every type of wave after solving the eigenvalue problem. Figure 16 shows the numerical results for this dispersion relation<sup>12</sup>.

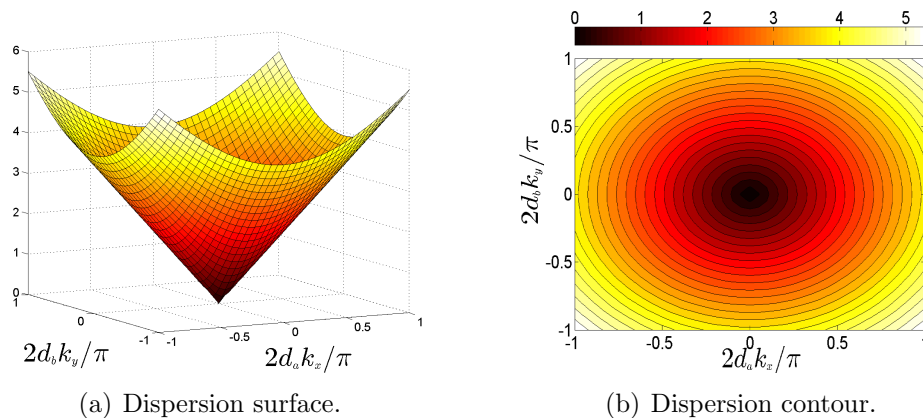


Figure 16: Numerical results for a homogeneous and isotropic material. These results correspond to the longitudinal wave (second calculated eigenvalue).

The dispersion relations are plotted in the First Brillouin zone, i.e., for a square cell  $2d_a k_x / \pi = [-1, 1]$  and  $2d_b k_y / \pi = [-1, 1]$ . Wave vectors  $\mathbf{k}$  outside the First Brillouin Zone can be written as:

$$\mathbf{k}_{n,m} = \left[ k_x + \frac{n\pi}{d_a}, k_y + \frac{m\pi}{d_b} \right]^T, \quad (19)$$

where  $n$  and  $m$  are integers counting cells to the right (or left) and up (or down). The vector  $[k_x, k_y]^T$  belongs to the First Brillouin Zone.

The wave numbers can also be written as

$$k_{n,m} = \sqrt{\left(k_x + \frac{n\pi}{d_a}\right)^2 + \left(k_y + \frac{m\pi}{d_b}\right)^2},$$

and thus, the angular frequency would be

---

<sup>12</sup>In the literature, one frequently finds the iso-frequency contours: a projection of every formed dispersion surface into the  $[k_x, k_y]$  plane, as shown in Figure 16 for this particular case.

$$\omega_{n,m} = c\sqrt{\left(k_x + \frac{n\pi}{d_a}\right)^2 + \left(k_y + \frac{m\pi}{d_b}\right)^2}.$$

The complete band structure is constructed covering the range  $[0, \pi/2d]$  ( $2d_a = 2d_b = 2d$ ): the IBZ since the material is isotropic. This region will capture also the data corresponding to the wave vectors outside the Brillouin zone. Figure 17 represents the theoretical and numerical dispersion curves for the homogeneous and isotropic material.

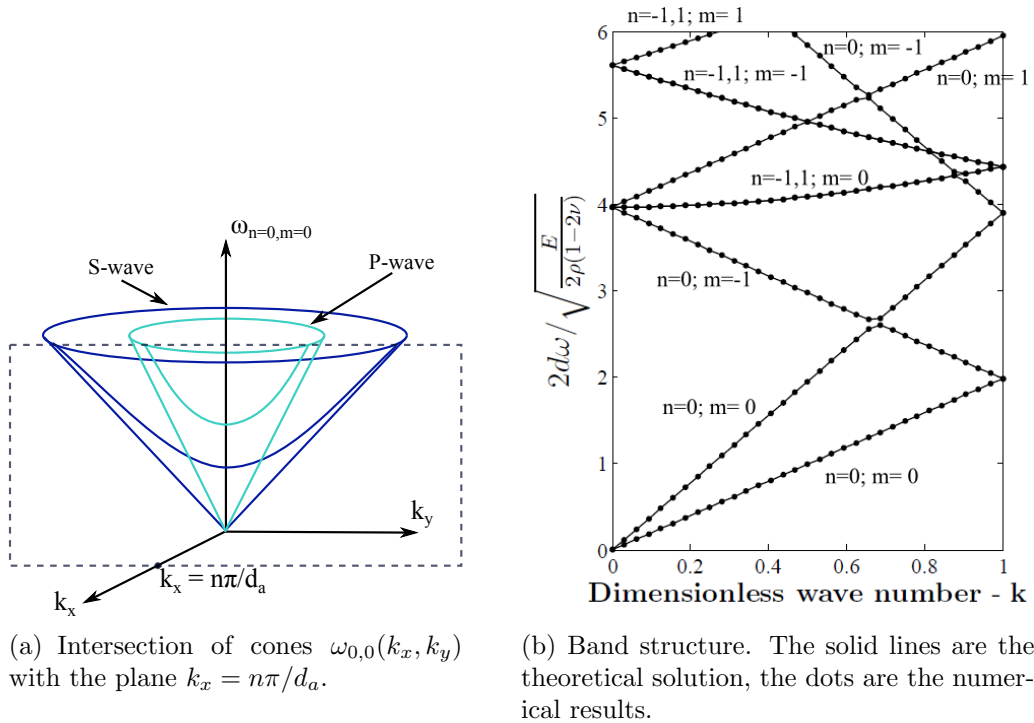


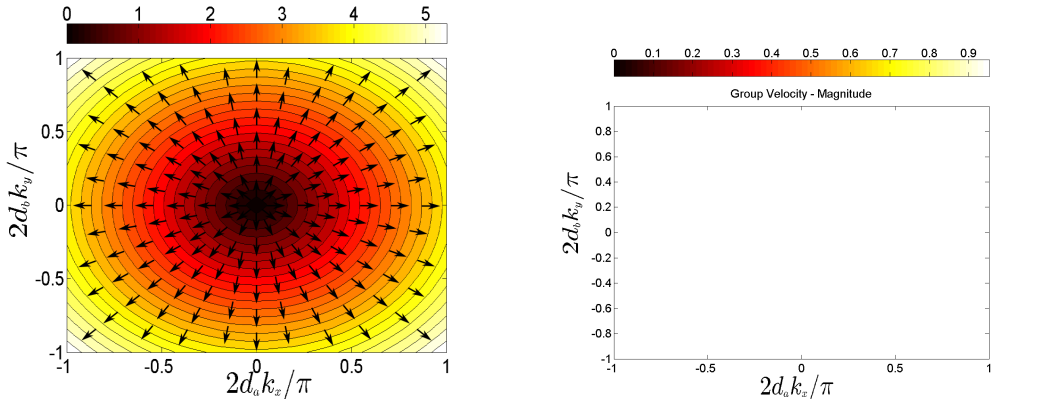
Figure 17: Branches of the dispersion curves in a homogeneous and isotropic material.

For an incident wave taken in the  $y$ -direction, with  $k_x = 0$ , the branches of curves that are observed correspond to

- If  $n = m = 0$ , the obtained curves are straight lines of the form  $\omega = c|k_y|$ .
- If  $n = 0$  and  $m \neq 0$ , the curves are folds of the straight lines corresponding to  $n = m = 0$  in the First Brillouin Zone:  $\omega = c|k_y + m\pi/d|$ .

- If  $n \neq 0$  and  $m = 0$ , the curves are hyperboles, resulting from the intersection of the cones  $\omega_{0,0}(k_x, k_y)$  with the plane  $k_x = n\pi/d$  (Figure 17 a).
- If  $n \neq 0$  and  $m \neq 0$ , the curves are folds of the hyperboles from the First Brillouin Zone.

The group and phase velocities will provide an indication of the anisotropy of the material. The group velocity is calculated from the dispersion relation using equation (15). The result is a vector field whose components point in the direction of the greatest rate of increase of the function (perpendicular direction to each contour line in Figure 16), and with a magnitude given by the slope of the graph in that direction. Figure 18 shows the group velocity vector field and its magnitude for the homogeneous and isotropic material.

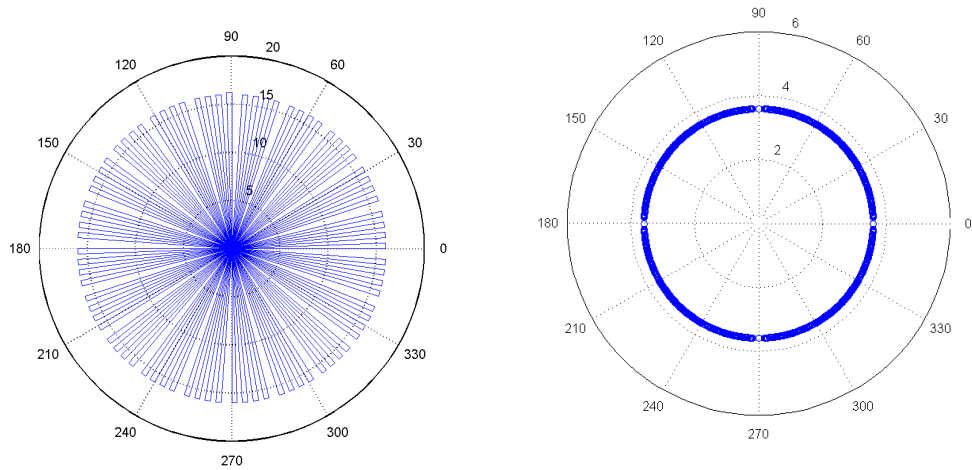


(a) Vector field superimposed to the dispersion contour. The arrows are perpendicular to each contour line.

(b) Magnitude: the colorbar value is normalized to  $\alpha$ .

Figure 18: Group velocity for the second eigenvalue (longitudinal wave) of a homogeneous and isotropic material.

Since there is no dispersion the group velocity must be the same for all wave vectors and the magnitude graph is monochromatic. Another very helpful way to read the vector field data is using a polar histogram: how many vector arrows point to a specific direction. This graph shows the preferred direction of energy propagation in the material but it does not have information about the magnitude (if the wave packets are faster in that direction). Figure 19 displays the polar histogram together with a polar graph of iso-frequency directivity, both for a homogeneous and isotropic material.



(a) Polar histogram: how many vector arrows point to a specific direction.

(b) Iso-frequency directivity: The direction of group velocity for a specific value of the angular frequency (or contour level). The chosen value  $2d\omega/5000 \approx 3.8$

Figure 19: Directivity of the material using the group velocity direction.

The polar histogram in Figure 19, shows that there is not a preferred direction of energy propagation in the material and there is the same number of wave vectors propagating energy in every direction. On the other hand, the iso-frequency directivity shows the preferred directions of energy propagation for just one value of the angular frequency, i.e., for a contour level in the dispersion contour. It is also observed how the chosen angular frequency does not present a preferred direction for energy propagation.

The phase velocity is obtained using equation (14). It shows which wave vectors (with a particular direction of incidence) are comparatively faster. Again, there is no dispersion leading to a monochromatic graph for the homogeneous and isotropic material (Figure 20).

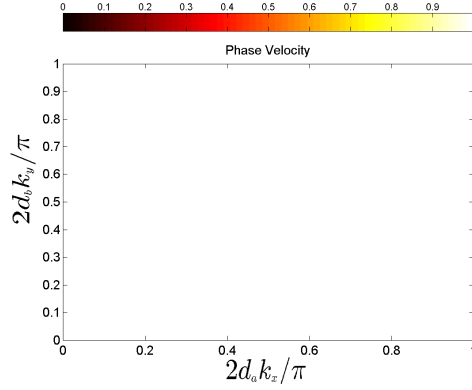


Figure 20: Phase velocity of the second eigenvalue (longitudinal wave) for a homogeneous and isotropic material. The colorbar value is normalized to  $\alpha$ .

### 3.2 Square inclusion

Consider now a cell composed of a square inclusion embedded in a matrix of an homogeneous material. The mechanical properties of the matrix are the same as in the previous case (Aluminum), while the inclusion has a Young's modulus  $E = 9.2 \times 10^{10} Pa$ , a Poisson's ratio  $\nu = 0.33$  and a mass density  $\rho = 8270 kg/m^3$  (brass). The dimensions are presented in Figure 21.

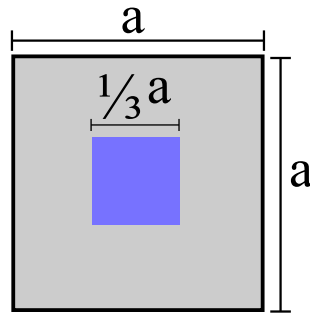


Figure 21: Primitive cell for a square inclusion.

The band structure is presented along the IBZ for a square cell (Figure 22), the region  $\Gamma - X - M - \Gamma$  correspond to:

$$\overline{\Gamma X} \longrightarrow k_y \frac{a}{\pi} = 0 \text{ and } k_x \frac{a}{\pi} = [0, 1], \quad (20)$$

$$\overline{XM} \longrightarrow k_x \frac{a}{\pi} = 1 \text{ and } k_y \frac{a}{\pi} = [0, 1], \quad (21)$$

$$\overline{M\Gamma} \longrightarrow k_x \frac{a}{\pi} = k_y \frac{a}{\pi} = [0, 1]. \quad (22)$$

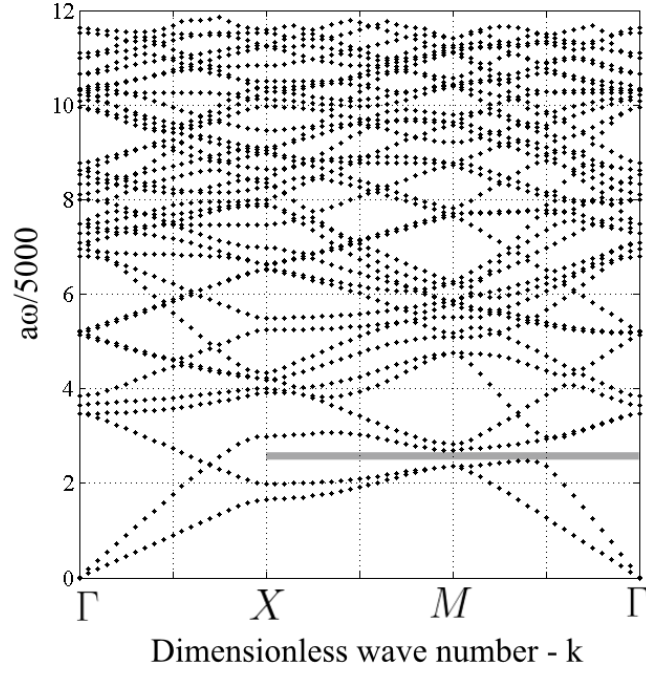


Figure 22: Band structure for a square inclusion.

From Figure 22 it is evident that there are no full band gaps along the complete IBZ. This is in contrast with the diffraction condition which implies that band gaps appear every time  $k_{x,y} = \pi/a$ . However, in the case of 2D elasticity, the fact that several wave modes interact inside the material implies that the diffraction condition must hold for every wave mode and its corresponding phase difference. For instance, with reference to Figure 23 the blue dashed line corresponds to a shear wave. It can be observed that band gaps occur every time  $ka/\pi = 1$  (region in light gray). However, the longitudinal waves (red solid line) with a band gap at higher frequencies

can propagate along this region. In order to have a full band gap is thus necessary that the two forbidden regimes coincide.

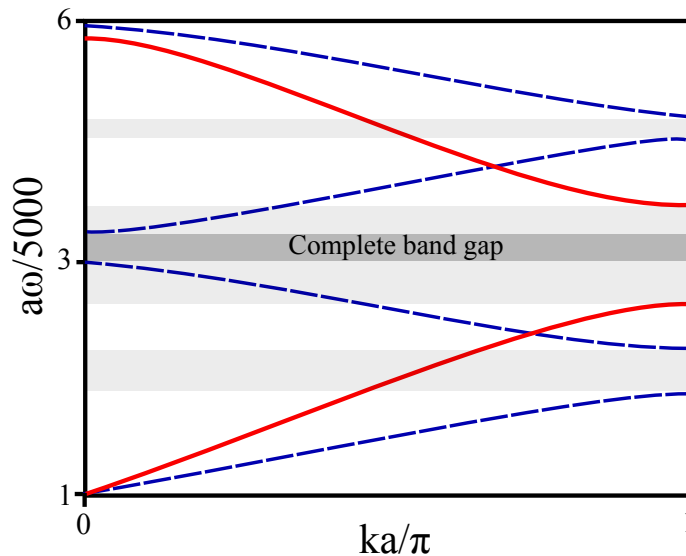


Figure 23: Band structure for a bilayer cell.

From the analysis above it is clear that a complete band gap can be reached under very specific combinations of geometric conditions and material properties. These parameters control the slopes of the curves in the band structure. As a conclusion, in elasticity the existence of periodicity does not guarantee the existence of band gaps.

On the other hand, partial band gaps in the IBZ (usually known as pseudo band gaps) can exist. Considering again the square inclusion it is also observed that in the dark gray region there is a band gap for all the possible waves. However, it is constrained to the directions of  $X - M$  and  $M - \Gamma$ , i.e., for waves with an incidence of  $[0^\circ, 45^\circ)$  and  $45^\circ$ , respectively <sup>13</sup>.

The dispersion contours of the first two eigenvalues for the square inclusion are shown in Figure 24. At low frequencies both contours show the behavior of a homogeneous and isotropic material, with stronger directional effects at higher frequencies. The directionality of the material is shown in Figure 25.

<sup>13</sup>The segment  $\overline{\Gamma X}$  represents the propagation in horizontal direction, i.e.  $0^\circ$ ;  $\overline{XM}$  in the directions from  $0^\circ$  to  $45^\circ$ ; and  $\overline{MT}$  in the direction of  $45^\circ$ .

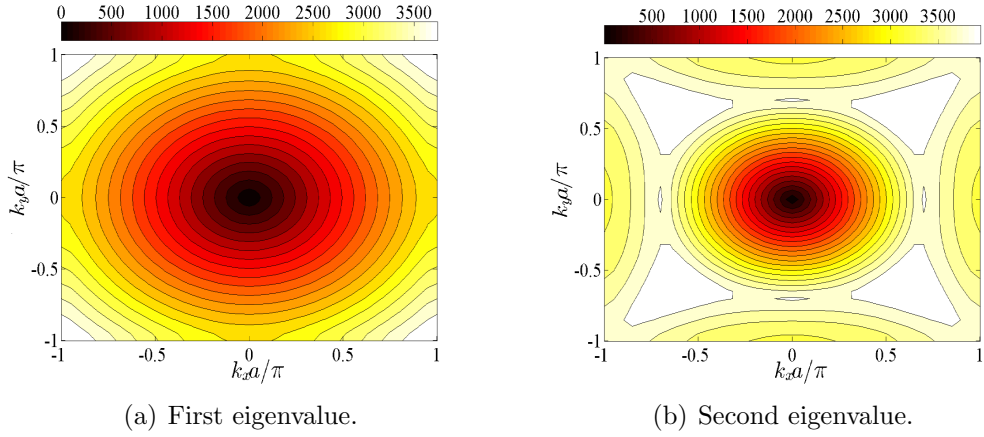


Figure 24: Dispersion contour for a square inclusion.

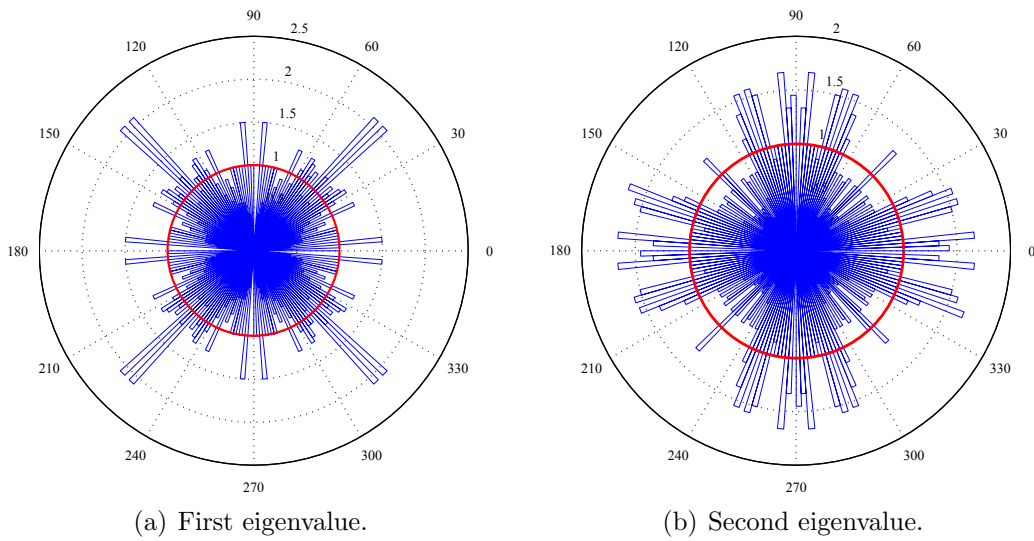


Figure 25: Polar histogram for a square inclusion. The data is normalized to the homogeneous and isotropic material, then, the red circle with radius= 1 corresponds to the homogeneous case.

The polar histograms in Figure 25 show that the material propagates energy specially along the diagonals. This is particularly strong for the first eigenvalue, although energy propagation is also observed along the vertical and horizontal axes.

The opposite behavior occurs for the second eigenvalue where it is observed that there is propagation along the diagonals but the preferred directions are around the principal axes, in the regions between  $(-30^\circ, 30^\circ)$  and  $(-150^\circ, 150^\circ)$  taken from each axis, approximately.

The iso-frequency directivity in Figure 26 supports what has been observed in the contours: the material behaves as homogeneous and isotropic at low frequencies, even at high frequencies for the second eigenvalue. The first eigenvalue presents preferred directions of energy propagation at high frequencies: it is highly directional in the diagonals.

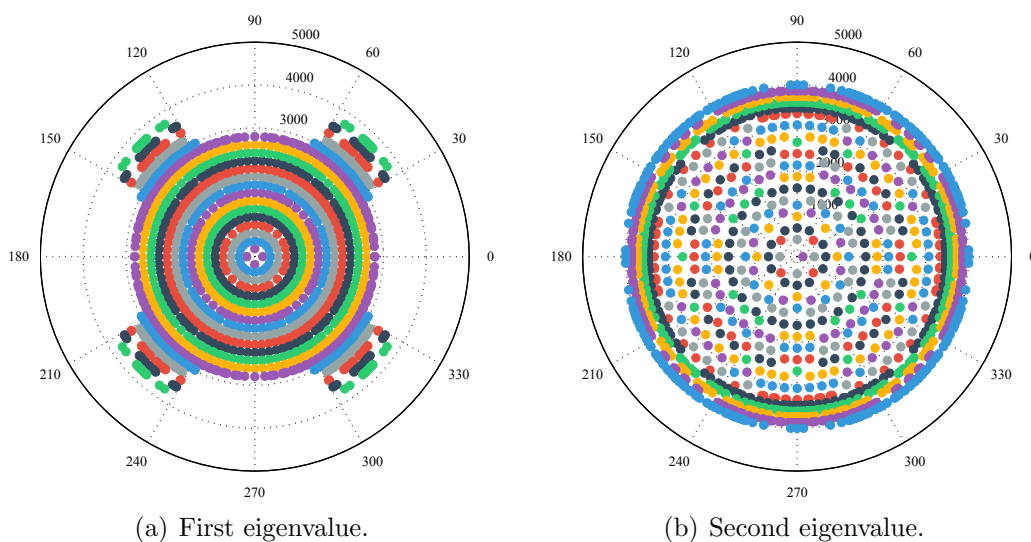
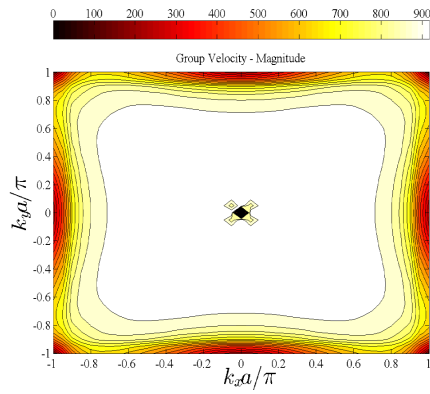
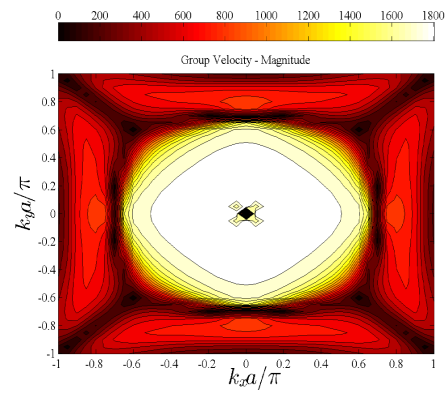


Figure 26: Iso-frequency directivity for a square inclusion. Every color represents a value of the angular frequency.

The group and phase velocities are presented in Figure 27 and 28. All images are monochromatic at low values of the wave number (with the highest velocity), and start to change in color towards the borders. This agrees with the analysis of the dispersion contours: the material behaves as homogeneous and isotropic in the monochromatic region. For both velocity graphs, it is observed that the contours of the first eigenvalue are slightly expanded along the diagonals. In the second eigenvalue of the group velocity, the contours lean towards the vertical and horizontal directions. This also supports what has been identified in the polar directivity graphs (Figure 25).

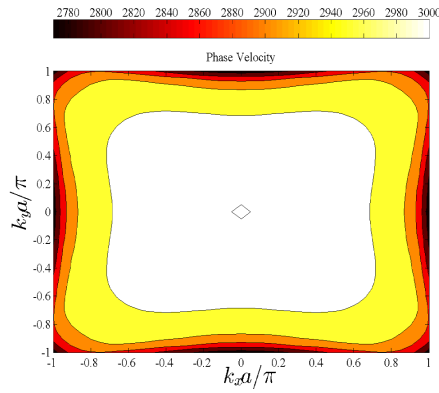


(a) First eigenvalue.

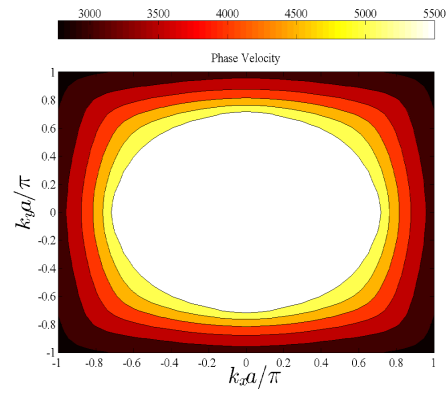


(b) Second eigenvalue.

Figure 27: Group velocity for a square inclusion.



(a) First eigenvalue.



(b) Second eigenvalue.

Figure 28: Phase velocity for a square inclusion.

## Part II

# Wave propagation in a bistable material

This section is dedicated to the analysis of wave propagation in a phase transforming cellular material. The material was originally introduced by Restrepo et al. [4], in a project formulated between the Computational Multi-Scale Materials Modeling Laboratory of Purdue University, and the Research Laboratory in Smart Materials and Structures of General Motors Global Research & Development.

In the phase transforming cellular material, the primitive cell in its periodic representation has multiple stable configurations with each one of them corresponding to a phase. The change from one stable phase to the other is achieved through large elastic deformations thus consuming energy during the process<sup>14</sup>. This feature combined with the periodic character of the material suggests the existence of complex and varying band structures opening the possibility for alternative forms of wave filtering and guiding. In this particular study the aim is to explore how to control the wave propagation behavior in the material and switch the propagation properties when the phase transition is triggered.

## 1 A cellular material that exhibits bistability

The cellular material consists of a primitive cell that can undergo phase transformation. This corresponds to a change in geometry that leads to stable configurations while keeping its original topology.

The phase transforming cellular material (PXCM) is presented in Figure 29. The primitive cell comprises a compliant bistable mechanism that exhibits a force-displacement relation with a sawtooth shape (see Figure 30). The relation presents two limit points:  $(d_I, F_{II})$  and  $(d_{II}, F_{II})$ , which define three regimes in the mechanical response [4] described as follows:

- Regimes I and III are characterized by a positive stiffness, and represent the deformation of stable configurations of the primitive cell. These configurations correspond to a local minimum in the potential energy of the mechanism.

---

<sup>14</sup>For more details please review reference [4].

- Regime II is characterized by a negative stiffness and corresponds to a transition of the mechanism from one limit point to the other.

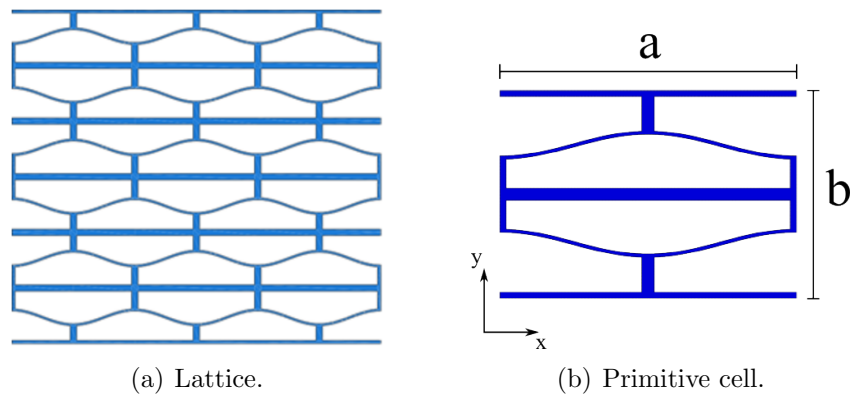


Figure 29: The Phase Transforming Cellular Material (PXCM).

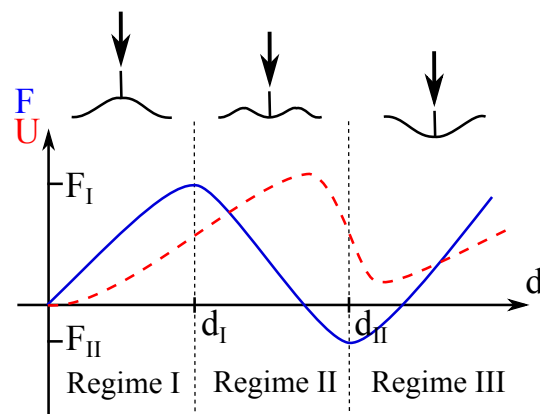


Figure 30: Force Vs Displacement relation for the PXCM and its change of potential energy  $U$  [4].

The material is expected to dissipate energy when subjected to impact and cyclic loading. The dissipation is achieved through large deformations that trigger the phase transitions and keep the elastic reversibility, as opposed to classical dissipation associated to plastic deformation.

The main question arising for the PXCM is whether the wave propagation is different for each stable phase, considering that there are only geometrical changes while the topology remains constant. This study explores how such particular features influence the dispersion relations of each phase and what are the controlling parameters in the wave propagation properties.

The three phases considered in this study are described by primitive cells referred to as open, intermediate and closed cell (see Figure 31). It is important to clarify that the study does not address the propagation properties during the phase change (Regime II). Furthermore, as the infinite material is deformed, the phase transition takes place one row at the time and the periodicity is broken. This suggests that the wave propagation properties also undergo a transition and the intermediate phase is an approximation when every row in the material has experienced half a collapse. In this study, we assume that during wave propagation the phase of the cellular material remains constant.

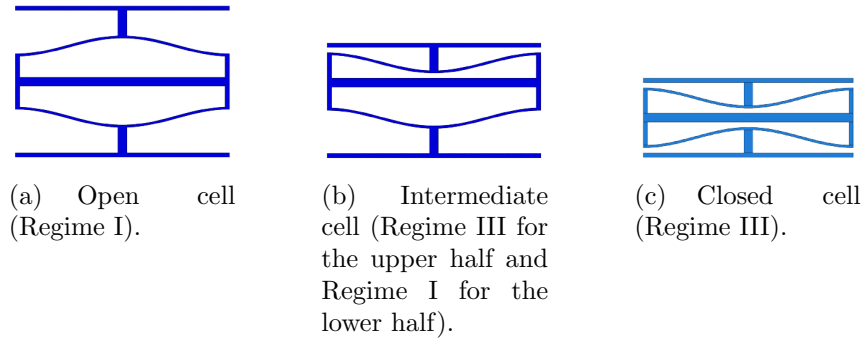


Figure 31: Primitive rectangular cells used to describe the cellular material in each stable phase

In order to understand the response of each one of the considered phases, the analysis starts by studying the band structure of a progressively built open cell, that is a cell that is built in several stages after considering the contribution from additional elements. This analysis is followed by the study of the three stable phases and by a final analysis considering pre-stresses. Accordingly, the last section explores the effects of a topological change in a closed cell.

All of the analyses in this part of the document were performed with FEMs using Bloch-periodicity conditions through MPCs in the commercial code Abaqus (Part

I). Since the depth (cross section) of the PXCM is considered to be larger than any other delimited area inside the primitive cell, the model follows a plane strain idealization. Also, all of the primitive cells used for the analyses are rectangular and its IBZ correspond to the perimeter pointed in Figure 6 and equations (20)-(22). The mechanical properties and lattice parameters used during the analysis are:

- Young Modulus  $E = 1 \text{ GPa}$ .
- Poisson's ratio  $\nu = 0.49$ .
- Density  $\rho = 1000 \text{ kg/m}^3$ .
- For each phase  $a = 60 \text{ mm}$ ; in the open cell  $b \approx 42 \text{ mm}$ , intermediate cell  $b \approx 32 \text{ mm}$  and closed cell  $b \approx 22 \text{ mm}$ .

## 2 Building an open cell

In order to build the open cell, consider the five intermediate stages shown in Figure 32. Figure 33 displays the differences in dimensions between the different stages together with the proportions of the open cell compared to the first stage. The remaining cases will maintain the same dimensions as the components in the open cell. Figure 34 shows the formed cellular materials based on each stage.

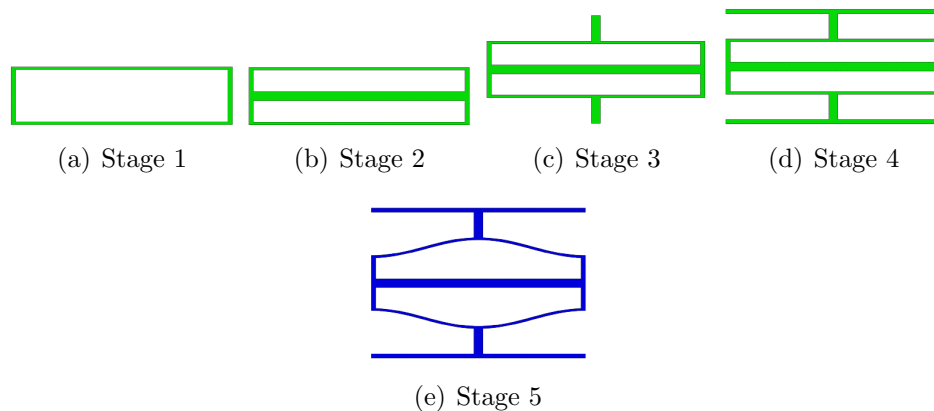


Figure 32: Primitive rectangular cells of the stages while building an open cell.

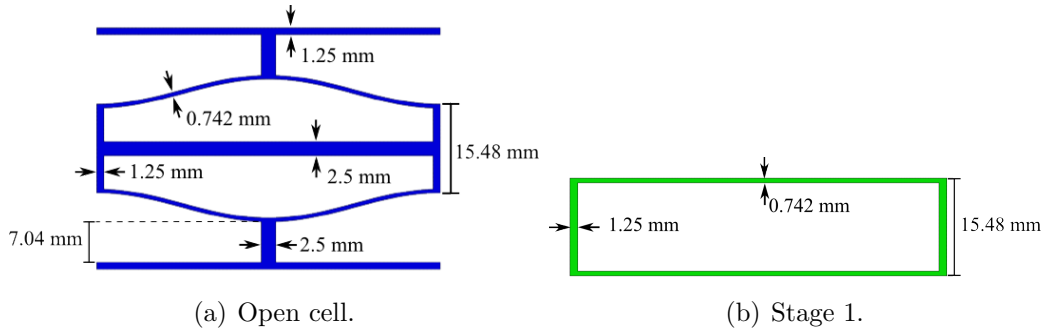


Figure 33: Dimensions of the open cell and the stage 1.

Figure 35 shows the band structure for each one of the stages. The way in which the dots are connected is important as each line will correspond to a type of wave defining the limits of the band gap. However, the identification of the different types of waves for a connected line (i.e., telling if it is a P, S, or a combination mode) is still complex and an analysis of the eigenvectors would be necessary in order to have an idea of the propagation (of the deformation shape).

The most noticeable feature is the appearance of band gaps for the stage 1 and 3 and also, the fact that the eigenvalues decrease and the curves are compressed when new elements are considered in each following stage. With respect to the band gap of stage 1, it must be observed that although the cell is very similar to the stage 2, the band gap vanishes for the last one<sup>15</sup>.

Figure 36 shows a close up of the band structure for the first nine eigenvalues of each stage. The existence of pseudo band gaps is evident, and also, it is observed how the band structure changes in stage 3 just because the addition of vertical bars.

<sup>15</sup>We can not say that stage 2 is the vertical alignment of two cells of stage 1, aligning two cells results in a middle bar with thickness 1.484 mm, while that bar in stage 2 has a thickness of 2.5 mm.

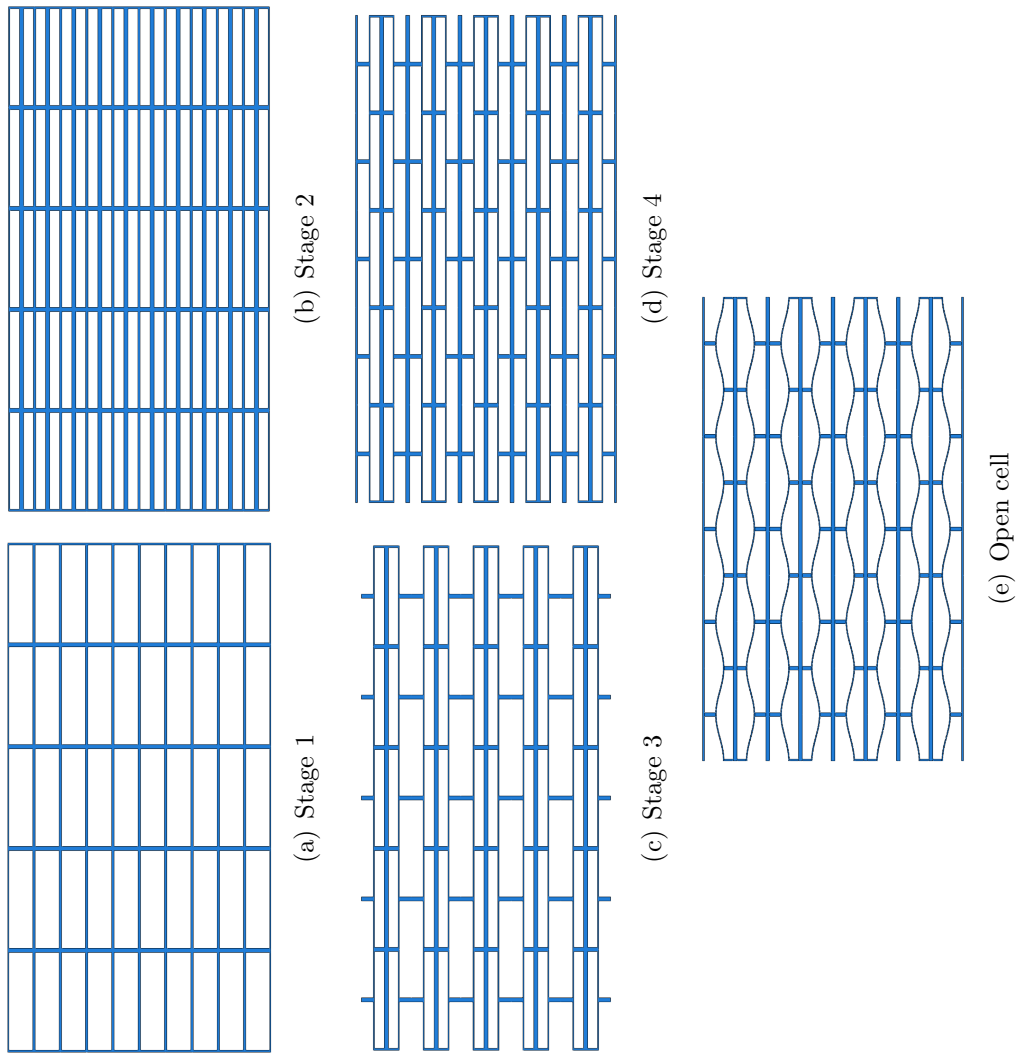
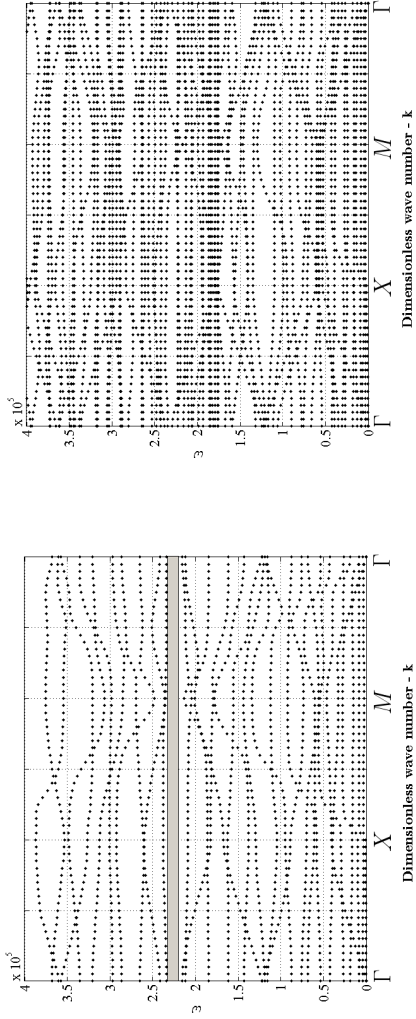
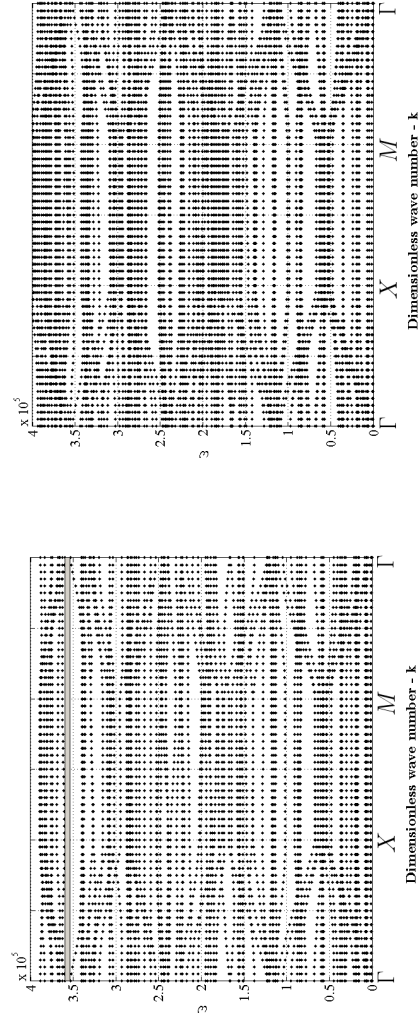


Figure 34: Cellular materials based on the primitive cells considered for each stage

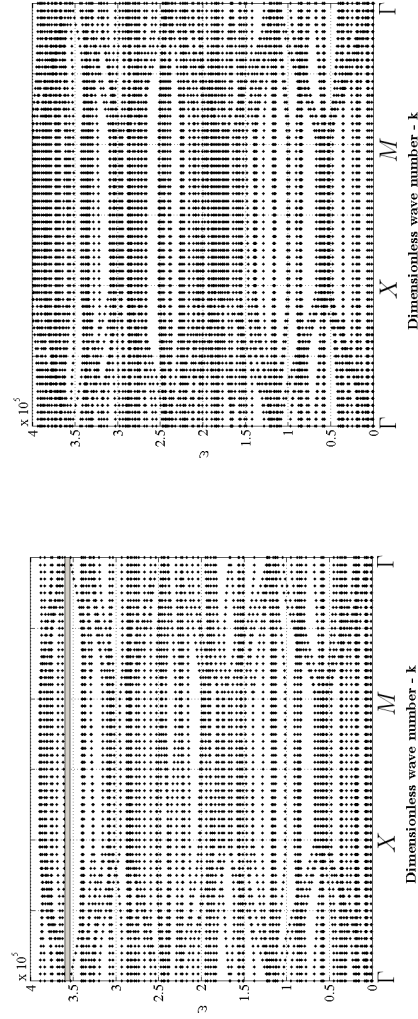


(a) Stage 1

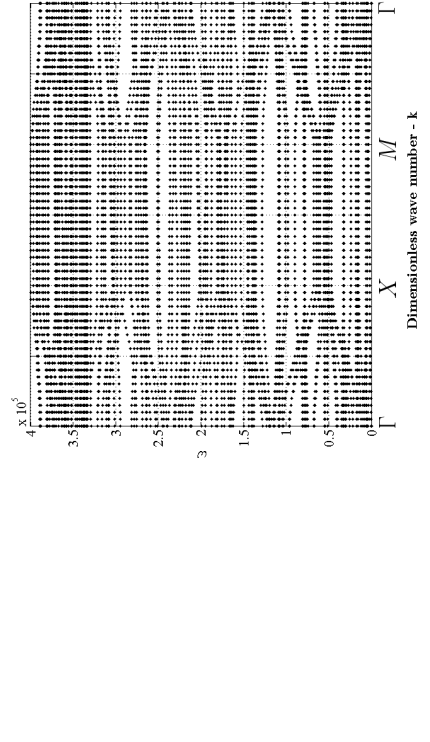


(b) Stage 2

(c) Stage 3

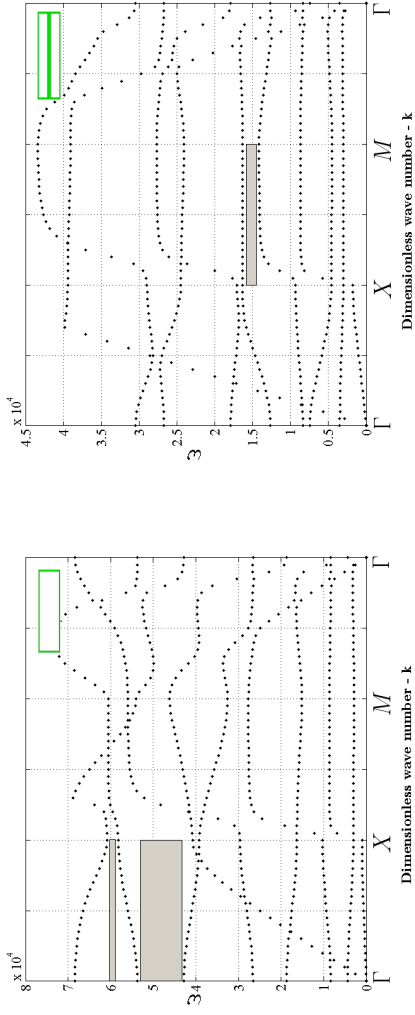


(d) Stage 4

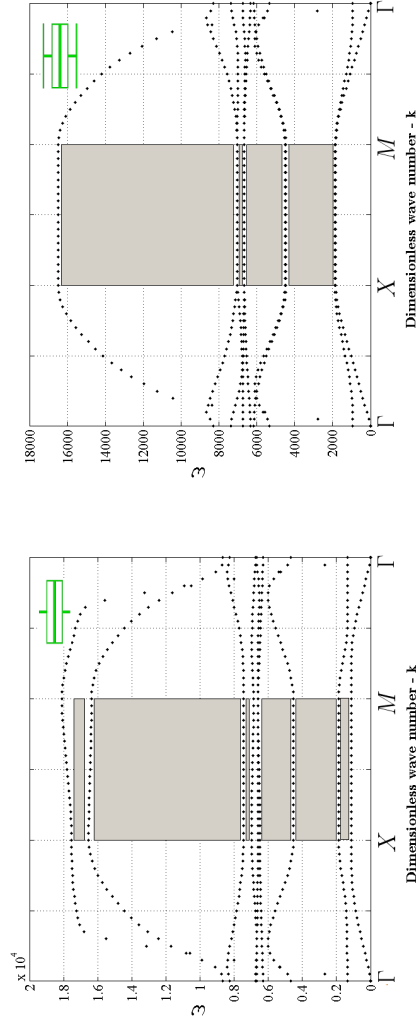


(e) Open cell

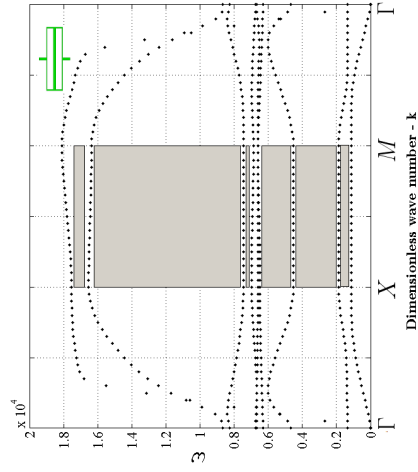
Figure 35: Band structure evolution: stages while building an open cell.



(a) Stage 1

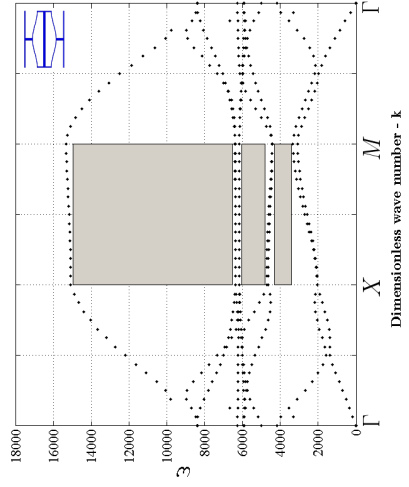


(b) Stage 2



(c) Stage 3

(d) Stage 4



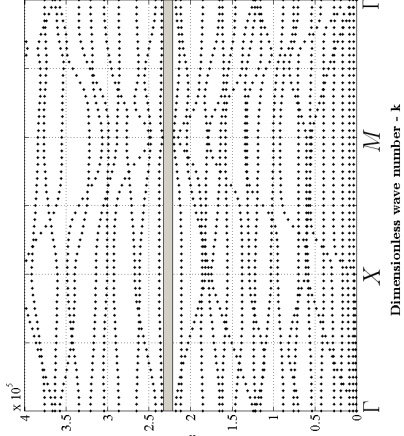
(e) Open cell

Figure 36: Close up for the band structure of each stage. Nine eigenvalues are considered.

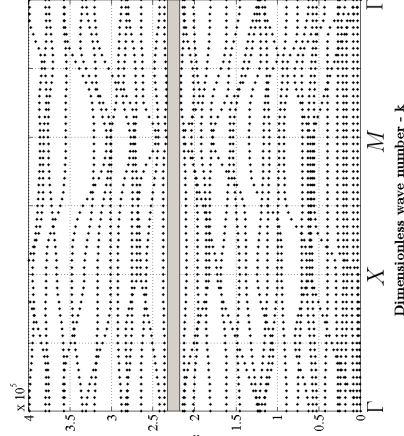
In order to track the band gap found in stage 1, an analysis for cells corresponding to stage 2 with increasing density in the middle bar was conducted. We started from  $\rho = 1 \text{ kg/m}^3$  with the assumption of absence of material. Figures 37 show the band gap evolution.

The band structure of stage 1 and stage 2 with  $\rho = 1 \text{ kg/m}^3$  agree. More eigenvalues appear as the density of the middle bar increases. By contrast the band gap, between  $\rho = 70 \text{ kg/m}^3$  and  $\rho = 85 \text{ kg/m}^3$  vanishes at a low value of the density considering the  $1000 \text{ kg/m}^3$  bound. The next step is exploring the region between  $100 \text{ kg/m}^3$  and  $1000 \text{ kg/m}^3$ , where it was found that around  $500 \text{ kg/m}^3$  the band gap reappears but is lost again for higher values.

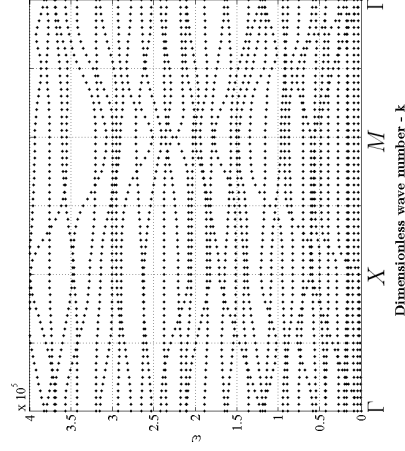
The results suggest that full band gaps require specific combinations of geometry and material properties. Such problem is the subject of future work.



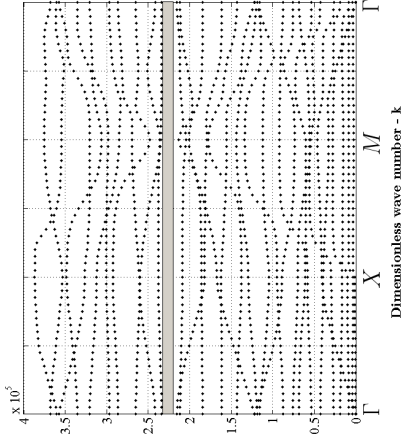
(b) Stage 2  $\rho = 1 \text{ kg/m}^3$ .



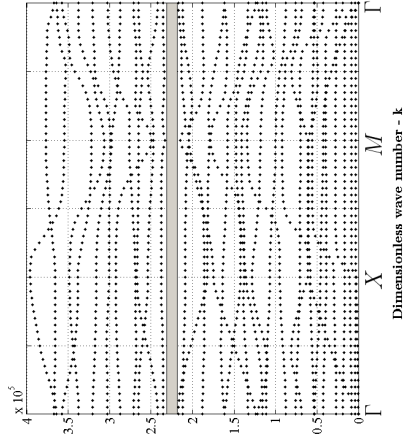
(d) Stage 2  $\rho = 50 \text{ kg/m}^3$ .



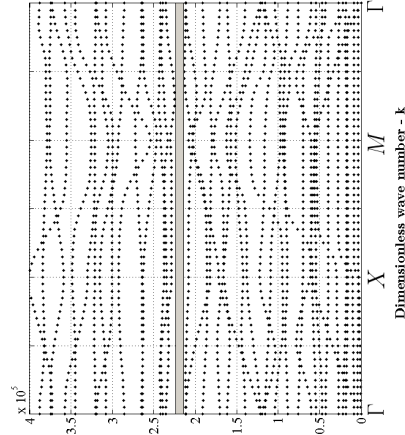
(f) Stage 2  $\rho = 85 \text{ kg/m}^3$ .



(a) Stage 1.



(c) Stage 2  $\rho = 10 \text{ kg/m}^3$ .



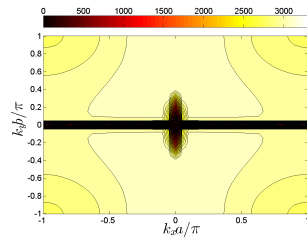
(e) Stage 2  $\rho = 70 \text{ kg/m}^3$ .

Figure 37: Tracking the band gap of stage 1. The analysis used cells of stage 2 with increasing density in the middle bar and starting from  $\rho = 1 \text{ kg/m}^3$  (absence of material).

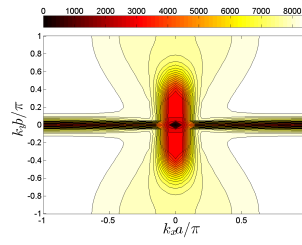
The anisotropy and directivity of each stage is now studied for the first two eigenvalues. The dispersion contours in Figure 38 and the polar histograms in Figure 39 and 40, show that all stages in both eigenvalues, except for the open cell, propagate energy preferably along the horizontal direction: the contours are compressed mainly towards the  $y$  axis. The open cell presents a difference between the eigenvalues, the first one propagates energy mostly in the vertical direction while the second one does it in the horizontal direction.

We note also the similarity between stages 1 and 2. The contours are highly similar with the only difference in the polar histogram: stage 2 has a sharper angle around the horizontal direction. This could be explained from Figure 34, where the presence of an additional horizontal bar in the cell facilitates the energy propagation along this direction. From the cellular material of stages 3 and 4, it is observed that the lost in continuity of the vertical bar could also explain why the contours are compressed towards the  $y$  axis and the pronounced directionality along the horizontal direction.

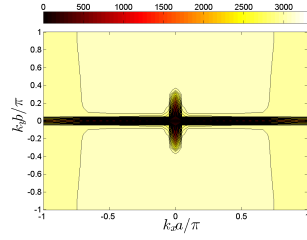
The directionality results for the first four stages, show the cells prefer a narrow region around the horizontal direction for the energy propagation. The open cell with the sinusoidal bars reinforces the energy propagation in the other directions, specially the vertical direction for the first eigenvalue and the horizontal direction for the second eigenvalue. We can think of these sinusoidal bars as wave guides.



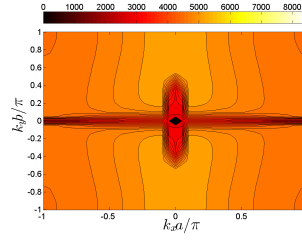
Stage 1: First eigenvalue.



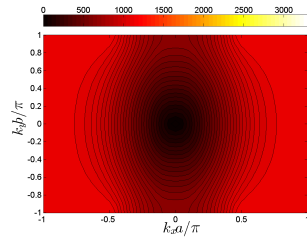
Stage 1: Second eigenvalue.



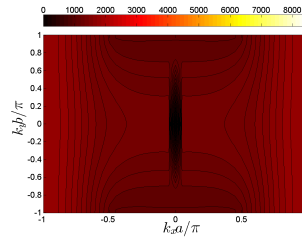
Stage 2: First eigenvalue.



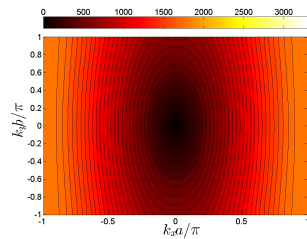
Stage 2: Second eigenvalue.



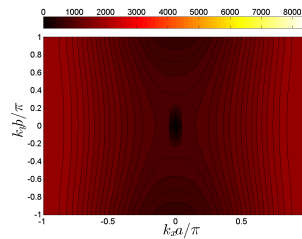
Stage 3: First eigenvalue.



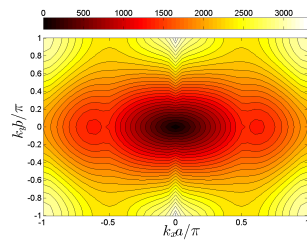
Stage 3: Second eigenvalue.



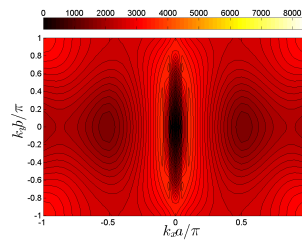
Stage 4: First eigenvalue.



Stage 4: Second eigenvalue.

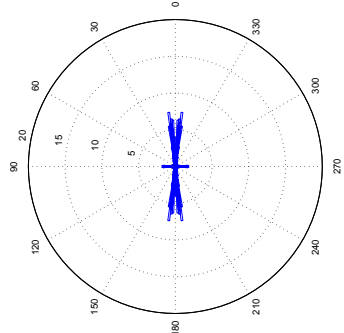


Stage 5: First eigenvalue.

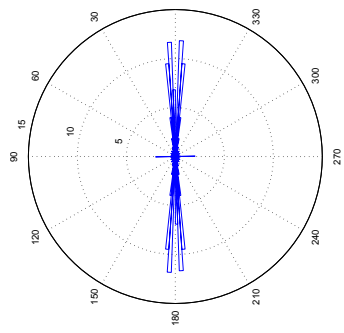


Stage 5: Second eigenvalue.

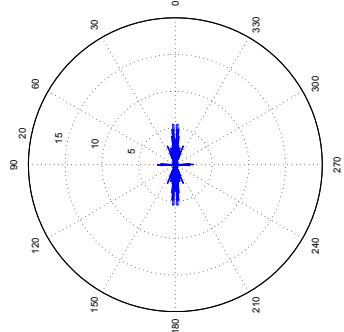
Figure 38: Dispersion contour evolution: stages while building an open cell.



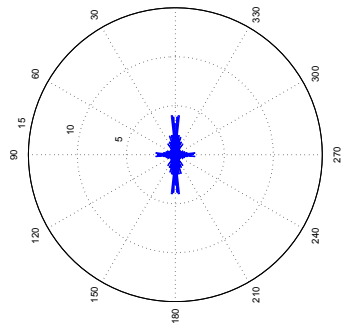
Stage 2: Second eigenvalue.



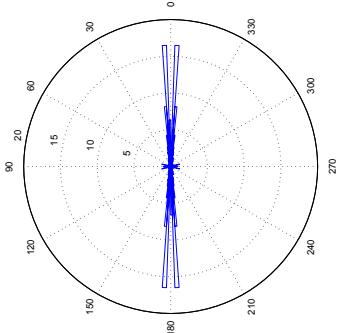
Stage 2: First eigenvalue.



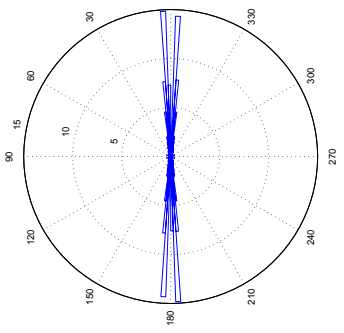
Stage 1: Second eigenvalue.



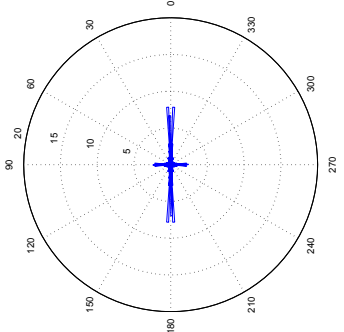
Stage 1: First eigenvalue.



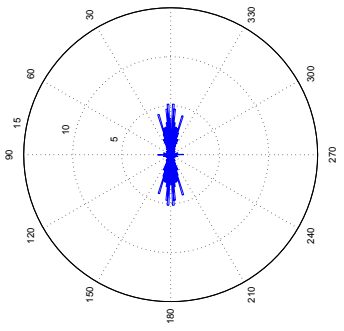
Stage 4: Second eigenvalue.



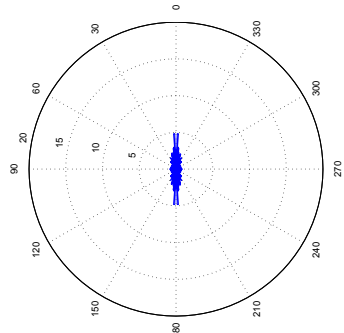
Stage 4: First eigenvalue.



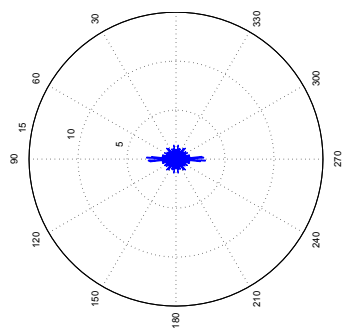
Stage 3: Second eigenvalue.



Stage 3: First eigenvalue.



Stage 5: Second eigenvalue.



Stage 5: First eigenvalue.

Figure 39: Polar histogram evolution: stages while building an open cell.

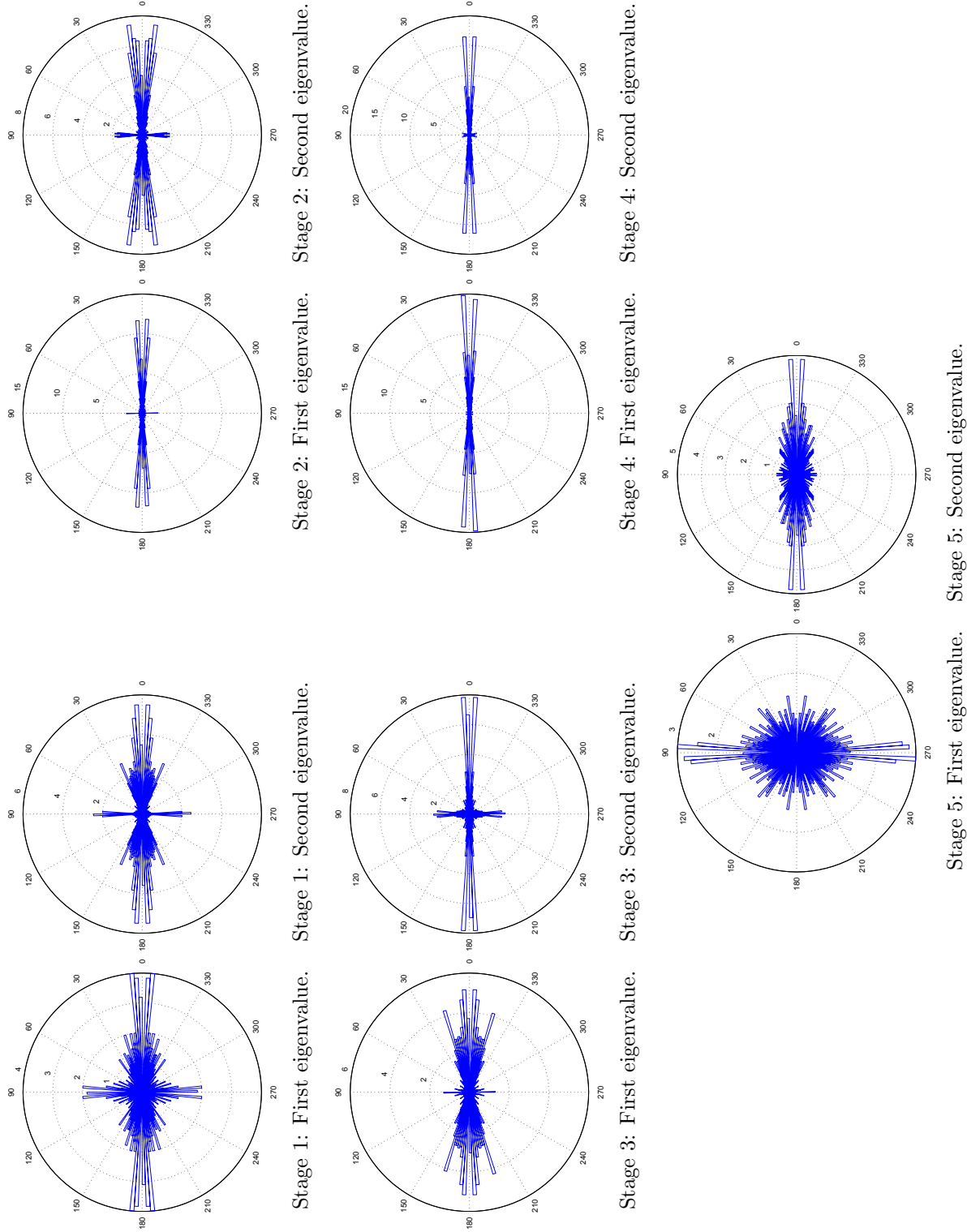


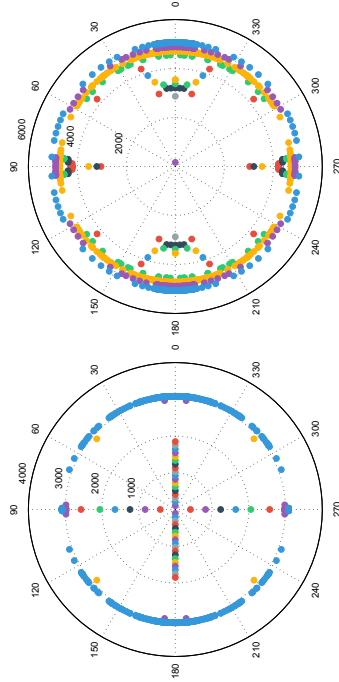
Figure 40: Close up for the polar histogram evolution. Each polar plot is presented with relative scale.

In the case of the polar iso-frequency plot shown in Figure 41, we obtain the directivity behavior for a single angular frequency (each color corresponds to a frequency value). For stage 1 and 2, the first eigenvalue shows that at low frequencies the energy is distributed along the horizontal and vertical directions. At higher frequencies the energy propagation tends to be in all directions. For the second eigenvalue, the first frequencies confine the energy around the horizontal direction of the material and the angle of energy propagation becomes wider as frequency increases.

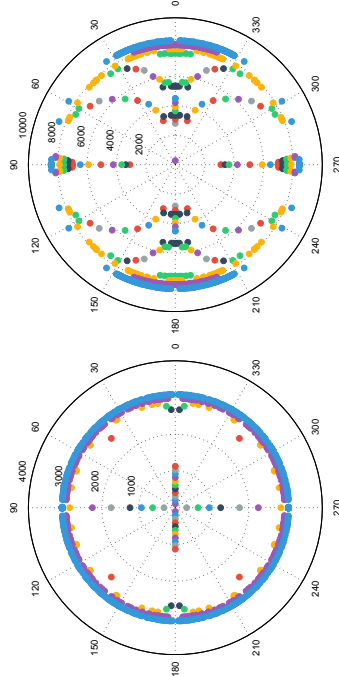
Stages 3 and 4 are also similar. For both eigenvalues, the energy of lower frequencies is propagated in all directions, but as the frequency increases, the energy is distributed around the horizontal direction of the material. Stage 5 is different. The energy propagation at low frequencies is given in all directions for both eigenvalues. After increasing the frequency, the first eigenvalue presents energy propagation in the vertical direction and the second eigenvalue in the horizontal direction.

In Figures 42 and 44, we can identify what directions and magnitudes of the incident waves reach the highest values of the group and phase velocity. The axes in Figures 43 and 45 have different scales in order to appreciate the values variation.

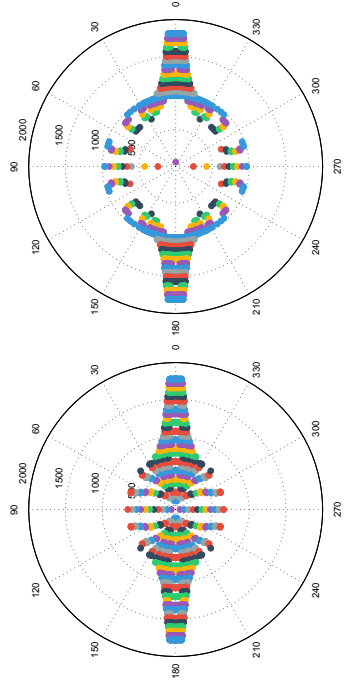
For the first four stages in the first eigenvalue, the velocity values (both the group and phase velocities) are higher for waves with an incidence along the horizontal axis, having larger angles as we pass to the next stage. In the open cell, the fastest waves have a narrow incidence angle along the vertical axis. This is consistent and complements the directivity plots. The case of the second eigenvalue is the same for all stages: the highest values correspond to wave vectors close to the origin and with an incidence angle around the horizontal axis.



Stage 1: First eigenvalue. Stage 2: Second eigenvalue.



Stage 3: First eigenvalue. Stage 4: Second eigenvalue.



Stage 5: First eigenvalue. Stage 6: Second eigenvalue.

Stage 1: First eigenvalue. Stage 2: Second eigenvalue.

Stage 3: First eigenvalue. Stage 4: Second eigenvalue.

Stage 5: First eigenvalue. Stage 6: Second eigenvalue.

Stage 5: First eigenvalue. Stage 6: Second eigenvalue.

Figure 41: Polar iso-frequency directivity: stages while building an open cell.

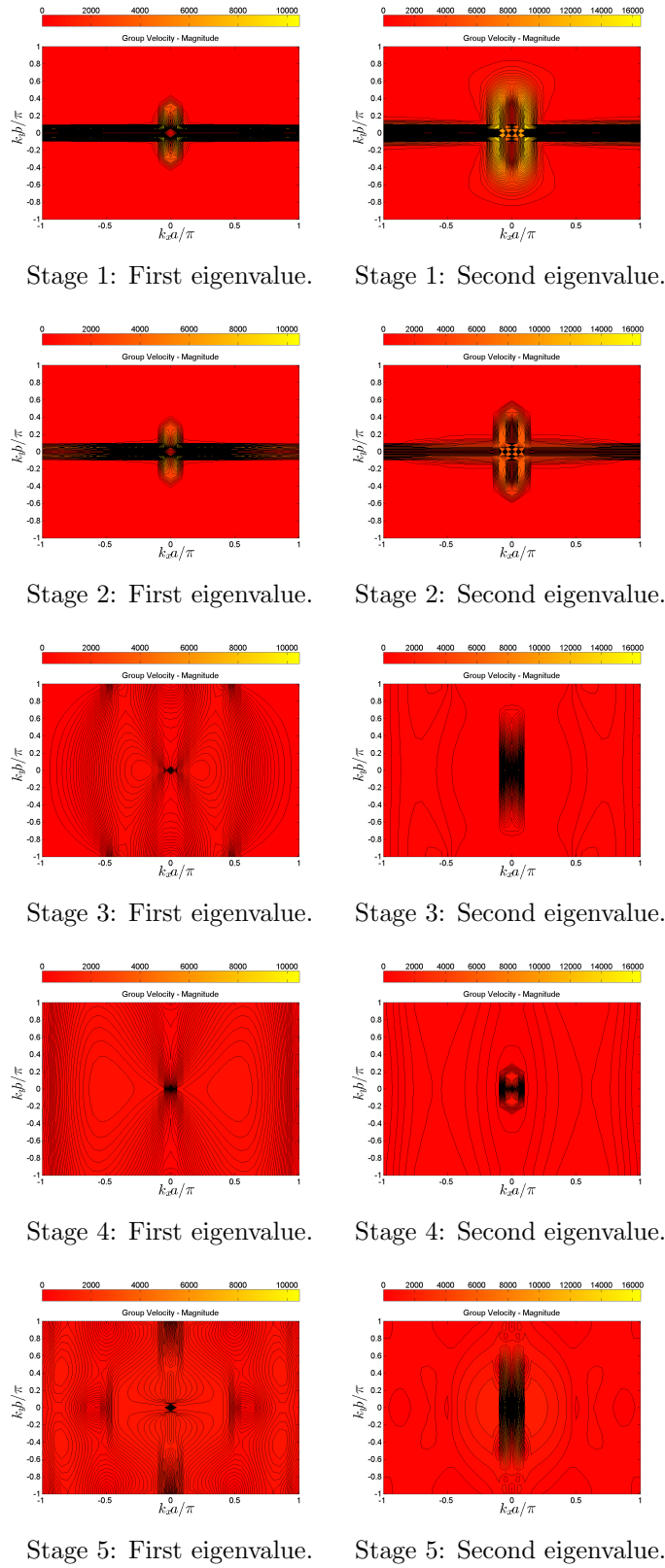


Figure 42: Group velocity magnitude, evolution: stages while building an open cell.

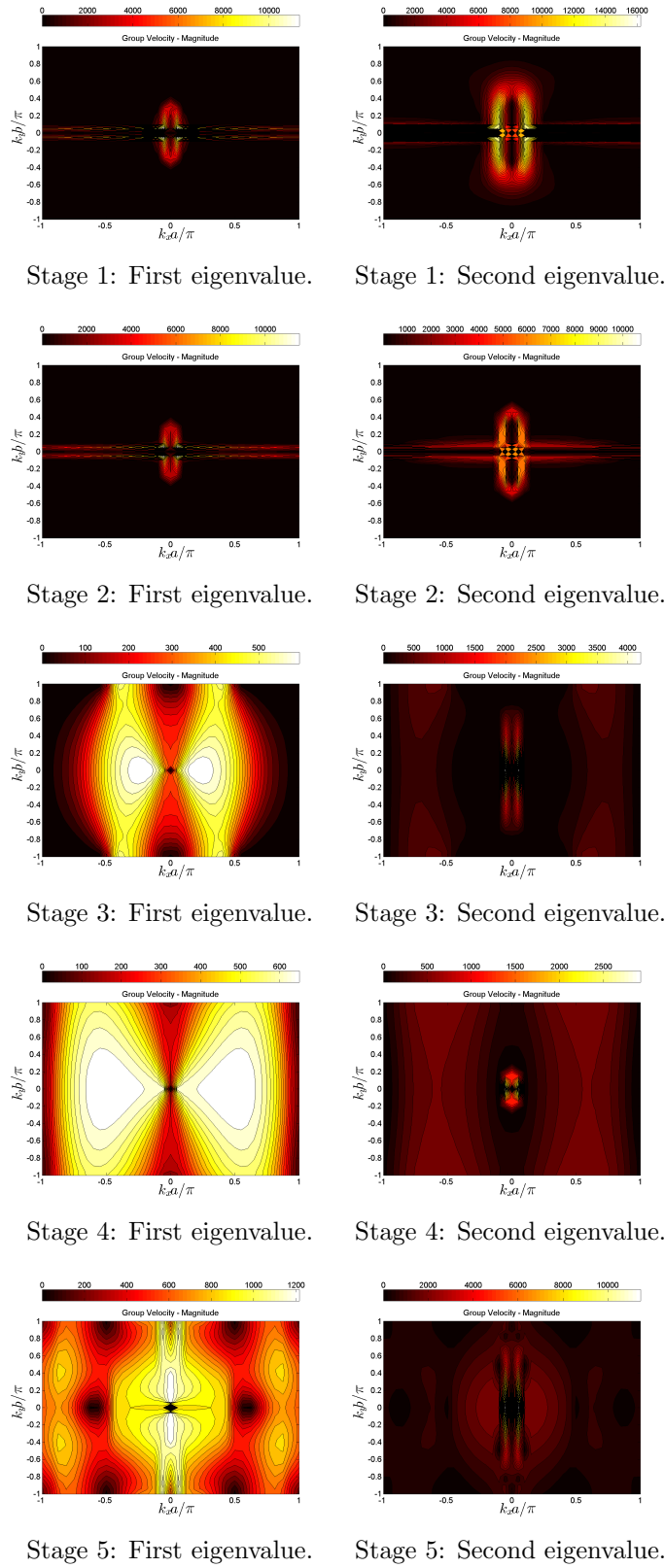


Figure 43: Group velocity magnitude, evolution: stages while building an open cell. Each contour is presented with relative scale.

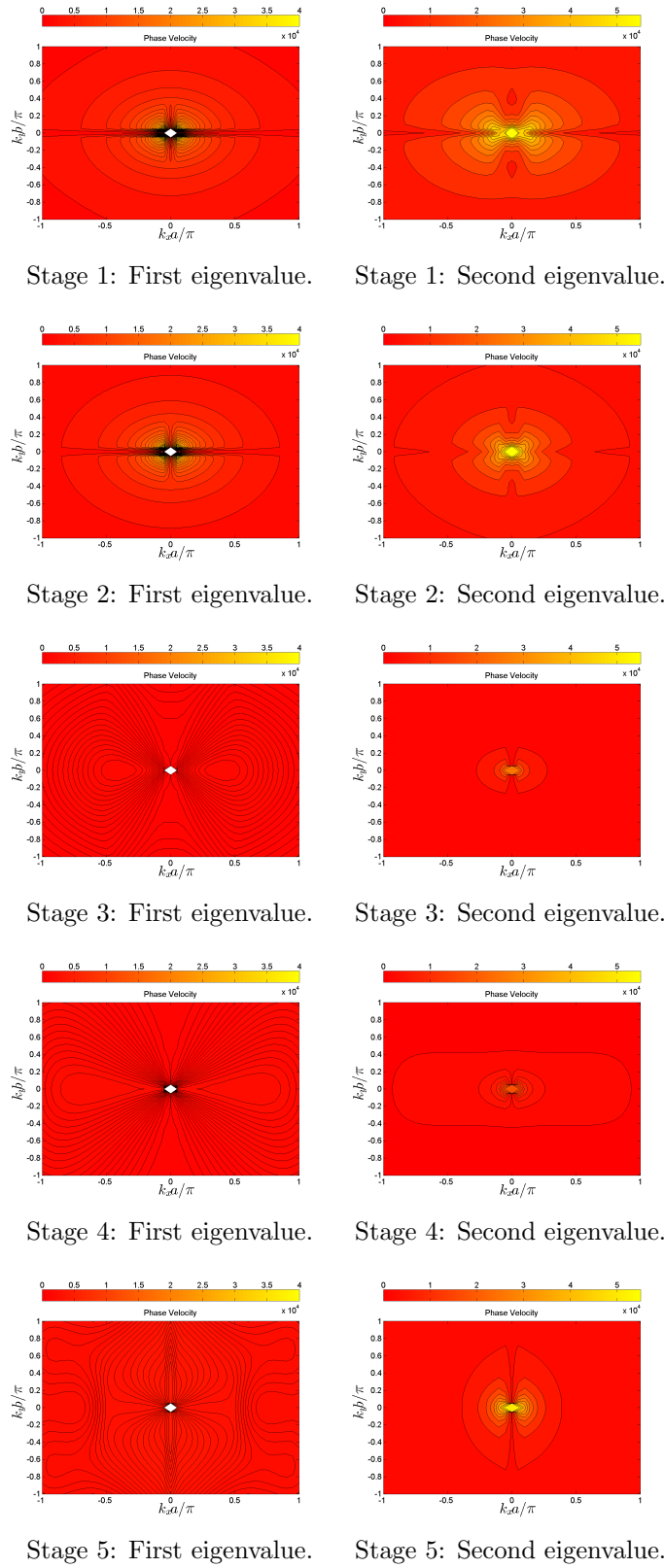
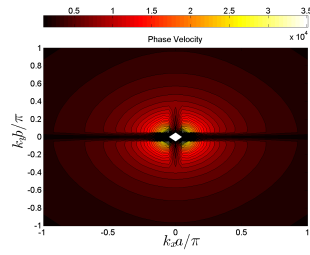
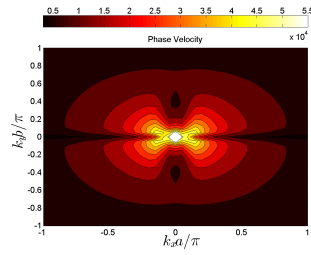


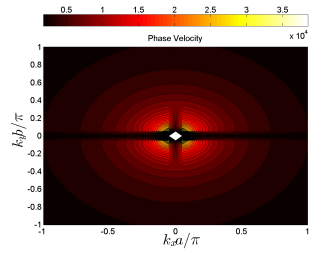
Figure 44: Phase velocity evolution: stages while building an open cell.



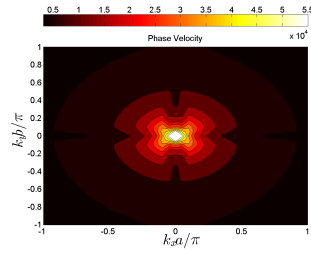
Stage 1: First eigenvalue.



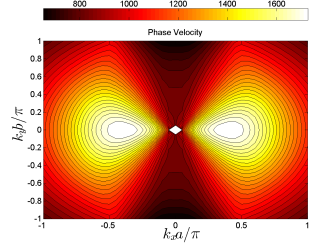
Stage 1: Second eigenvalue.



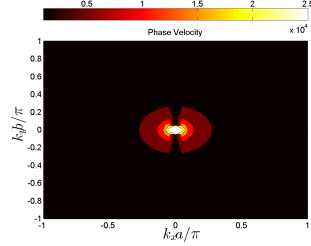
Stage 2: First eigenvalue.



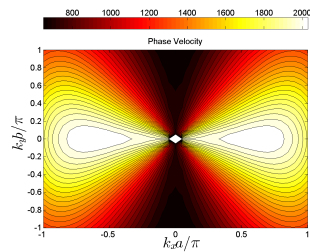
Stage 2: Second eigenvalue.



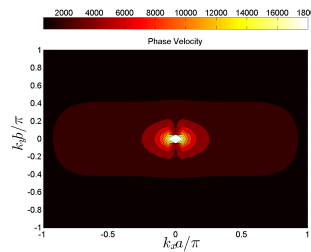
Stage 3: First eigenvalue.



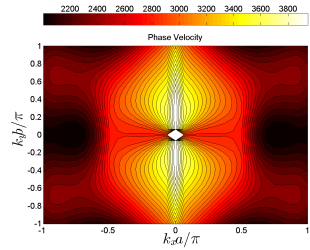
Stage 3: Second eigenvalue.



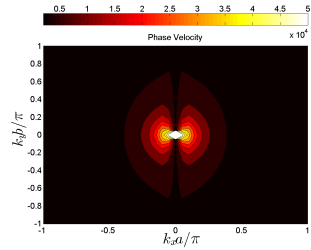
Stage 4: First eigenvalue.



Stage 4: Second eigenvalue.



Stage 5: First eigenvalue.



Stage 5: Second eigenvalue.

Figure 45: Phase velocity evolution: stages while building an open cell. Each contour is presented with relative scale.

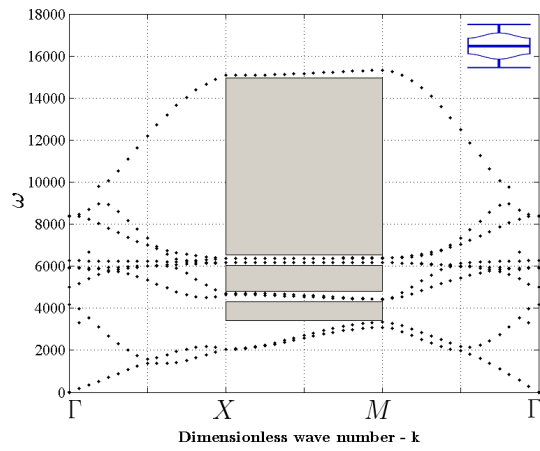
### 3 Dispersion diagrams of the stable configurations

The analysis that follows corresponds to low frequencies, therefore, the band structures show the first nine eigenvalues and the dispersion diagrams are analyzed for the first two (Figure 31). As shown in Figure 46 there are no complete band gaps in any stable phase. By contrast pseudo gaps appear in  $\overline{XM}$ : waves with an incidence angle from  $0^\circ$  to  $45^\circ$ . The remarkable feature of these band structures is that there is not a significant difference between the phases. The geometrical differences in this case have a weak influence on the band structure, at least at low frequencies.

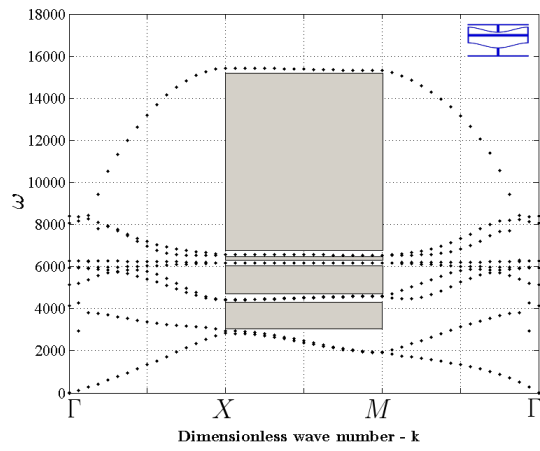
The previous idea is also evidenced, although partially, in the dispersion contours of Figure 47. For the open and closed cell, the contours of both eigenvalues are similar, however, the differences are highlighted in the polar histograms of Figure 48. In these plots, the closed cell shows a strong directionality around the vertical axis for the first eigenvalue; the angle opening is about  $\pm 30^\circ$  around the vertical axis. In the case of the open cell, we have that the energy propagation is given mainly in a narrow angle around the vertical axis, but also is distributed in the other directions (also notably around the horizontal direction). For the second eigenvalue, both, the closed and open cells propagate energy horizontally in a very similar way.

The intermediate phase is more interesting: for the first eigenvalue, it is highly directional around the horizontal axis with an angle opening about  $\pm 30^\circ$ . The second eigenvalue also propagates energy horizontally, but in a wider angular region as compared the other phases.

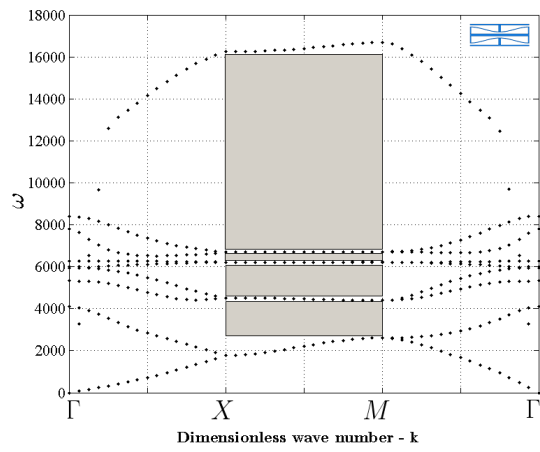
The contrast in directionality when comparing the intermediate cell with the other two phases, suggests the possibility of a waveguide device for low frequencies. This is an important result to take into account for future applications and the idea should be explored through a time domain analysis.



(a) Open Cell



(b) Intermediate Cell



(c) Closed Cell

Figure 46: Dispersion curves for each phase of the cell.

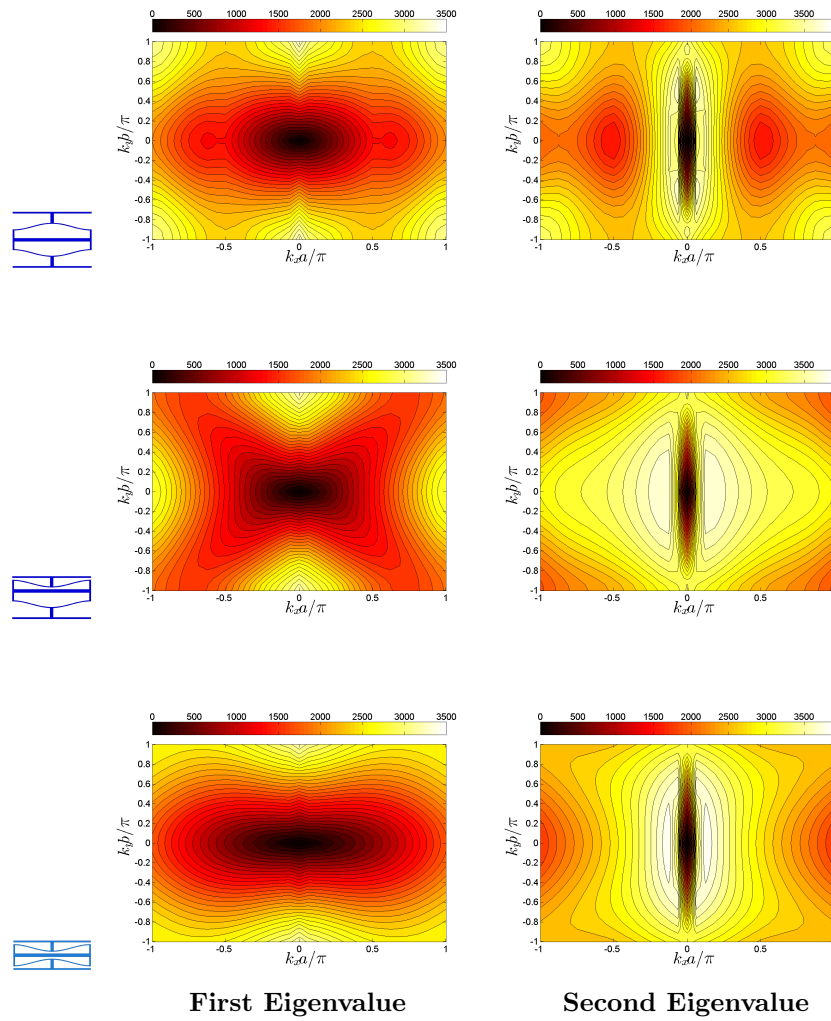


Figure 47: Dispersion contours for the first two eigenvalues. Each row corresponds to one type of cell (open, intermediate and closed) and each column to the specified eigenvalue.

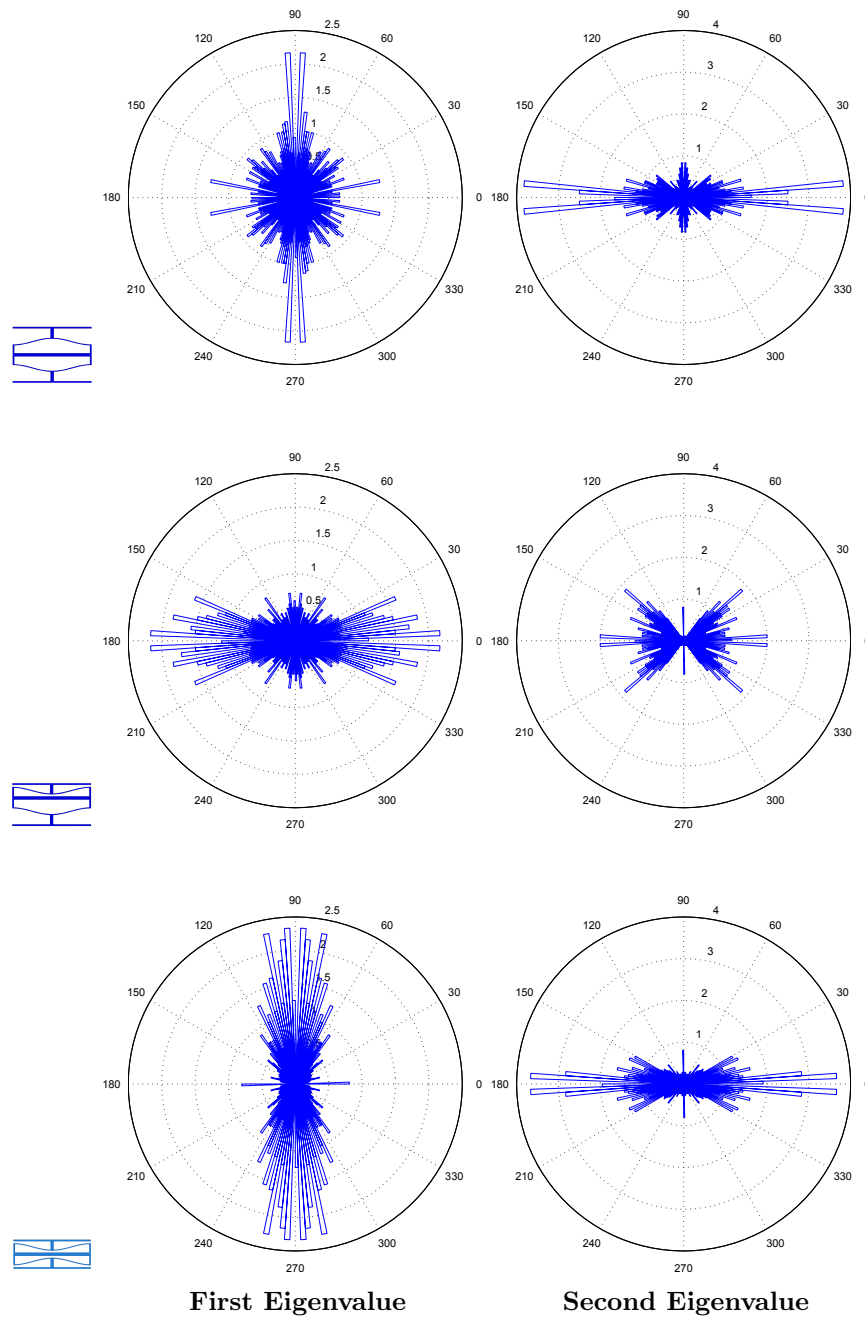


Figure 48: Polar histograms for the first two eigenvalues. Each row corresponds to one type of cell (open, intermediate and closed) and each column to the specified eigenvalue.

The iso-frequency directivity in Figure 49 is a simple way to read the dispersion contours in Figure 47, in terms of the material directionality. These show what directions of energy propagation are chosen for an individual frequency value.

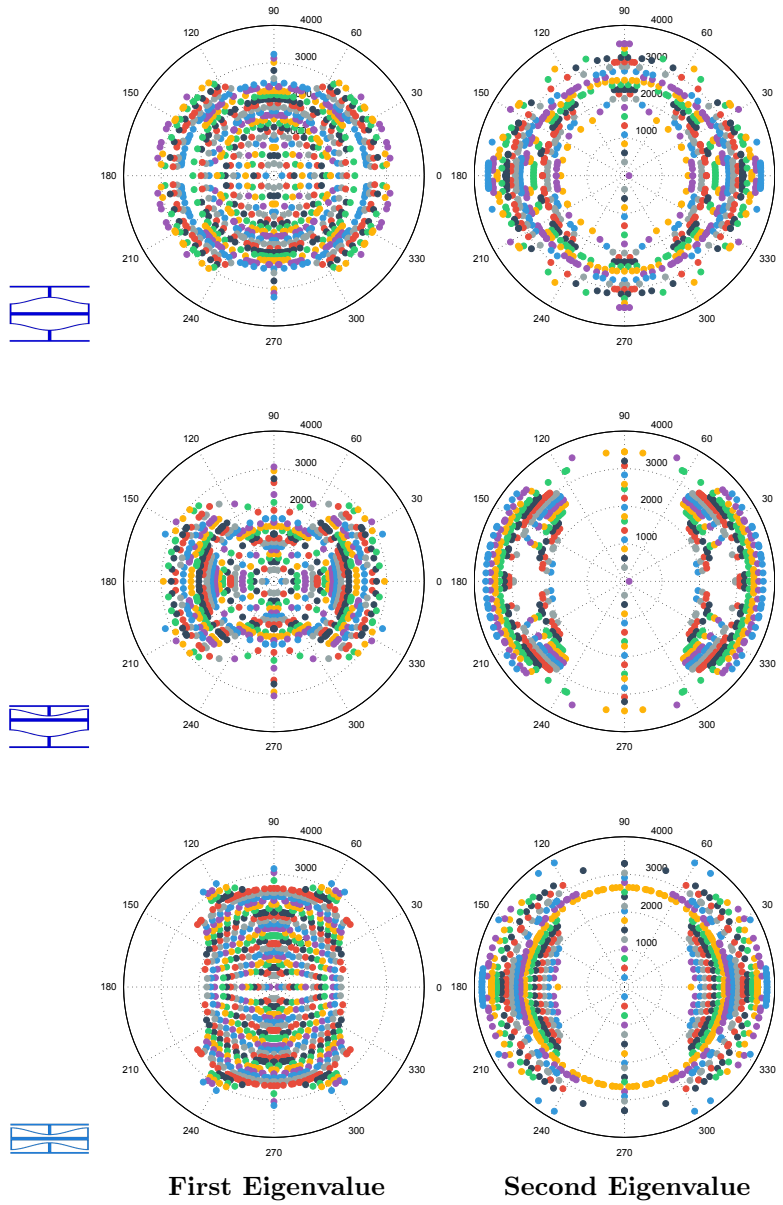


Figure 49: Polar polar iso-frequency directivity. Each row corresponds to one type of cell (open, intermediate and closed) and each column to the specified eigenvalue.

The “fastest” waves in terms of the group and phase velocities (Figures 50 and 51, respectively) are highlighted with yellow. What should be observed is that the “lowest” waves in the first eigenvalue, for the intermediate cell, have diagonal incidences, while in the closed cell they have horizontal incidence. The second eigenvalue shows that wave vectors lose velocity very quickly as its magnitude increases.

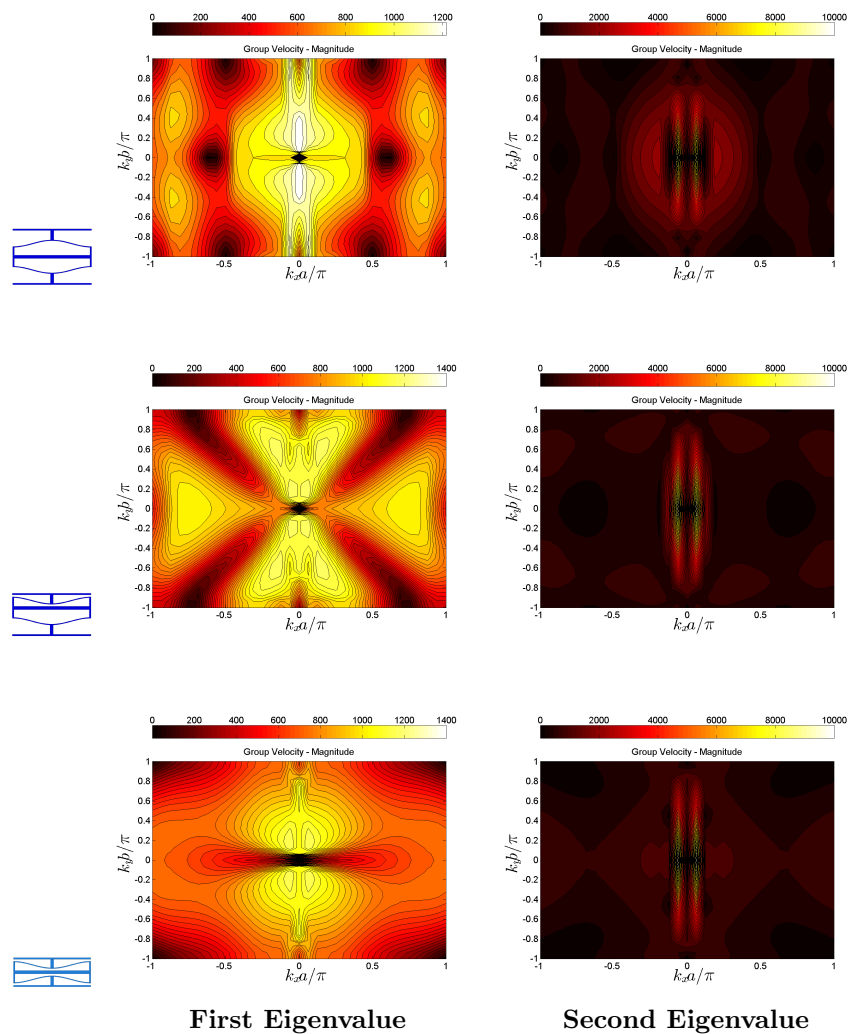


Figure 50: Group velocity magnitude. Each row corresponds to one type of cell (open, intermediate and closed) and each column to the specified eigenvalue.

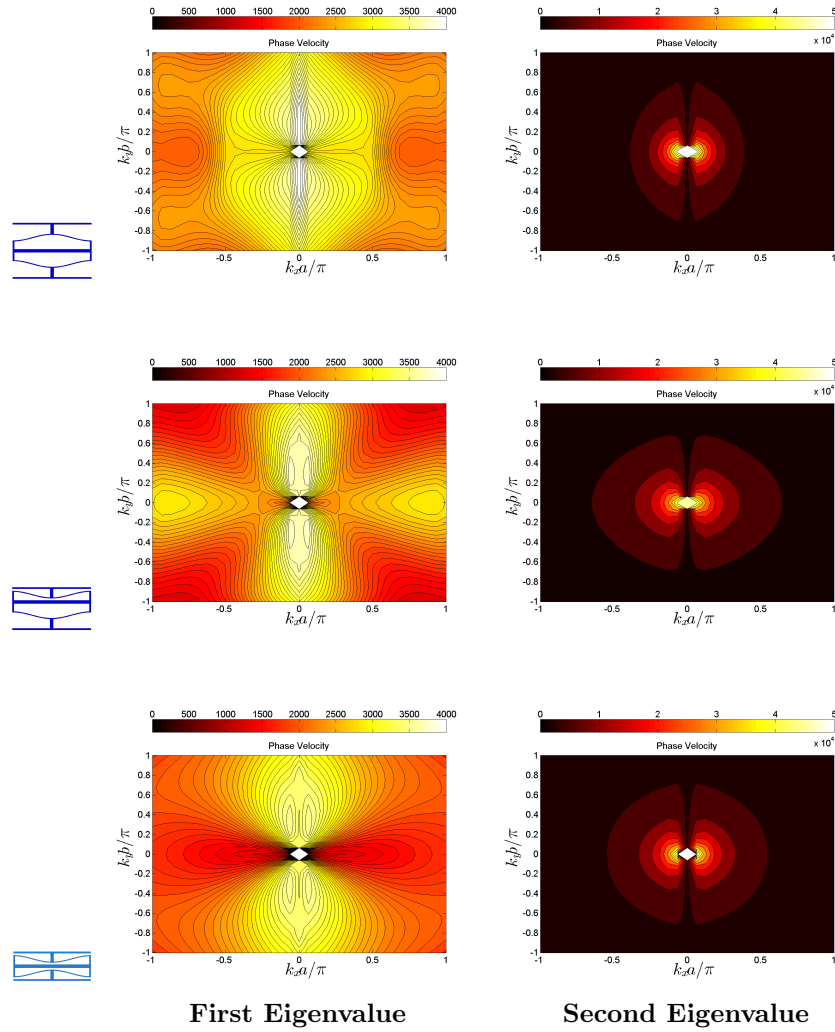


Figure 51: Phase velocity. Each row corresponds to one type of cell (open, intermediate and closed) and each column to the specified eigenvalue.

## 4 Considering pre-stresses

The analysis from the previous section revealed that it is possible to take advantage of the differences in the directivity between each phase suggesting the possibility of applications in wave guides. However, wave filtering has not been observed since there are not observable complete band gaps. On the other hand, the band struc-

ture does not change between phases. We can assume that the geometry variations between the three phases of the cell, determine the differences in the energy distribution at low frequencies.

Now, in order to consider the effect of a phase transition, we analyse the consequences of the remaining pre-stresses after the open cell collapses to the closed cell. We study if these pre-stresses change the dispersion diagrams and alter the propagation properties found for a closed cell in the last section. The model used in the estimation of the pre-stresses consists of an open cell with periodic boundary<sup>16</sup>. We imposed the displacement needed to reach a phase transition. Figure 52 shows the resulting Von Mises stress.

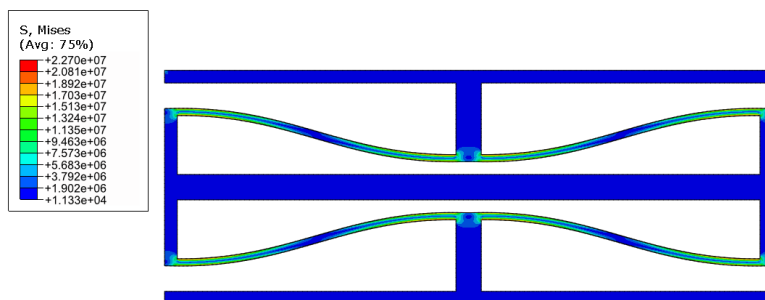


Figure 52: Von Mises pre-stress after the open cell collapsed to the closed cell.

During the phase transition, the force-displacement curve of saw-tooth shape was reproduced (Figure 53). The computed pre-stress used for Bloch analysis, corresponds to the step marked with the red dot in the curve. This dot is located when the force equals zero, i.e., a stability point, just in the transition to the closed cell.

<sup>16</sup>The boundary conditions were applied through Dummy nodes ( [120]).

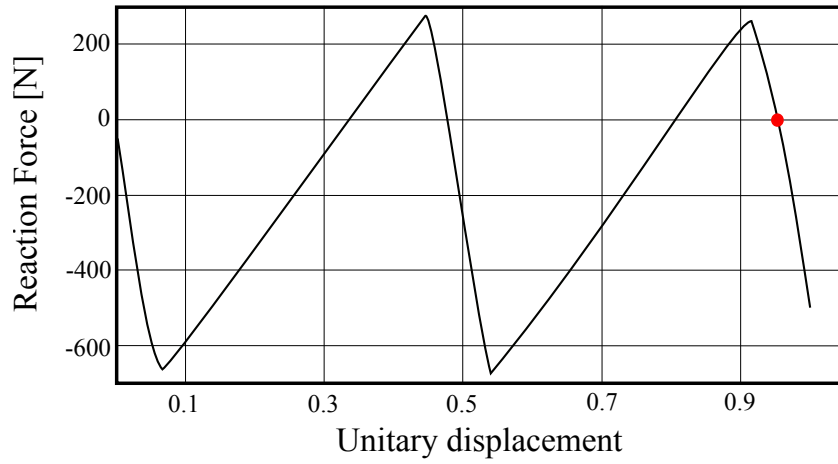
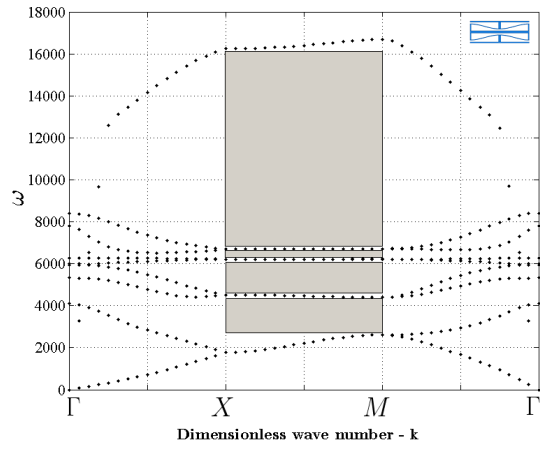
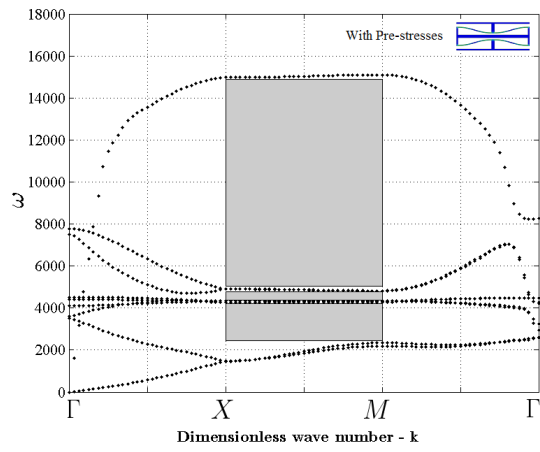


Figure 53: Force-Displacement curve of the open cell while being compressed and reaching the closed stable configuration.

We conclude that there are almost no changes in the dispersion diagrams, an the only relevant observation is that the eigenvalues are lower when considering the pre-stresses. This is supported by the comparison shown in Figures 54 and 55. We don't present the remaining dispersion diagrams used in previous sections, as they will be almost the same: they are derived from the dispersion contours.



(a) Closed Cell



(b) Closed Cell with Pre-stresses

Figure 54: Band structure for a closed cell, with and without pre-stresses.

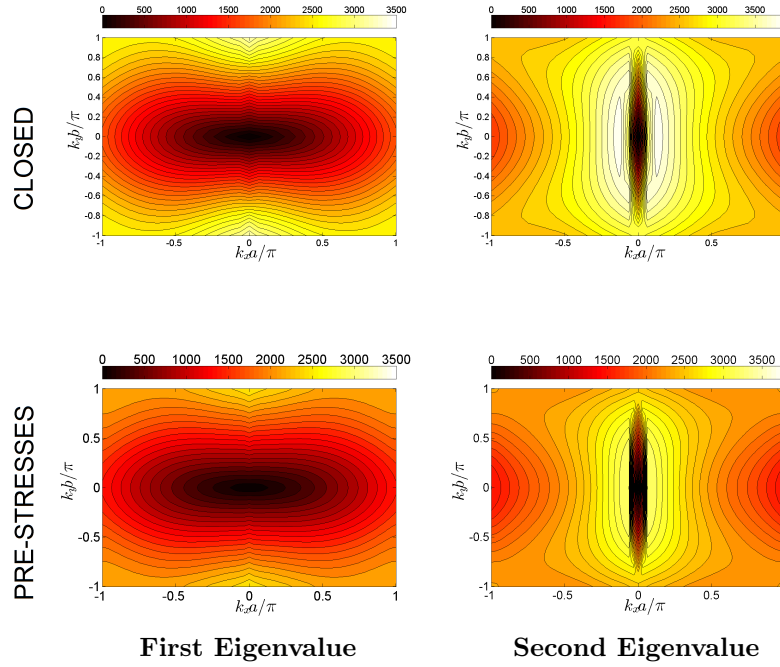


Figure 55: Dispersion contours comparison: Closed cell with and without pre-stresses.

## 5 Modifying the topology

This section considers the effects of a topological change in a closed cell. This is an attempt to alter drastically the band structure and the dispersion diagrams and thus, find mechanisms to switch the propagation properties between phases. Figure 56 shows the primitive cells: the closed cell and the cell with topological modifications, the resulting cellular materials are also presented (Figure 57).

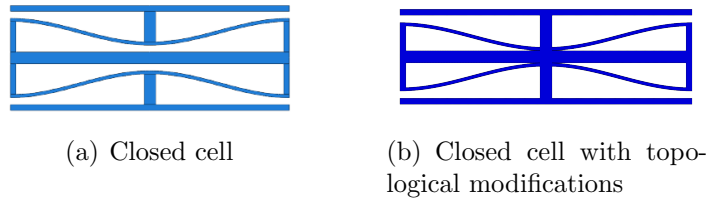
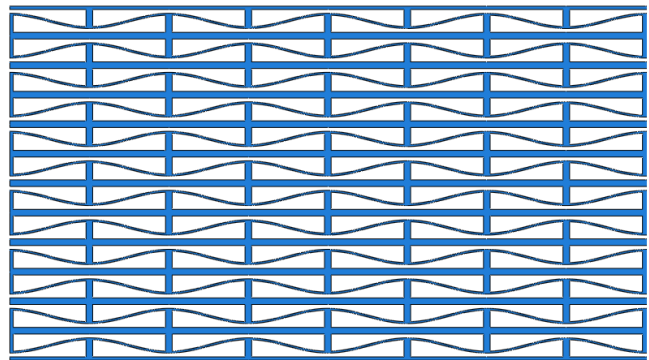
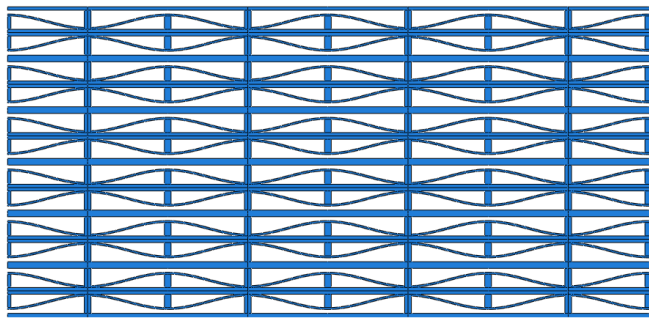


Figure 56: Primitive cells: closed configuration, with and without topological modifications.



(a) Closed cell



(b) Closed cell with topological modifications

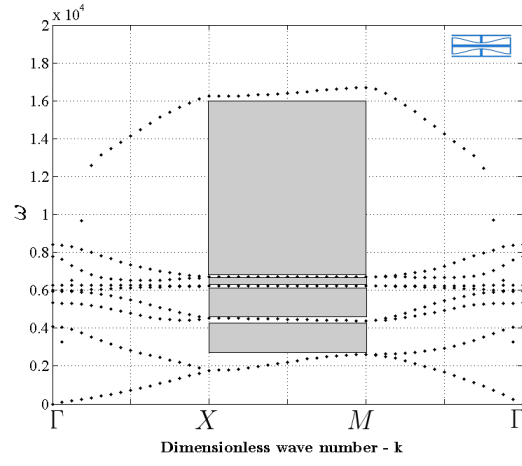
Figure 57: Lattices for the closed configuration, with and without topological modifications.

The cellular materials reveal a particular condition that surely affects the band diagrams: the material with topological modifications has continuous vertical bars while the typical material in closed configuration does not. The differences are observed from the band structures in Figure 58. The number of pseudo band gaps is smaller in the modified cell along  $\overline{XM}$  than the typical closed cell. Also the complete band structure resembles the one of stages 1 and 2 when an open cell is built (Figure 36). This last characteristic makes sense since the cellular material with modified topology is a combination of both, a rectangular grid and the sinusoidal bars.

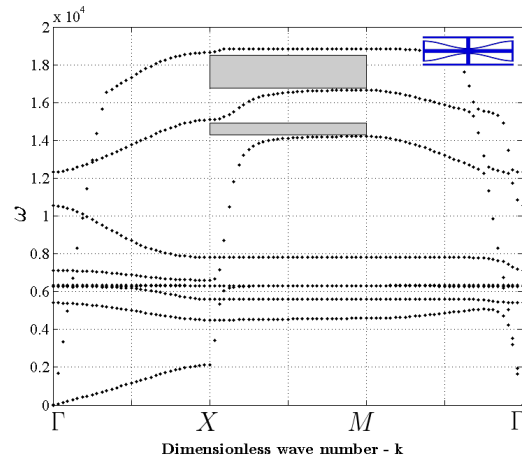
The dispersion contours (Figure 59) also reinforce the observation that stages 1 and 2 are very similar to this case of modified topology. Thus, the directionality contrast between the typical cell and the modified cell, is obvious. The polar histograms in Figure 60 show how the energy is now distributed almost only in the vertical and horizontal directions, with preference along the horizontal direction. It is clear that the continuity of bars facilitates the energy propagation in these directions.

The differences in the wave propagation are also observed in the iso-frequency directivity plot of Figure 61. For the modified cell, at lower frequencies, the waves propagate energy either around the horizontal or vertical directions for both eigenvalues. At higher frequencies the energy flux is directed almost in all directions. It has already been discussed how the typical closed cell confines the energy around the vertical direction for the first eigenvalue, and around the horizontal direction for the second eigenvalue.

In general, the modified topology exhibits the “fastest waves” for group and phase velocity (Figures 62 and 63). The energy is propagated faster for waves with a narrow angular incidence around the horizontal and vertical axes. In the case of phase velocity, we observe that waves with diagonal incidence have faster wave fronts.



(a) Closed Cell



(b) Closed Cell with Pre-stresses

Figure 58: Band structure for a closed cell, with and without topological modifications

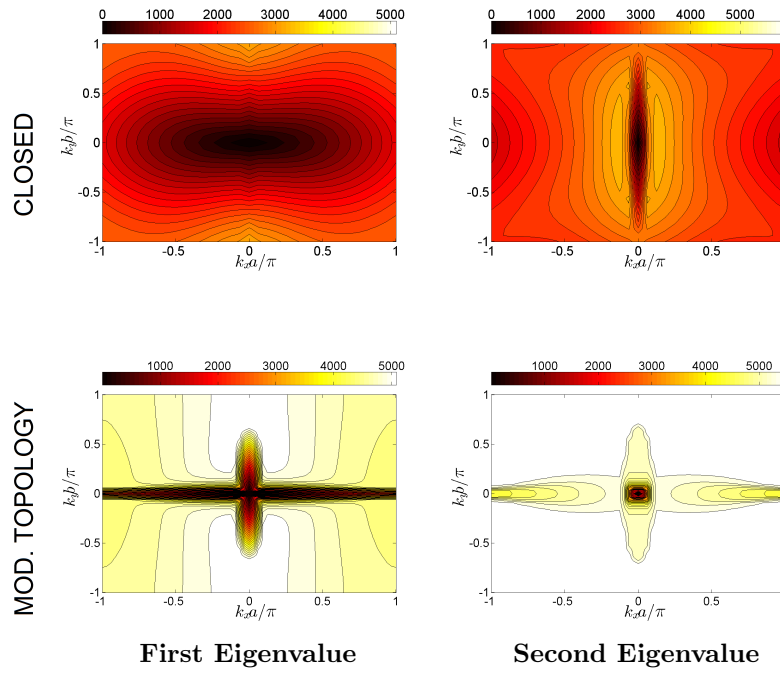


Figure 59: Dispersion contours comparison: Closed cell with and without modifications.

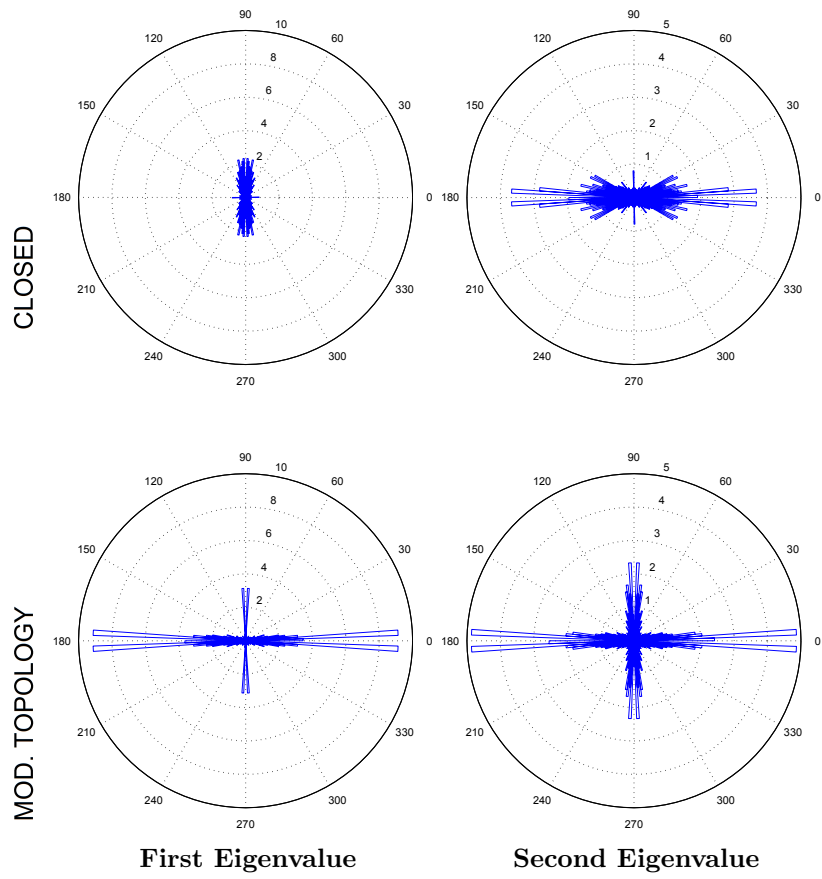


Figure 60: Polar histograms comparison: Closed cell with and without modifications.

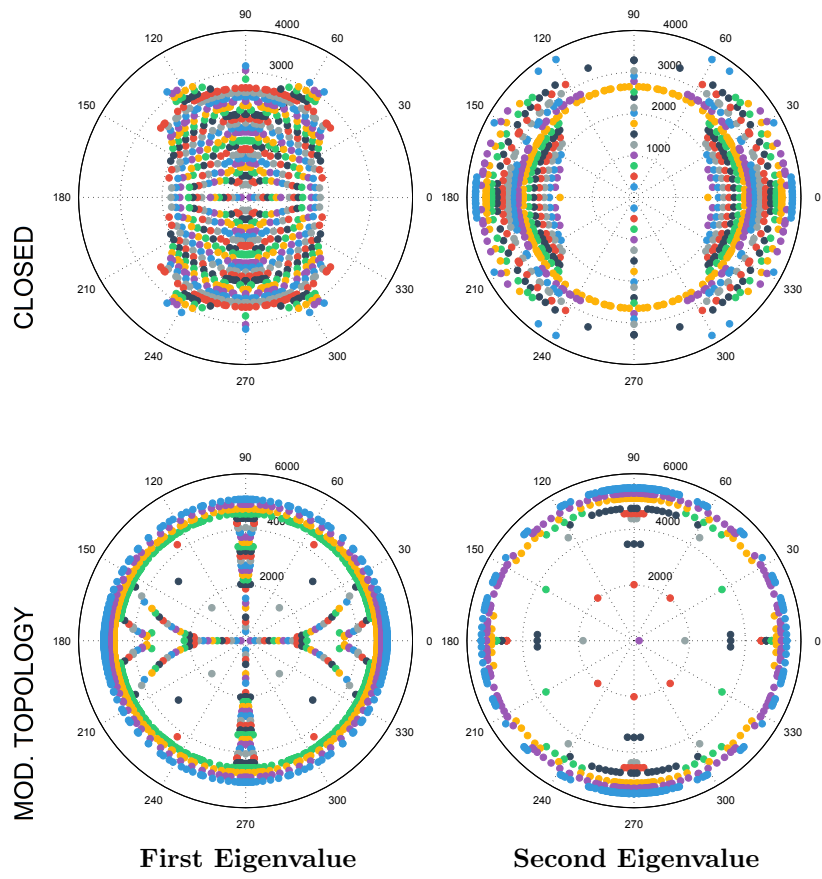


Figure 61: Iso-frequency directivity comparison: Closed cell with and without modifications.

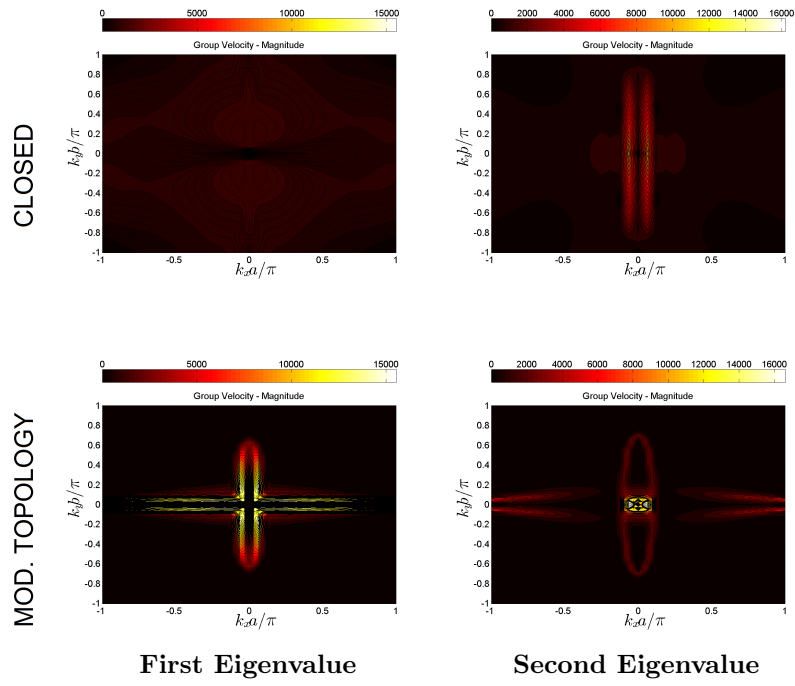


Figure 62: Group velocity comparison: Closed cell with and without modifications.

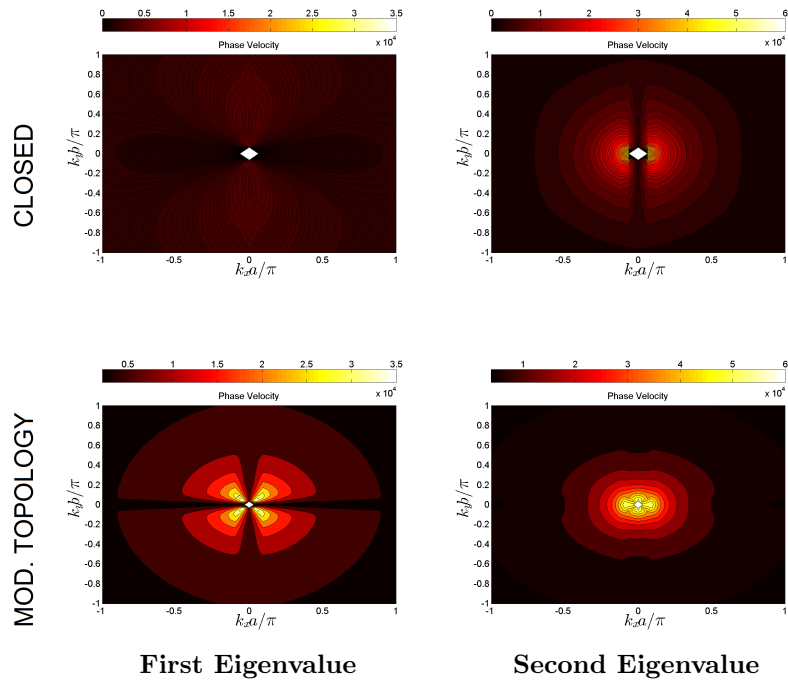


Figure 63: Phase velocity comparison: Closed cell with and without modifications.

# Conclusions

- Complete band gaps in the case of elastic in plane motion requires specific combinations of geometry and material properties. This problem must be studied in future works aimed at identifying the physical mechanisms that control the band structure in this more general case.
- Directionality results for the first four stages during the process termed here "building an open cell", show the cells prefer a narrow region around the horizontal direction for the energy propagation. The open cell with the sinusoidal bars reinforces the energy propagation in the other directions. These sinusoidal bars may be considered as wave guides.
- In a cellular material, the continuity of bars facilitates the energy propagation in the direction of alignment of the bars.
- The geometrical differences between the stable phases (closed, intermediate and open) have a weak influence on the band structure, at least at low frequencies.
- The contrast in directionality when comparing the intermediate cell with the other two phases, suggests the idea of a waveguide device at low frequencies. This is an important result to take into account in future applications and therefore, a time domain analysis is really worth it.
- If pre-stresses are included, there are almost no changes in the dispersion diagrams. The only relevant observation is the decrease in the eigenvalues.
- The complete band structure of the closed modified cell resembles the one of stage 1 or 2 when we built an open cell. This last characteristic makes sense since the cellular material with modified topology is a combination of both a rectangular grid and the sinusoidal bars.

## References

- [1] L. J. Gibson, Biomechanics of cellular solids, *J. Biomech.* 38 (3) (2005) 377–399.
- [2] M. A. Meyers, J. McKittrick, P. Y. Chen, Structural biological materials: critical mechanics-materials connections, *Science* 339 (6121) (2013) 773–779.
- [3] L. J. Gibson, M. F. Ashby, B. A. Harley, *Cellular materials in nature and medicine*, Cambridge University Press, 2010.
- [4] D. Restrepo, N. D. Mankame, P. D. Zavattieri, Phase transforming cellular materials, *Extreme Mechanics Letters* 4 (2015) 52–60.
- [5] J. Gomez, J. Jaramillo, M. Saenz, J. Vergara, A superposition based diffraction technique to study site effects in earthquake engineering, *Int. J. of Geo.*
- [6] D. Restrepo, J. Bielak, R. Serrano, J. Gomez, J. Jaramillo, Effects of realistic topography on the ground motion of the colombian andes - a case study at the aburrá valley, antioquia, *Geo. J. Int.*
- [7] N. Guarín-Zapata, J. Gomez, N. Yaraghi, D. Kisailus, P. D. Zavattieri, Shear wave filtering in naturally-occurring bouligand structures, *Acta Biomaterialia*.
- [8] N. Guarín-Zapata, J. Gomez, Evaluation of the spectral finite element method with the theory of phononic crystals, *J. of Comp. Acous.*
- [9] Z. Y. Liu, X. X. Zhang, Y. W. Mao, Y. Y. Zhu, Z. Y. Yang, C. T. Chan, P. Sheng, Locally resonant sonic materials, *Science* 289 (2000) 1734–1736.
- [10] M. I. Hussein, M. J. Leamy, M. Ruzzene, Dynamics of phononic materials and structures: Historical originis, recent progress and future outlook, *Applied Mechanics Reviews* 66 (2014) 040802(1–38). doi:10.1115/1.4026911.
- [11] L. Brilluoin, *Wave propagation in periodic structures.*, Dover Publications, 2003.
- [12] G. Floquet, Sur les équations différentielles linéaires a coefficients périodiques, *Comptes Rendu de l'Académie des sciences Paris* 91 (1880) 880–882.
- [13] F. Bloch, über die quantenmechanik der elektronen in kristallgittern, *Zeitschrift für Physik A Hadrons and Nuclei* 52 (1929) 555–600.

- [14] J. V. Sánchez-Pérez, D. Caballero, R. Martínez-Sala, C. Rubio, J. Sánchez-Dehesa, F. Meseguer, J. Llinares, F. Gálvez, Sound attenuation by a two-dimensional array of rigid cylinders, *Phys. Rev. Lett.* 80 (1998) 5325–5328.
- [15] D. Richards, D. J. Pines, Passive reduction of gear mesh vibration using a periodic drive shaft, *J. Sound Vib* 264 (2003) 317–342.
- [16] M. I. Hussein, G. M. Hulbert, R. A. Scott, Dispersive elastodynamics of 1d banded materials and structures: Analysis, *J. Sound Vib* 289 (2006) 779–806.
- [17] M. I. Hussein, G. M. Hulbert, R. A. Scott, Dispersive elastodynamics of 1d banded materials and structures: design, *J. Sound Vib* 307 (2007) 865–893.
- [18] H. Policarpo, M. M. Neves, A. M. Ribeiro, Dynamical response of a multi-laminated periodic bar: Analytical, numerical and experimental study, *Shock Vib* 17 (2010) 521–535.
- [19] J. Sánchez-Dehesa, V. M. García-Chocano, D. Torrent, F. Cervera, S. Cabrera, Noise control by sonic crystal barriers made of recycled materials, *J. Acoust. Soc. Am* 129 (2011) 1173–1183.
- [20] M. Ruzzene, F. Scarpa, F. Soranna, Wave beaming effects in two-dimensional cellular structures, *Smart Materials and Structures*.
- [21] M. M. Sigalas, Elastic wave band gaps and defect states in two-dimensional composites, *J. Acoust. Soc. Am* 101 (1997) 1256–1261.
- [22] M. M. Sigalas, Defect states of acoustic waves in a two-dimensional lattice of solid cylinders, *J. Appl. Phys* 84 (1998) 2026–3030.
- [23] M. Torres, F. R. M. de Espinosa, D. García-Pablos, N. García, Sonic band gaps in finite elastic media: Surface states and localization phenomena in linear and point defects, *Phys. Rev. Lett* 82 (1999) 3054–3057.
- [24] M. Kafesaki, M. M. Sigalas, N. García, Frequency modulation in the transmissivity of wave guides in elastic wave band gap materials, *Phys. Rev. Lett* 85 (2000) 4044–4047.
- [25] A. Khelif, A. Choujaa, S. Benchabane, B. Djafari-Rouhani, V. Laude, Guiding and bending of acoustic waves in highly confined phononic crystal waveguides, *Appl. Phys. Lett* 84 (2004) 4400–4402.

- [26] S. Mohammadi, A. A. Eftekhar, A. Khelif, W. D. Hunt, A. Adibi, Evidence of large high frequency complete phononic band gaps in silicon phononic crystal plates, *Appl. Phys. Lett* 92.
- [27] Y. Pennec, B. Djafari-Rouhani, J. O. Vasseur, A. Khelif, P. A. Deymier, Tunable filtering and demultiplexing in phononic crystals with hollow cylinders, *Phys. Rev. E* 69 (2004) 046608 – 046611.
- [28] M. I. Hussein, G. M. Hulbert, R. A. Scott, Hierarchical design of phononic materials and structures, *Proc. of 2005 ASME Int. Mech. Eng. Cong. and Exp (IMECE2005-81325)* (2005) 163–172.
- [29] S. Mohammadi, A. Adibi, On chip complex signal processing devices using coupled phononic crystal slab resonators and waveguides, *AIP Adv* 1 (2011) 041903 – 041906.
- [30] S. Bringuier, N. Swintek, J. O. Vasseur, J. F. Robillard, K. Runge, K. Muralidharan, P. A. Deymier, Phase-controlling phononic crystals: realization of acoustic boolean logic gates, *J. Acoust. Soc. Am* 130 (2011) 1919–1925.
- [31] R. Lucklum, J. Li, Phononic crystals for liquid sensor applications, *Meas. Sci. Technol* 20.
- [32] R. Wilson, J. Reboud, Y. Bourquin, S. L. Neale, Y. Zhang, J. M. Cooper, Phononic crystal structures for acoustically driven microfluidic manipulations, *Lab Chip* 11 (2011) 323–328.
- [33] D. Nardi, E. Zagato, G. Ferrini, C. Giannetti, F. Banfi, Design of a surface acoustic wave mass sensor in the 100 GHz range, *Appl. Phys. Lett* 100.
- [34] J. J. Shi, S. C. S. Lin, T. J. Huang, Wide-band acoustic collimating by phononic crystal composites, *Appl. Phys. Lett* 92 (2008) 111901 – 111911.
- [35] X. D. Zhang, Z. Y. Liu, Negative refraction of acoustic waves in two-dimensional phononic crystals, *Appl. Phys. Lett* 85 (2004) 341–343.
- [36] S. X. Yang, J. H. Page, Z. Y. Liu, M. L. Cowan, C. T. Chan, P. Sheng, Focusing of sound in a 3d phononic crystal, *Phys. Rev. Lett.* 93.
- [37] B. Liang, B. Yuan, J. C. Cheng, Acoustic diode: rectification of acoustic energy flux in one-dimensional systems, *Phys. Rev. Lett* 103.

- [38] B. Liang, X. S. Guo, J. Tu, D. Zhang, J. C. Cheng, An acoustic rectifier, *Nature Mater* 9 (2010) 989–992.
- [39] M. Maldovan, E. L. Thomas, Simultaneous localization of photons and phonons in two-dimensional periodic structures, *Appl. Phys. Lett* 88.
- [40] C. Goffaux, J. P. Vigneron, Theoretical study of a tunable phononic band gap system, *Phys. Rev. B* 64.
- [41] O. Thorp, M. Ruzzene, A. Baz, Attenuation and localization of wave propagation in rods with periodic shunted piezoelectric patches, *Smart Mater. Struct* 10 (2001) 979–989.
- [42] Z. Hou, F. Wu, Y. Liu, Phononic crystals containing piezoelectric materia, *Solid State Commun* 130 (2004) 745–749.
- [43] V. Laude, M. Wilm, S. Benchabane, A. Khelif, Full band gap for surface acoustic waves in a piezoelectric phononic crystal, *Phys. Rev. E* 71.
- [44] C. J. Rupp, M. Dunn, K. Maute, Switchable phononic wave filtering, guiding, harvesting, and actuating in polarization-patterned piezoelectric solids, *Appl. Phys. Lett* 96.
- [45] J. Baumgart, M. Zvyagolskaya, C. Bechinger, Tailoring of phononic band structure in colloidal crystals, *Phys. Rev. Lett* 99.
- [46] J. Y. Yeh, Control analysis of the tunable phononic crystal with electrorheological material, *Physica B* 400 (2007) 137–144.
- [47] F. M. L. Y. Z. Wang, W. H. Huang, X. A. Jiang, Y. S. Wang, K. Kishimoto, Wave band gaps in two-dimensional piezoelectric/piezomagnetic phononic crystals, *Int. J. Solids Struct* 45 (2008) 4203–4210.
- [48] M. Ruzzene, A. Baz, Control of wave propagation in periodic composite rods using shape memory inserts, *ASME J. Vib. Acoust* 122 (2000) 151–159.
- [49] A. Evgrafov, C. J. Rupp, M. L. Dunn, K. Maute, Optimal synthesis of tunable elastic wave guides, *Comput. Methods Appl. Mech. Eng.* 198 (2008) 292–301.
- [50] K. Bertoldi, M. C. Boyce, Mechanically triggered transformations of phononic band gaps in periodic elastomeric structures, *Phys. Rev. B* 77.

- [51] K. Bertoldi, P. M. Reis, S. Willshaw, T. Mullin, Negative poisson's ratio behavior induced by an elastic instability, *Advanced Materials* 22 (2010) 361 – 366.
- [52] P. Wang, J. Shim, K. Bertoldi, Effects of geometric and material nonlinearities on tunable band gaps and low frequency directionality of phononic crystals, *Phys. Rev. B* 88.
- [53] S. Babae, N. Viard, P. Wang, N. X. Fang, K. Bertoldi, Harnessing deformation to switch on and off the propagation of sound, *Adv. Mat.*
- [54] C. Pouya, J. T. B. Overvelde, M. Kolle, J. Aizenberg, K. Bertoldi, J. C. Weaver, P. Vukusic, Characterization of a mechanically tunable gyroid photonic crystal inspired by the butterfly *parides sesostris*, *Adv. Optical Mater.*
- [55] E. N. Economou, M. M. Sigalas, Classical wave propagation in periodic structures: cermet versus network topology, *Phys. Rev. B* 48 (1993) 13434 – 13438.
- [56] R. S. Langley, On the modal density and energy flow characteristics of periodic structures, *J. Sound Vib.* 4 (1994) 491 – 511.
- [57] R. S. Langley, The response of two-dimensional periodic structures to point harmonic forcing, *J. Sound Vib* 197 (1996) 447 – 469.
- [58] R. S. Langley, N. S. Bardell, H. M. Ruivo, The response of two-dimensional periodic structures to harmonic point loading: A theoretical and experimental study of beam grillage, *J. Sound Vib.* 207 (1997) 521 – 535.
- [59] M. Ruzzene, L. Mazzarella, P. Tsopeles, F. Scarpa, Wave propagation in sandwich plates with periodic auxetic core, *J. Intell. Mater. Syst. Struct* 13 (2002) 587 – 597.
- [60] P. G. Martinsson, A. B. Movchan, Vibrations of lattice structures and phononic band gaps, *Q. J. Mech. Appl. Math* 56 (2003) 45 – 64.
- [61] O. Sigmund, J. S. Jensen, Systematic design of phononic band gap materials and structures by topology optimization, *Philos. Trans. R. Soc. London, Ser. A* 361 (2003) 1001 – 1019.
- [62] M. Ruzzene, F. Scarpa, Directional and band gap behavior of periodic auxetic lattices, *Phys. Status Solidi B* 242 (2005) 665 – 680.

- [63] A. S. Phani, J. Woodhouse, N. A. Fleck, Wave propagation in two-dimensional periodic lattices, *J. Acoust. Soc. Am* 119 (2006) 1995–2005.
- [64] S. Gonella, M. Ruzzene, Homogenization and equivalent in-plane properties of two-dimensional periodic lattices, *Int. J. Solids Struct* 45 (2008) 2897–2915.
- [65] O. R. Bilal, M. I. Hussein, Ultrawide phononic band gap for combined in-plane and out-of-plane waves, *Phys. Rev. E* 84.
- [66] M. S. Kushwaha, P. Halevi, Band gap engineering in periodic elastic composites, *Appl. Phys. Lett* 64 (1994) 1085–1087.
- [67] C. M. Reinke, M. F. Su, R. H. Olsson, I. El-Kady, Realization of optimal band gaps in solid-solid, solid-air, and hybrid solid-air-solid phononic crystal slabs, *Appl. Phys. Lett* 98.
- [68] C. T. Sun, J. D. Achenbach, G. Herrmann, Time-harmonic waves in a stratified medium propagating in the direction of the layering, *ASME J. Appl. Mech.*
- [69] S. Nemat-Nasser, General variational methods for waves in elastic composites, *J. Elasticity*.
- [70] A. L. Abrahamson, The response of periodic structures to aero-acoustic pressures with particular reference to aircraft skin-rib-spar structures, Ph.D. thesis, University of Southampton, Southampton, U.K. (1973).
- [71] D. J. Mead, A general theory of harmonic wave propagation in linear periodic systems with multiple coupling, *J. Sound Vib.*
- [72] D. J. Ewins, Vibration characteristics of bladed disk assemblies, *J. Mech. Eng. Sci.*
- [73] J. H. Griffin, T. M. Hoosac, Model development and statistical investigation of turbine blade mistuning, *J. Vib., Acoust., Stress Reliab. Des.*, 106 (1984) 204–210.
- [74] V. S. Deshpande, N. A. Fleck, High strain rate compressive behaviour of aluminium alloy foams, *Int. J. Impact Eng.* 24 (2000) 277–298.
- [75] M. A. Hazizan, W. J. Cantwell, The low velocity impact response of foam-based sandwich structures, *Composites, Part B* 33 (2002) 193–204.

- [76] J. P. Talbot, H. E. M. Hunt, A computationally efficient piled-foundation model for studying the effects of ground-borne vibration on buildings, *Proc. Inst. Mech. Eng., Part C* 217 (2003) 975–989.
- [77] J. Bao, Z. F. Shi, H. J. Xiang, Dynamic responses of a structure with periodic foundations, *J. Eng. Mech.* 138 (2012) 761–769.
- [78] M. Brun, A. B. Movchan, I. Jones, Phononic band gap systems in structural mechanics: Finite slender elastic structures and infinite periodic waveguides, *ASME J. Vib. Acoust.* 135.
- [79] M. M. Sigalas, E. N. Economou, Elastic and acoustic wave band structure, *J. Sound Vib.* 158 (1992) 377–382.
- [80] M. M. Sigalas, E. N. Economou, Band structure of elastic waves in two dimensional systems, *Solid State Commun.* 86 (1993) 141–143.
- [81] M. S. Kushwaha, P. Halevi, L. Dobrzynski, B. Djafari-Rouhani, Acoustic band structure of periodic elastic composites, *Phys. Rev. Lett.* 71 (1993) 2022–2025.
- [82] M. S. Kushwaha, P. Halevi, G. Martínez, L. Dobrzynski, B. Djafari-Rouhani, Theory of acoustic band structure of periodic elastic composites, *Phys. Rev. B* 49 (1994) 2313–2322.
- [83] J. O. Vasseur, B. Djafari-Rouhani, L. Dobrzynski, M. S. Kushwaha, P. Halevi, Complete acoustic band gaps in periodic fibre reinforced composite materials: The carbodepoxy composite and some metallic systems, *J. Phys.: Condens. Matter* 6 (1994) 8759–8770.
- [84] E. N. Economou, M. M. Sigalas, Stop bands for elastic waves in periodic composite materials, *J. Acoust. Soc. Am.* 95 (1994) 1734–1740.
- [85] I. E. Psarobas, N. Stefanou, A. Modinos, Scattering of elastic waves by periodic arrays of spherical bodies, *Phys. Rev. B* 62 (2000) 278–291.
- [86] M. M. Sigalas, N. Garcia, Theoretical study of three dimensional elastic band gaps with the finite-difference time-domain method, *J. Appl. Phys* 87 (2000) 3122–3125.
- [87] M. S. Kushwaha, P. Halevi, Giant acoustic stop bands in two-dimensional periodic arrays of liquid cylinders, *Appl. Phys. Lett* 69 (1996) 31–33.

- [88] M. S. Kushwaha, P. Halevi, Stop bands for cubic arrays of spherical balloons, *J. Acoust. Soc. Am* 101 (1997) 619–622.
- [89] F. R. M. de Espinosa, E. Jiménez, M. Torres, Ultrasonic band gap in a periodic two-dimensional composite, *Phys. Rev. Lett* 80 (1998) 1208–1211.
- [90] I. E. Psarobas, N. Stefanou, A. Modinos, Surface acoustic waves in two-dimensional periodic elastic structures, *Phys. Rev. B* 58 (1998) 7958–7965.
- [91] F. Meseguer, M. Holgado, D. Caballero, N. Benaches, J. Sánchez-Dehesa, C. López, J. Llinares, Rayleigh-wave attenuation by a semi-infinite two-dimensional elastic band gap crystal, *Phys. Rev. B* 59 (1999) 12169–12172.
- [92] B. Manzanares-Martínez, F. Ramos-Mendieta, Surface elastic waves in solid composites of two-dimensional periodicity, *Phys. Rev. B* 68.
- [93] T. T. Wu, Z. G. Huang, S. Lin, Surface and bulk acoustic waves in two-dimensional phononic crystal consisting of materials with general anisotropy, *Phys. Rev. B* 69.
- [94] J. J. Chen, B. Qin, J. C. Cheng, Complete band gaps for lamb waves in cubic thin plates with periodically placed inclusions, *Chin. Phys. Lett* 22 (2005) 1706–1708.
- [95] J. C. Hsu, T. T. Wu, Efficient formulation for band-structure calculations of two-dimensional phononic-crystal plates, *Phys. Rev. B* 74.
- [96] A. Khelif, B. Aoubiza, S. Mohammadi, A. Adibi, V. Laude, Complete band gaps in two-dimensional phononic crystal slabs, *Phys. Rev. B* 74.
- [97] R. Sainidou, N. Stefanou, Guided and quasi-guided elastic waves in phononic crystal slabs, *Phys. Rev. B* 73.
- [98] C. Charles, B. Bonello, G. Ganot, Propagation of guided elastic waves in two-dimensional phononic crystals, *Ultrasonics* 44 (2006) E1209–E1213.
- [99] A. B. Movchan, N. V. Movchan, R. C. Mcphedran, Bloch-floquet bending waves in perforated thin plates, *Proc. R. Soc. A* 463 (2007) 45–64.
- [100] J. O. Deymier, P. A. Deymier, B. Djafari-Rouhani, Y. Pennec, A. C. Hladky-Hennion, Absolute forbidden bands and waveguiding in two-dimensional phononic crystal plates, *Phys. Rev. B* 77.

- [101] I. El-Kady, R. H. Olsson, J. G. Fleming, Phononic band-gap crystals for radio frequency communications, *Appl. Phys. Lett* 92.
- [102] Y. Pennec, J. O. Vasseur, B. Djafari-Rouhani, L. Dobrzynski, P. A. Deymier, Two-dimensional phononic crystals: Examples and applications, *Surf. Sci. Rep* 65 (2010) 229–291.
- [103] T. T. Wu, J. C. Hsu, J. H. Sun, Phononic plate waves, *IEEE Trans. Ultrason., Ferroelectr., Freq. Control* 58 (2011) 2146–2161.
- [104] T. T. Wu, L. C. Wu, Z. G. Huang, Frequency band gap measurement of two-dimensional air/silicon phononic crystals using layered slanted finger interdigital transducers, *J. Appl. Phys* 97.
- [105] S. Benchabane, A. Khelif, J. Y. Rauch, L. Robert, V. Laude, Evidence for complete surface wave band gap in a piezoelectric phononic crystal, *Phys. Rev. E* 73.
- [106] D. Torrent, J. Sánchez-Dehesa, Radial wave crystals: radially periodic structures from anisotropic metamaterials for engineering acoustic or electromagnetic waves, *Phys. Rev. Lett* 103 (2009) 64301–64306.
- [107] W. Steurer, D. Sutter-Widmer, Photonic and phononic quasicrystals, *J. Phys. D: Appl. Phys* 40 (2007) R229–R247.
- [108] A. L. Chen, Y. S. Wang, Y. F. Guo, Z. D. Wang, Band structures of fibonacci phononic quasicrystals, *Solid State Commun* 145 (2008) 103–108.
- [109] S. C. neira Ibáñez, V. Romero-García, J. V. Sánchez-Pérez, L. M. García-Raffi, Overlapping of acoustic band gaps using fractal geometries, *Eur. Phys. Lett* 92.
- [110] V. Laude, Y. Achaoui, S. Benchabane, A. Khelif, Evanescent bloch waves and the complex band structure of phononic crystals, *Phys. Rev. B* 80 (2009) 092301–092309.
- [111] V. Romero-García, J. V. Sánchez-Pérez, S. C. neira Ibáñez, L. M. García-Raffi, Evidences of evanescent bloch waves in phononic crystals, *Appl. Phys. Lett* 96.
- [112] P. Langlet, These: Analyse de la propagation des ondes acoustiques dans les matériaux periodiques a l aide de la methode des elements finis, Ph.D. thesis, LUniversité de Valenciennes et du Hainaut-Cambresis (1993).

- [113] N. G. Zapata, Simulacin numrica de problemas de propagacin de ondas: Dominios infinitos y semi-infinitos, Master's thesis, Universidad EAFIT (2012).
- [114] C. Kittel, Introduction to Solid State Physics, 8th Edition, Wiley, 2005.
- [115] K. F. Graff, Wave Motion in Elastic Solids, Dover Publications, 1975.
- [116] E. Hecht, Optics, Addison-Wesley, 2001.
- [117] L. Brillouin, Wave Propagation and Group Velocity, Academic Press, 1960.
- [118] B. Banerjee, An introduction to metamaterials and waves in composites, CRC Press, Taylor and Francis Group, 2011.
- [119] M. Åberg, P. Gudmundson, The usage of standard finite element codes for computation of dispersion relations in materials with periodic microstructure, J. Acoust. Soc. Am.
- [120] G. A. Kassem, Micromechanical material models for polymer composites through advanced numerical simulation techniques, Tech. rep., Aachen University and RWTH (2009).